

Thulium Doped Fibre Lasers in Continuous-Wave and Pulsed Regimes

by

Riaan Stuart Coetzee

*Dissertation presented for the degree of Master of Science in the Faculty
of Science at
Stellenbosch University*



Supervisor: Prof. Erich G Rohwer
Co-supervisors: Dr. Daniel Esser, Dr. Pieter Neethling

December 2013

Declaration

By submitting this thesis electronically, I declare that the entirety of the work contained therein is my own, original work, that I am the sole author thereof (save to the extent explicitly otherwise stated), that reproduction and publication thereof by Stellenbosch University will not infringe any third party rights and that I have not previously in its entirety or in part submitted it for obtaining any qualification.

December 2013

Copyright © 2013 Stellenbosch University

All rights reserved

Abstract

The following work focuses on the development and characterization of efficient, high-power, Thulium doped fibre lasers. Lasers emitting light around $\sim 2 \mu\text{m}$ have generated a large amount of interest owing to the range of applications requiring and utilizing light centred on this wavelength. Laser light in this emission band is considered “eye-safe” which makes it ideal for applications where eye-safety is paramount. The aim of this work is to develop expertise in Thulium doped fibre lasers. Background information relevant to the functioning of Thulium doped fibre lasers is presented. An existing diode pumped, CW Thulium doped fibre laser is characterized. The wavelength output as well as the efficiency of the fibre laser was characterized for different fibre temperatures, indicating shorter wavelength output for lower fibre temperatures. Additionally, initial results indicate that without any wavelength control (fibre Bragg gratings, volume Bragg grating), the spectrum and laser output is temporally unstable. The design, development and characterization of a diode pumped, CW and Q-switched Thulium doped fibre laser is discussed. The design process and considerations are discussed in detail. Different feedback elements, including a volume Bragg Grating, are utilized to constitute the laser resonator as well as two lengths of doped fibre. The CW fibre laser is characterized with regard to its slope efficiency, spectral output, temporal behaviour, beam profile and polarization. A maximum slope efficiency of 37 % was obtained for 6.5 metres of active fibre, only limited by the onset of thermal damage of the fibre ends. Pulsed mode of the fibre laser was facilitated with the aid of an Acousto Optic Modulator (AOM). At a pulse repetition rate of 10 kHz and average power of 2 W, a maximum pulse energy of 200 μJ is obtained with pulse durations of 77 ns. This corresponds to a maximum peak power of 2.6 kW

Opsomming

Hierdie tesis fokus op die ontwikkeling en karakterisering van doeltreffende, hoë-drywing vesellasers met Tulium as aktiewe ioon. Lasers met uitset golflengte rondom $\sim 2 \mu\text{m}$ verwek groot akademiese belangstelling gegewe die verskeidenheid praktiese toepassings wat lig by $\sim 2 \mu\text{m}$ vereis en benut. Laserlig in hierdie golflengtegebied word beskou as "oogveilig", wat dit ideaal maak vir toepassings waar oogveiligheid uiters belangrik is. Die doel van hierdie werk is om kundigheid in vesellasers, met Tulium as aktiewe ioon, te ontwikkel. Agtergrondinligting met betrekking tot die funksionering van Tulium vesellasers word eerstens bespreek. Daarna word 'n bestaande diode-gepompde Tulium vesellaser bespreek in terme van die karakterisering van die uitset laser spektrum, asook die doeltreffendheid van die vesel laser vir verskillende temperature, wat dui op korter golflengtes vir laer temperature. Daarbenewens het die aanvanklike resultate daarop gedui dat sonder enige golflengte beheer (vesel Bragg roosters, volume Bragg rooster), die spektrum en uitsetdrywing tydelik onstabiel is. Die ontwerp, ontwikkeling en karakterisering van 'n diode-gepompde kontinuedrywing en Q-geskakelde Tulium vesellaser word bespreek. Die ontwerp-proses en oorwegings word in detail bespreek. Verskillende hoë-reflekerende elemente, insluitend 'n volume Bragg rooster, word gebruik om die laserresonator te vorm. Twee lengtes van die aktiewe vesel word ook eksperimenteel ondersoek. Die kontinuedrywing vesel laser word gekarakteriseer met betrekking tot die helling van die doeltreffendheidskurwe, spektrale uitset, tydsgedrag, straalprofiel en polarisasie. 'n Maksimum hellingsdoeltreffendheid van 37% was behaal vir 6,5 meter van 'n aktiewe vesel maar was beperk deur die aanvang van skade aan die vesel endpoint as gevolg van hitteoorlading. Pulsering van die vesellaser is bewerkstelling met 'n Akoestiese Optiese Modulator (AOM). Teen 'n pulstempo van 10 kHz en met 'n gemiddelde uitsetdrywing van 2 W, was die maksimum pulsenergie van 200 μJ verkry met pulslengte van 77 ns. Dit stem ooreen met 'n maksimum piekdrwywing van 2,6 kW.

To Life

Acknowledgements

I would like to express my sincere gratitude to the following people:

- My supervisor Prof Erich Rohwer, for always providing insight and guidance into the work and situation at hand. I am grateful for your door always being open to me.
- Dr PH Neethling, for your valued contributions, advice and help with regard to any experimental and theoretical work I needed to do.
- Dr Daniel Esser, for promoting my love for science and your contributions towards my life, both in terms of academics and personal matters.
- Dr Hencharl Strauss, for being a good, honest friend and for contributions and guidance towards this work.
- Oliver Collet, for your friendship and input into furthering my understanding.
- Cobus Jacobs & Wayne Koen. For your friendship and assistance with regard to experimental work.
- All the technical staff at the LRI and NLC for their assistance with any technical matters related to this work.
- My Family, my father(s), mother(s) and brothers. For always being there for me regardless of the situation. Allowing me to see myself through your eyes has enriched and grown the love I have for life.
- I would also like to acknowledge and give thanks to the LRI, NLC and ARMSCOR for funding my MSc studies, I am truly grateful.
- Life.

Table of Contents

Abstract	ii
Acknowledgements	vi
List of Figures	ix
List of Tables	xii
1 Introduction.....	1
1.1 Thulium-Doped Fibre Lasers.....	1
2 Theory & Background	5
2.1 Gaussian Beams	5
2.2 Overview of Thulium-Doped Silica.....	7
2.2.1 Typical Glass Hosts for Fibres.....	11
2.2.2 Silica Glass & Oxide Dopants	13
2.3 Literature Review of CW & Pulsed Thulium-doped Fibre Lasers	13
2.3.1 Pulsed Operation of Thulium-Doped Fibre Lasers	15
2.4 Review of General Fibre Laser Designs in Literature	20
2.4.1 Resonator Designs	21
2.5 Conclusion	23
3 Wavelength Characterization of a Thulium Doped Fibre Laser	24
3.1 Design Considerations & Experimental Setup	24
3.1.1 Pump Source	25
3.1.2 Lenses & Mirrors	27
3.1.3 The Thulium-Doped Fibre	28
3.1.4 The Grating Spectrometer & Calibration.....	30
3.2 Experimental Results	33
3.2.1 Output Power Dependence on Temperature	33
3.2.2 Output Spectra and Wavelength Dependence on Temperature	34
3.3 Discussion.....	38
3.4 Recommendations.....	38
4 Design & Development of a CW & Q-switched Thulium-Doped Fibre Laser.....	40

4.1	Design Considerations & Experimental Setup	41
4.1.1	The Active Fibre	41
4.1.2	The Pump Source(s).....	47
4.1.3	Pump Optic Design	51
4.1.4	Resonator Design for CW Operation.....	56
4.1.5	Resonator Design for Locking the Laser Wavelength.....	59
4.1.6	Q-switch.....	59
4.1.7	Optical Layout for Q-switched operation	62
4.1.8	Cooling Design	64
4.1.9	Diagnostic Layout.....	64
4.2	Experimental Results	68
4.2.1	Laser Efficiencies.....	68
4.2.2	Output Spectra	71
4.2.3	Temporal Behaviour/Fluctuations	76
4.2.4	The Beam Profile of the Laser Beam.....	79
4.2.5	M ² measurement	82
4.2.6	Polarization	83
4.2.7	Q-switched Operation	84
4.3	Summary & Discussion	88
4.4	Recommendations & Future Work	89
5	Conclusion	92
6	List of Presentations.....	95
7	References.....	96

List of Figures

Figure 1-1: An optical fibre, viewed along a direction perpendicular to the fibre axis [14].	4
Figure 2-1: The beam radius w as a function of propagation distance z .	5
Figure 2-2: Collection of adjacent Thulium ions within silica, indicating energy and Stark levels, energy transfer via cross-relaxation and relaxation processes.	8
Figure 2-3: Energy transfer processes between two rare-earth ions. Migration (a), cross-relaxation (b), upconversion (c).	9
Figure 2-4: Absorption spectra of Thulium within silica glass [32].	11
Figure 2-5: Loss spectrum of silica optical fibre in the near-IR region [37].	12
Figure 2-6: Schematic of the 1 kW all-fibre laser [8].	14
Figure 2-7: >1kW of power output at 2045nm - Q-peak [8].	14
Figure 2-8: Graphical representation of laser behaviour during Q-switching.	16
Figure 2-9: Representation of an AOM during operation or Q-switching.	17
Figure 2-10: A simple fibre laser configuration.	20
Figure 2-11: An all-fibre laser.	22
Figure 3-1: Schematic of the Tm: fibre laser setup.	24
Figure 3-2: Fibre coupled laser diodes - Jenoptik (JOLD-75-CPXF-2P W).	26
Figure 3-3: Laser diode output power (W) as a function of diode current (A).	26
Figure 3-4: Cross sectional representation of the fibre (not to scale) [62].	28
Figure 3-5: The monochromator, indicating the optical layout and auxiliary components.	30
Figure 3-6: Calibration measurement of the Jarrel-Ash monochromator with two well known laser sources.	32
Figure 3-7: Slope efficiency plot for the Thulium doped fibre laser (room temperature).	33
Figure 3-8: Initial spectrum for the Thulium doped fibre laser.	34
Figure 3-9: Measured Tm-fibre laser spectrum at constant temperature of 25°C and pump power of 21.9 W.	35
Figure 3-10: Measured Tm-fibre laser spectrum at constant temperature of 25°C and pump power of 21.9 W, second scan.	36
Figure 3-11: Output spectrum of the Thulium laser, with a cooled (0°C) water bath and constant pump power of 21.9 W.	37
Figure 3-12: Cooled and un-cooled spectra of the LRI laser, at a constant pump power of 21.9 W.	37
Figure 4-1: Schematic of the Thulium doped fibre laser setup.	40
Figure 4-2: Top-view photo of the CW laser setup.	41
Figure 4-3: 1-8 Imaging layout used to confirm the core and pump cladding diameters.	43

Figure 4-4: Imaged fibre face indicating the core and octagonal pump cladding – greyscale x 4.	43
Figure 4-5: Sony Ericsson EFC-11 cleaver and optical fibre polishing pads.	46
Figure 4-6: The active fibre after cleaving (left) and after polishing (right).	46
Figure 4-7: 150 W, 200 μm core diameter, fibre coupled laser diode - Apollo Instruments.	47
Figure 4-8: Power (W) vs. Current (A) calibration - 150 W, Apollo diode.	49
Figure 4-9: Spectrum of the 150 W Apollo diode at full power (60A), $\sim 28^\circ\text{C}$	50
Figure 4-10: Wavelength dependence on diode temperature - 150 W Apollo diode. .	50
Figure 4-11: Comparison of light guidance between a standard lens and a GRIN lens.	52
Figure 4-12: Mounted Gadium lenses.	54
Figure 4-13: Interior structure of the Gadium lens tube.	54
Figure 4-14: Propagation of pump light via the Gadium lenses.	55
Figure 4-15: HR mirror functioning as feedback element within the resonator.	57
Figure 4-16: Mounted HR mirror with surrounding dry air enclosure.	58
Figure 4-17: The mounted Volume Bragg Grating.	59
Figure 4-18: RF signal (orange) generated during specific time intervals.	60
Figure 4-19: On-axis view of the mounted Acousto-Optic Modulator.	61
Figure 4-20: Schematic of the extension to the CW setup for Q-switched operation. .	62
Figure 4-21: Optical layout for Q-switched operation.	62
Figure 4-22: Optical layout for Q-switched operation with 1 metre active fibre length.	63
Figure 4-23: Diagnostic layout for the Thulium fibre laser.	65
Figure 4-24: Calibration plot for the Jarrel-Ash monochromator, utilizing a frequency doubled Nd: YVO laser (532 nm).	66
Figure 4-25: CW Slope efficiency with the curved HR mirror and ~ 6.5 metre fibre length.	68
Figure 4-26: Photo of the Thulium fibre during lasing.	69
Figure 4-27: Slope efficiency of the Q-switched setup during CW operation, ~ 6.5 metres fibre length.	70
Figure 4-28: Slope efficiency for the 1 metre fibre laser, using a flat HR mirror and VBG.	71
Figure 4-29: low power (0.336 W) spectrum for the Thulium fibre laser, fibre length of ~ 6.5 m.	72
Figure 4-30: Spectral output for varying output powers, ~ 6.5 m fibre length.	73
Figure 4-31: Output spectra for the two fibre lengths at constant output power of ~ 3 W.	74
Figure 4-32: Output spectrum of the 1 metre fibre laser, with broadband HR and VBG, 1 W output.	75

Figure 4-33: Schematic of the diagnostic layout used to observe temporal behaviour of the laser output.....	76
Figure 4-34: Temporal jitter of the 6.5 m fibre laser for two different time scales (1 W output).....	77
Figure 4-35: Output signal for the 1 metre fibre laser, with the VBG has feedback element (1 W output).....	77
Figure 4-36: Self-pulses in the output signal for increasing pump powers, 1 metre fibre length, with VBG.....	78
Figure 4-37: Self-pulse durations and frequency for varying pump powers.....	78
Figure 4-38: Beam profile of the laser beam for increasing output powers.....	79
Figure 4-39: Distortion in the beam profile of the laser beam due to minor misalignment of the HR mirror – 3.7 W & 3.5 W output power.....	80
Figure 4-40: Gradual improvement of the beam profile for the 1 metre fibre laser with VBG. Angled cleaved fibre end. 1 W output power.....	81
Figure 4-41: M^2 measurement for the Thulium fibre laser.....	82
Figure 4-42: Transmitted output power through the polarizing cube, for different rotation angles. 80 mW total power.....	83
Figure 4-43: Stable pulse generation (a) followed by erratic pulsing (b), repetition rate of 90 kHz, 12 W output power, 6.5 metre fibre length.....	85
Figure 4-44: A stable pulse train at 30 kHz repetition rate, 2 W output power, 6.5 metre fibre length.....	85
Figure 4-45: Breakthrough lasing during Q-switched operation seen at two different time scales and output powers. 30 kHz, 2W and 3W output power.....	86
Figure 4-46: An irregular Pulse train, 150 kHz, 1 W output power.....	86
Figure 4-47: Pulse Energy (μ J) and Pulse Duration (ns) for varying repetition rates (kHz) at a constant output power of 2 W.....	87
Figure 4-48: Proposed Dual end pumped configuration for the Thulium-doped fibre laser.....	91

List of Tables

Table 2-1: important properties of common fibre materials [36].	12
Table 2-2: Table of results for Q switched Tm doped fibre laser, with varying modulating elements [48].	19
Table 3-1: Parameter values for the CorActive Thulium-doped fibre.	28
Table 3-2: Spectrometer drive speeds ($\text{\AA}/\text{min}$).	31
Table 4-1: Parameter data for the doped Nufern fibres.	41
Table 4-2: Measured data for various beam diameters incident on the active fibre face.	56
Table 4-3: Summary of results obtained for the Thulium doped fibre laser.	88

1 Introduction

Thulium doped fibre lasers are promising sources of mid-infrared ($\sim 2 \mu\text{m}$) light. There is a range of applications which require light that is centred on this wavelength. These include, but are not limited to: LIDAR and remote sensing [1], medical surgery [2], directed infrared counter measures (DIRCM) [3] and optical pumping of other laser systems [4,5,6]. Fibre lasers have certain properties which make them ideal for these applications. They are robust, potentially more efficient and can be scaled to very high powers ($> 1 \text{ kW}$). The aim of this work was to develop expertise in this technology. To achieve this, an existing continuous-wave (CW) laser was characterized (Chapter 3). Additionally a new CW and Q-switched Thulium doped fibre laser was designed, developed and characterized (Chapter 4). The experimental setup and results are discussed in detail. The results obtained indicate the potential of these devices as mid-infrared laser sources and indicate some of the current limitations hindering further power-scaling.

1.1 *Thulium-Doped Fibre Lasers*

Thulium doped fibre lasers have a broad, tuneable emission spectrum of $\sim 1900 \text{ nm} - 2100 \text{ nm}$ [7]. Thulium doped fibre lasers have already managed to reach powers exceeding 1 kW under CW operation [8]. In addition, Thulium ions benefit from a resonant energy transfer process known as cross-relaxation [9], essentially providing two $\sim 2 \mu\text{m}$ photons per pump photon. By optimizing this process, while simultaneously minimizing other energy loss processes, high CW slope efficiencies may be obtained, the highest recorded to date being $\sim 74\%$ [10]. Due to the longer lasing wavelength of thulium, thulium doped fibres may be scaled to larger mode areas while still maintaining single mode operation. The larger fibre geometries available ensure that the thresholds of unwanted non-linear processes, such as Stimulated Brillouin Scattering, are raised [11]. This is particularly important for pulsed fibre lasers. These features coupled with excellent beam qualities ($M^2 < 1.5$), and robustness in design, pave the way for a large amount of potential applications as previously mentioned.

Research into rare-earth doped fibre lasers has experienced an exponential growth over the past two decades [12]. Fibre lasers enjoy specific advantages which distinguish them from other lasers. A few of these are:

- Mechanically durable and robust designs, utilizing less free space optics.

An all fibre system is possible, implying minimal use of free space optics. Thus one would obtain less loss overall, each loss introduced by the addition of each optical element in the setup. Certain elements that serve a specific function (for example, polarizing cubes in bulk-solid state lasers) are not necessary for fibres, as the fibre itself can be made to compensate for and maintain polarization [13]. The possibility of an all fibre system, also removes the risk of misalignment of the laser optics. For applications outside the laboratory, this is critical. This resilience to mechanical disturbances, allows the fibre laser to continue to lase under such a disturbance and this might be a strict requirement for certain applications. The fibre can also be coiled thereby utilizing less space overall.

- Broad absorption and emission line-widths.

For Thulium in particular, there are many available pumping bands (as will be shown later). These pumping bands can be quite broad, which relaxes the width of the pumping wavelength required to obtain lasing. This affords the possibility to make use of commercial laser diodes, instead of complicated pumping schemes.

- High optical-to-optical conversion efficiencies.
- High beam quality.

Certain applications require the divergence of the laser beam to be minimal over a considerable distance. This is only possible if the laser beam has a high beam-quality (low M^2) and is near diffraction limited (implying lasing in the lowest order mode TEM_{00} or LP_{01} for fibres in general). Due to the small diameter of the fibre core (typically $8\ \mu\text{m} - 30\ \mu\text{m}$), it is possible to obtain single mode-operation. This requires the structure of fibre geometry to be chosen in such a way as to allow this. Thermal effects upon the beam profile are largely negligible due

to the shielding property of the fibre as well as the lack of thermal lensing. This is in direct contrast to bulk solid-state lasers, where obtaining single mode operation is a challenge not limited to just the structure of the gain medium, but thermal management and resonator design as well. For Thulium fibre lasers in particular, it is easier to scale to higher powers while still maintaining single mode operation.

- Large degree of thermal resilience and efficient cooling due to the fibre geometry.

A fibre exhibits a large surface area to volume ratio owing to its cylindrical geometry. As a result of this property, a fibre is easily cooled by air or water as the cooling medium can easily come into direct contact with and surround the fibre allowing for efficient heat extraction from the core. This direct contact does not affect lasing in any detrimental sense. This fact, in conjunction with others mentioned, enables high efficiencies in fibre lasers.

- High gains.

The amount of gain can be much easier to extract within a fibre as opposed to solid-state lasers due the guiding property of the fibre itself. The typical gain per pass for a fibre can be in the order of 20 dB – 30 dB and 3 – 7 dB per pass for a solid-state laser [14]. This would require multiple passes for a solid-state laser as opposed to a fibre laser. The introduction of the single-clad structure of the active fibre facilitated the input coupling of pump light (Figure 1-1), [14,15]. Light enters the optical fibre and is confined and guided by means of total internal reflection. This is true provided that the angle of incident light falls within the angle defined by the numerical aperture (NA) of the fibre. Additionally, ongoing research and improvement into high power diode lasers ensured that the pumping of doped fibres with diode lasers, would potentially offer high optical gains, efficiency and power.

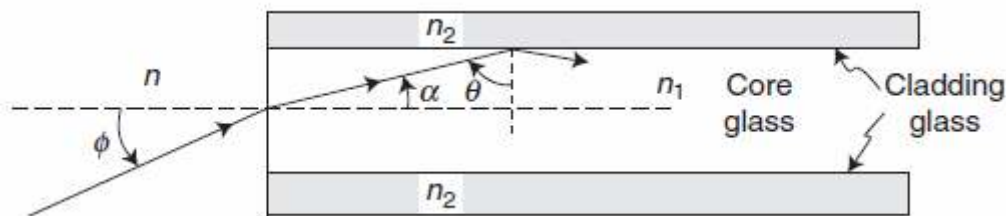


Figure 1-1: An optical fibre, viewed along a direction perpendicular to the fibre axis [14].

The most recent development with regard to Thulium fibres has been the introduction of Large Mode Area (LMA) fibres [16]. The motivation for LMA fibres is due to the following reasons:

- i. Owing to the larger fibre diameters, the onset of optical damage in the fibre is raised.
- ii. The larger area allows for easier thermal management within the fibre and relaxes the thermal load on the fibre ends. In addition this would imply a higher overall damage threshold.
- iii. The larger areas also raise the onset threshold of detrimental non-linear effects, due to the fact that they are intensity dependent.

Currently the main challenges hindering power scaling within fibre lasers falls into two categories. These are nonlinear effects and thermal damage, respectively. The main non-linear effects include Stimulated Raman Scattering (SRS) and Stimulated Brillouin Scattering (SBS) [17]. Other nonlinear effects do play a minor role, these being four-wave mixing [18] and self-focussing [19]. However for scaling to higher powers, SRS and SBS contribute the main limitation with regard to non-linear effects.

Thermal damage sets a limit on the maximum power obtained for Thulium doped fibre lasers and is the dominant factor inhibiting power scaling in this thesis. In order to obtain high efficiencies and fully exploit the cross-relaxation process in Thulium, a high doping concentration is required. As a consequence of this high doping, other energy transfer effects such as upconversion and excited-state absorption become pronounced (see Chapter 2.2). Relaxation from the states (excited by these effects), causes energy transferred into heat build up in the fibre, which will hamper

power-scaling. If scaling to high powers is required, it is therefore necessary to employ an effective cooling scheme for the active fibre of the fibre laser.

Much research has been undertaken into fibre lasers, utilizing different rare-earth doped elements (Yb^{3+} , Er^{3+} , Nd^{3+} , Ho^{3+} , Tm^{3+} , etc), however, investigating all of these falls outside of the scope of this thesis. The purpose of this study is to establish expertise in Thulium doped fibre lasers.

2 Theory & Background

This chapter will cover the spectroscopic characteristics of the Thulium ion, glass hosts for Thulium and the population dynamics relevant for Thulium doped fibre lasers. In addition, a brief literature review of CW and pulsed designs and results will be given. Also, theory relevant to Gaussian beam propagation will be discussed.

2.1 Gaussian Beams

This section will introduce the reader to common parameters and terms used in Gaussian propagation. Laser beams are frequently referred to as Gaussian beams. This is due to the fact that the intensity profile of these beams can often be described by Gaussian functions [14]. Consider Figure 2-1 given below.

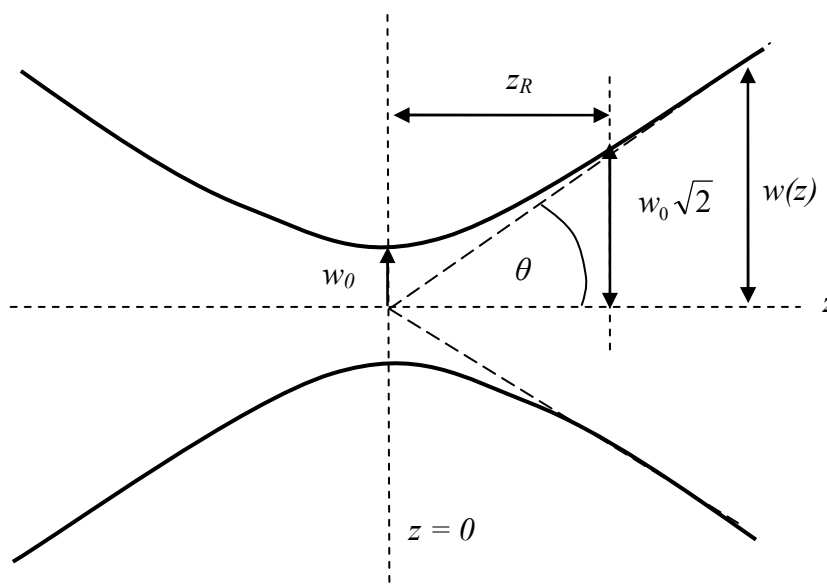


Figure 2-1: The beam radius w as a function of propagation distance z .

Figure 2-1 shows the variation of the beam radius $w(z)$ of a Gaussian beam with a propagation distance z . If a Gaussian beam is focused by a lens, the beam will be

focused to have a beam radius or spot size of w_0 . It can be shown that the beam radius $w(z)$ can be expressed as [20]:

$$w(z) = w_0 \sqrt{1 + \left(\frac{M^2 \lambda (z - z_0)}{\pi w_0^2} \right)^2} \quad (2.1)$$

Where w_0 is the beam radius at the beam waist ($z = z_0$), λ is the wavelength of the light, z is the propagation distance, z_0 is the position of the beam waist and M^2 is the beam quality factor. Equation (2.1) can be used to determine the beam radius of a Gaussian beam anywhere along its propagation length. This is important to know when designing the optical layout of a specific laser and will be elaborated on later. Another useful parameter commonly encountered in laser design is the Rayleigh range z_R . This is the distance from the beam waist where the area of the beam has effectively doubled, and occurs at a beam radius of $w_0 \sqrt{2}$.

From Figure 2-1, if we consider the case where $z \gg 0$ (the so-called far-field approximation), the angle θ can be expressed as $\frac{w(z)}{z}$. Applying the condition $z \gg 0$ to equation (2.1), it can be shown that this reduces to:

$$\theta = \frac{w(z)}{z} = \frac{\lambda}{\pi w_0} M^2 \quad (2.2)$$

Equation (2.2) gives the half-angle divergence for a Gaussian beam in the far-field. For this thesis, it will be relevant to adjust equation (2.2) to compensate for fibres. In order to do this, the position of the beam waist is considered to be the fibre face. The area of the Gaussian beam at the beam waist is equivalent to the area of the fibre core. The numerical aperture (NA) of a fibre is directly related to this half-angle. Therefore, for a fibre with fibre core of diameter D , equation (2.2) can be expressed as:

$$M^2 = \frac{\pi D}{2\lambda} NA \quad (2.3)$$

Using equation (2.3), the expected beam-quality factor for a fibre laser can be approximated, provided all other fibre parameters are known.

As was mentioned, the M^2 value is the beam-quality factor. The M^2 value of a given beam is the factor by which it differs from an ideal Gaussian beam ($M^2 = 1$). There are numerous techniques to measure the M^2 for a given beam. The general idea is as follows: A beam with an unknown M^2 value is converged with a lens. The diameter (and hence radius) is measured at various points along this length with a specific technique, such as a 90/10, 16/84 knife edge. Referring to the beam propagation formula (equation 2.1), the values $w(z)$ and z are measured. This data is then plotted (the beam radius $w(z)$ as a function of the distance z). With the data plotted, a least-squares fit of the beam propagation formula is fitted to the data, from which an M^2 value may be determined. In order to obtain consistent and accurate values for the M^2 , the International Standard ISO 111046 specifies the exact procedure to be employed for a specific measurement technique [21].

For a step-index optical fibre, it is possible to obtain single mode operation provided the so called “V-parameter” of the fibre is less than the cut off value of 2.405. The V-parameter for a fibre can be expressed as [14]:

$$V = \frac{2\pi a}{\lambda} \sqrt{n_1^2 - n_2^2} = \frac{2\pi a}{\lambda} NA \quad (2.4)$$

Where a is the fibre core radius, λ is the wavelength of the laser light, n_1 and n_2 are the refractive indices of the core and pump cladding respectively and NA is the numerical aperture of the core.

2.2 Overview of Thulium Doped Silica

This section will cover the structure of the Thulium ion within silica glass and relevant energy transfer processes which occur during laser operation. The choice of a dopant and fibre material is critical and will ultimately affect the final performance and output wavelengths of the fibre laser in question. Due to the fabrication process of fibre glasses, the active dopant incorporated into the host medium may undergo chemical changes regarding its oxidation state [22]. This may lead to varying dopant states incorporated into the fibre, which would act as impurities (giving rise to parasitic absorption/lasing and ion quenching) rather than active ions contributing to the desired lasing. However, rare-earth ions are highly stable within their trivalent

oxidation state [23], which makes them ideal candidates as active dopants for fibre lasers. Extensive research has been undertaken regarding the electronic structure of lanthanides, especially in glass hosts [24]. This work will focus on the main transition of interest within diode-pumped Thulium doped fibre lasers, this being ${}^3F_4 \rightarrow {}^3H_6$.

The ${}^3F_4 \rightarrow {}^3H_6$ transition within Thulium ions is of particular interest owing to its broad infrared emission ($\sim 1.9 - 2.1 \mu\text{m}$) [7]. Given below is a figure representing the energy levels of interest within Thulium (Figure 2-2).

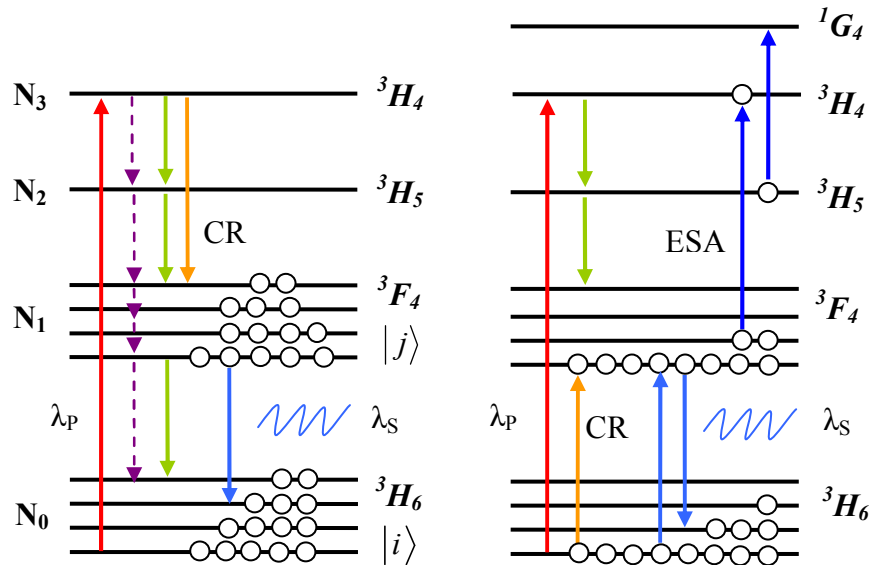


Figure 2-2: Collection of adjacent Thulium ions within silica, indicating energy and Stark levels, energy transfer via cross-relaxation and relaxation processes.

Thulium is optimally pumped with wavelengths in the range $\sim 790 - 800 \text{ nm}$. Typically, the pump sources utilized for this pumping scheme are commercial AlGaAs laser diodes [25]. By pumping in this absorption band, one is able to obtain high pump efficiencies. The absorption of the transition ${}^3H_6 \rightarrow {}^3F_4$ shares a spectral overlap with the ${}^3H_4 \rightarrow {}^3F_4$ and ${}^3F_4 \rightarrow {}^3H_6$ emission. This gives rise to a resonant energy transfer process known as cross-relaxation [10], which occurs between two adjacent Thulium ions. This process is more generally known as a Förster energy transfer process [26]. It is a dipole-dipole interaction between two Thulium ions. In Figure 2-2, the ion is excited via the laser pump source (λ_p) from the lower level (3H_6) to the third excited state (3H_4). The ion then de-excites into the lower levels by means of spontaneous decay(s) (green arrows), multi-phonon relaxation (purple arrows) and cross-relaxation (CR). Cross relaxation is dependant on the distance between neighbouring Thulium ions and therefore the doping concentration of Thulium within

the core plays a vital role in determining the laser efficiency [27]. However, high doping concentrations tend to result in the Thulium ions clustering with one another, leading to detrimental energy losses such as upconversion and re-absorption. Typical inter-ion energy transfer processes, between rare-earth ions, are indicated below in Figure 2-3.

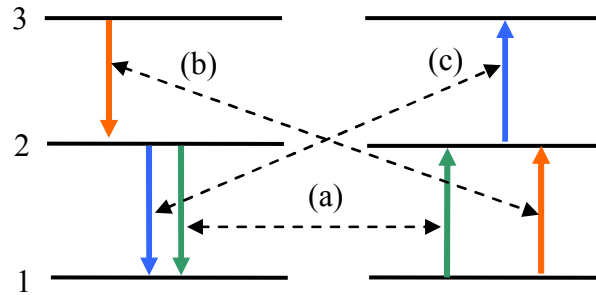


Figure 2-3: Energy transfer processes between two rare-earth ions. Migration (a), cross-relaxation (b), upconversion (c).

The energy levels represented in Figure 2-2, are actually energy manifolds and consist of many sub-levels known as Stark levels. A single Stark level within the 3F_4 and 3H_6 has been indicated by the notation $|j\rangle$ and $|i\rangle$ respectively. This broadening of the energy levels is due to the presence of the electric field which permeates the Thulium-doped silica and is known as the Stark effect [28]. The broadening is also said to be inhomogenous due to the amorphous glass structure of silica. This is the principal reason for the broad emission spectrum associated with Thulium-doped fibre lasers.

The McCumber relation (given by equation 2.5) shows that the value of the emission and absorption cross-sections, are dependent on the temperature T . This relation indicates how the temperature of a laser medium would have a direct effect on the emission and absorption cross-sections, and therefore the output wavelength of the laser [29].

$$\frac{\sigma_e(\lambda)}{\sigma_a(\lambda)} = \exp\left(\frac{-hc}{k_B T} \frac{1}{\lambda}\right) \quad (2.5)$$

In addition, the ground states of quasi-three level ions are populated at room temperature, also having an impact on the wavelengths of lasers based on certain rare-earth ions [30]. The loss for the laser is different at different temperatures, particularly the re-absorption loss. This will also affect the output wavelength of the laser.

The lifetime of the 3F_4 level has been determined both experimentally and theoretically, varying in a wide range [31]. The values vary according to the composition of the silica used i.e. the glass structure and doping, and whether there is a large amount of impurities and what these impurities are. Values of this lifetime for silica used in fibre lasers have been measured to be around 4.75 ms [29]. It is desirable for this level to have a long lifetime for pulsed operation, in order to obtain pulses with a higher energy. This implies an increase in the amount of extractable energy out of the laser as well as lowering the lasing threshold. Energy depletion via phonons also plays a fundamental role in de-exciting levels within the manifolds. This in turn may increase the probability of re-absorption occurring within the ion and also altering the absorption cross section of the manifold, both undesired effects. In addition, previous research has indicated that phonon energies have a significant effect on the lifetime of a specific energy level [29]. The high phonon energies in silica decrease the lifetimes of the 3F_4 , 3H_4 and 3H_5 levels and therefore lower phonon energy within a fibre medium is one motivation for choosing alternative glass hosts for fibre fabrication besides silica. Due to this shorter lifetime, the probability of the cross-relaxation process is also reduced, which will lower the efficiency of the laser.

The 3F_4 level emits light in a wavelength range of $\sim 1.9 - 2.1 \mu\text{m}$ and is de-excited to the ground state 3H_6 . Thulium has other absorption peaks (Figure 2-4, [32]), represented by the transitions: ${}^3H_6 \rightarrow {}^3H_5$ ($\sim 1210 \text{ nm}$) and ${}^3H_6 \rightarrow {}^3F_4$ ($\sim 1600 \text{ nm}$), however pumping these bands requires pump sources which are not readily available (Nd:YAG, Erbium fibre lasers, etc). These schemes do not offer high absorption in comparison to pumping at $\sim 790 \text{ nm}$. Also, the benefit of cross-relaxation is not utilized and hence lower efficiencies can be expected.

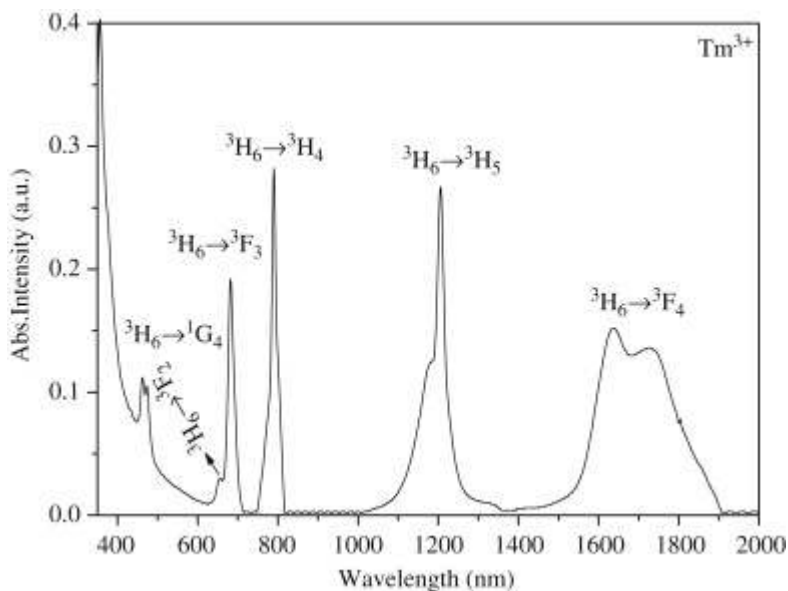


Figure 2-4: Absorption spectra of Thulium within silica glass [32].

Previous research has shown that the output of Thulium doped fibre lasers operating in CW configurations has displayed an erratic structure. The CW output resembles a periodic, pulsed structure and this behaviour has come to be known as self-pulsing or self-mode locking [33], [34], [35]. The origin of these self-pulses has been a matter of some debate, with explanations ranging from longitudinal modes and inter-ion effects such as cross-relaxation. Previous work has also shown a correlation between the parameters of these self-pulses and the amount of input pump power [33]. The CW output of the laser will jump between regimes of Quasi-CW and purely CW depending on the amount of input pump power. In [34], the authors numerically model the population dynamics of the Thulium ion, accounting for cross-relaxation, excited state absorption and upconversion. The authors rule out all factors and find that the influence of excited state absorption accounts for the measured parameters of the observed self-pulses, suggesting the origin of these pulses is attributed to excited state absorption.

2.2.1 Typical Glass Hosts for Fibres

A wide variety of host materials for rare-earth doped fibres have been used, each influencing the results of laser output. The choice of the material is dependent on a number of factors, such as:

- Phonon energies.
- Durability.
- Thermal conductivity, expansion, etc.

- Solubility of rare-earth dopants.
- Mechanical strength.
- Glass purity.
- Transparency in a specific wavelength range.

Silicates, fluorides (fluorozirconate – ZrF_4 , ZBLAN), chalcogenides, ceramics, Germanate and Tellurite are some of the most investigated fibre materials (Table 2-1, [36]).

Table 2-1: important properties of common fibre materials [36].

Fibre Material	Max Phonon Energy (cm^{-1})	Infrared Transparency Cut-off (μm)	Propagation losses (λ at minimum) (dB/km)	Thermal Conductivity (W/Km)
Silica	1100	< 2.5	0.2 (1.55 μm)	1.38
ZBLAN	550	< 6.0	0.05 (2.55 μm)	0.7 – 0.8
GLS	425	< 8.0	0.5 (3.50 μm)	0.43 – 0.5

For high power applications centred on $\sim 2 \mu m$, silica presents the best choice, owing to its high thermal and mechanical resilience, power scaling capability and acceptable transparency within the mid-infrared emission range of Thulium (Figure 2-5, [37]). Therefore all the fibres utilized in this thesis, make use of silica glass as the fibre medium.

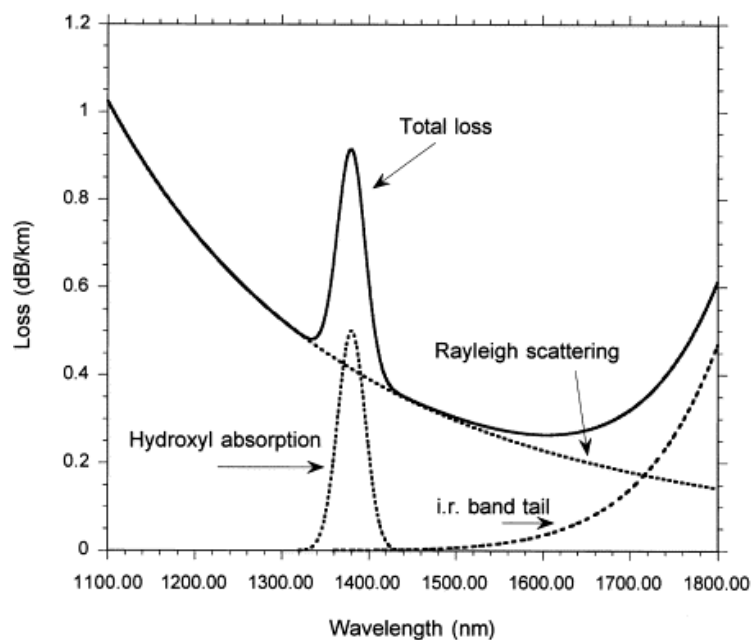


Figure 2-5: Loss spectrum of silica optical fibre in the near-IR region [37].

2.2.2 Silica Glass & Oxide Dopants

Silica glass (pure SiO_2) is an amorphous material that is covalently bonded. Owing to the strength of these bonds, it exhibits a high degree of mechanical and thermal durability. However this leads to high phonon energies within the glass medium, typically of the order of $\sim 1050 \text{ cm}^{-1}$. The high phonon energy presence leads to non-radiative decay between energy sub-levels of rare-earth doped ions, and as such these transitions are known as phonon assisted transitions [31].

The addition of certain oxides (Al_2O_3 , P_2O_5 , B_2O_3 , etc) into the glass host has been shown to increase the efficiency of rare-earth doped fibre lasers and has become common place for most fibres. For fibres utilizing Tm^{3+} as the principal dopant, aluminosilicate (Al_2O_3) has been particularly effective in minimizing clustering between adjacent Tm^{3+} ions and increasing the solubility of the rare-earth dopant within silica. Clustering between the dopant ions leads to losses due to energy transfer processes and affects the population inversion, dramatically decreasing laser performance [10]. The oxide additive also serves to increase the refractive index of the core, therefore assisting with confining light within the core. Another indirect benefit of the addition of Al_2O_3 is the increased mechanical strength of the silica medium.

2.3 Literature Review of CW & Pulsed Thulium doped Fibre Lasers

One of the first Thulium doped silica fibre laser was developed in 1988 by Hanna *et al* [38]. The fibre was pumped with a dye laser with a centre wavelength of 797 nm. Initial results indicated a slope efficiency of about 13 %, comparatively lower than recent efficiencies produced. However, this was prior to the development of cladding pumping, hence the lower efficiency. Also the cross-relaxation mechanism was not fully understood at this time and therefore could not be efficiently exploited. Further understanding of the resonant energy transfer processes between Tm^{3+} ions lead to the highest efficiency for such a fibre laser, reported to be $\sim 74 \%$ [10].

In terms of output power, a 885 W Thulium doped fibre laser with a slope efficiency of 49.2 % was produced in 2009 by P.F Moulton, *et al* [39]. The fibre was dual-end pumped by two commercial laser diodes at a wavelength of $\sim 795 \text{ nm}$, with a maximum pump power of $\sim 1 \text{ kW}$. Due to the high pump powers incident on the fibre,

the fibre utilized had larger core and pump cladding diameters of 35 μm and 625 μm respectively. The larger fibre core diameter resulted in a multimode beam.

This record was later broken in 2010 by a 1 kW continuous-wave fibre based, master-oscillator with two amplifier stages, which currently is the highest CW, single-mode output from a Thulium doped fibre laser system [8] (Figure 2-7). The fibre amplifiers were pumped by twelve fibre coupled laser diodes at $\sim 793 \text{ nm}$ and utilized fibre Bragg gratings to constitute the laser resonator (Figure 2-6). By combining the fibres of the pump diodes (beam-combining) with that of the active fibre, less thermal load is incident on the fibre ends. This technique allows fibre lasers to be scaled to higher powers.

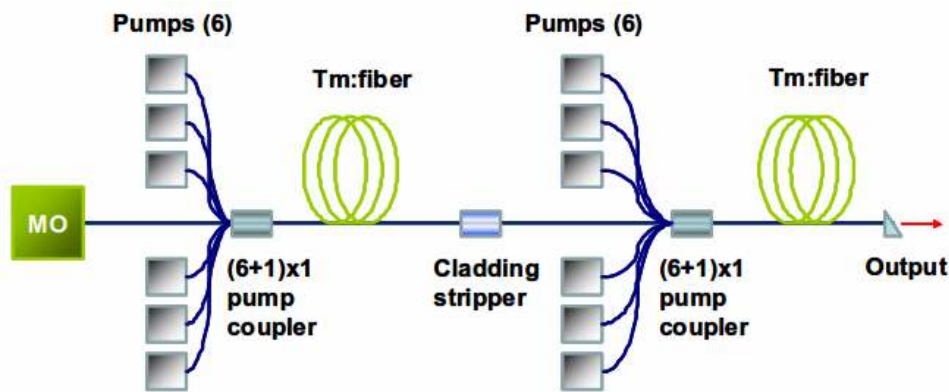


Figure 2-6: Schematic of the 1 kW all-fibre laser [8].

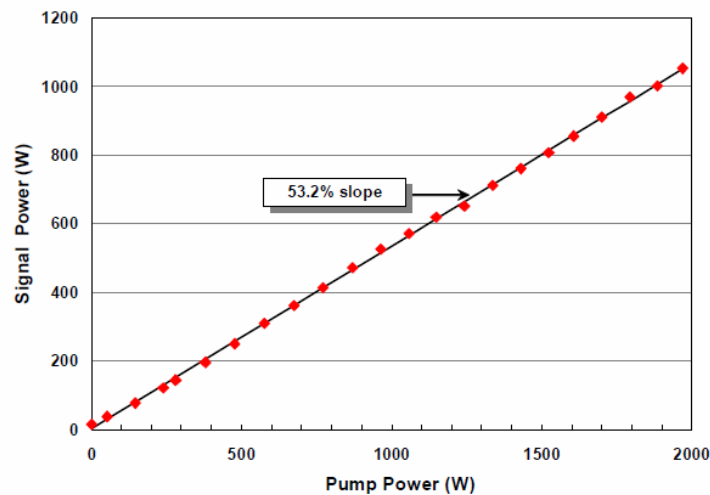


Figure 2-7: >1kW of power output at 2045nm - Q-peak [8].

Previous work has indicated that an inverse relationship exists between the number of Tm^{3+} ions and the core to cladding area ratio [40]. In this work, five different fibres

with varying parameters (core, cladding diameters, doping concentration, etc) were studied, measuring for example: output power and wavelength, lasing efficiencies, influence of temperature. From this, for higher core to cladding ratio there is a small number of Tm^{3+} ions present, leading to less re-absorption and shorter running wavelengths. The choice of fibre parameters is therefore crucial to determining the fibre laser output(s).

The addition of other rare-earth co-dopants into Thulium silica fibres has also been extensively investigated. Ytterbium was one of the first dopants to be incorporated [41]. This setup generated 75 W of output power and yielded a slope efficiency of 32%. At the time, the availability of ~ 790 nm diode lasers was poor and they were relatively costly. The addition of Yb^{3+} ions as a co-dopant opened the possibility of pumping with diodes at ~ 975 nm, which were widely available. However, Thulium-doped fibres that make use of Ytterbium co-doping suffer from thermal effects and heat build up in the fibre, lowering the scaling limit of devices based on these fibres [41].

Co-doping with Holmium ions (Ho^{3+}) has also been previously utilized [42]. Since Ho^{3+} doped fibres cannot be pumped efficiently with commercially available diodes, the Tm^{3+} ion serves as a facilitator for the Ho^{3+} ions, similar to the $\text{Yb}^{3+}/\text{Tm}^{3+}$ fibre. This might be of interest where wavelengths longer than $2 \mu\text{m}$ are required [5] for pumping non-linear crystals for longer ($3 - 5 \mu\text{m}$) infrared wavelength generation. Much work has gone into producing pulsed mid-infrared sources, that generate high pulse peak powers, short pulse durations at high repetition rates. One interesting application is the use of mid-infrared pulses in pumping non-linear media such as ZnGeP_2 (ZGP) crystals for longer wavelength generation [5], [6]. For such applications, pulse repetition rates of 50 - 100 kHz are required.

2.3.1 Pulsed Operation of Thulium-Doped Fibre Lasers

2.3.1.1 Q-switching

Q-switching is a technique frequently employed to generate laser pulses. The term ‘Q-switching’ refers the switching off the quality factor of a laser resonator, i.e. from a low loss to high loss and vice versa. This is achieved with some modulating element such as a chopper wheel or Acousto-Optic Modulator (AOM).

The technique works in the following manner. A laser medium is pumped with a pump source at a constant rate (Figure 2-8). With the Q-switch turned on the laser resonator becomes high-loss (low quality) instead of low-loss (high quality). During the on-time of the Q-switch, the gain medium of the laser is excited by the pump light and the upper laser level becomes populated, leading to an increasing population inversion. No lasing due to stimulated emission occurs during this time due to the resonator loss induced by the Q-switch. After a specific time, the Q-switch is turned off, leading to the high loss (low quality) laser resonator becoming low loss (high quality).

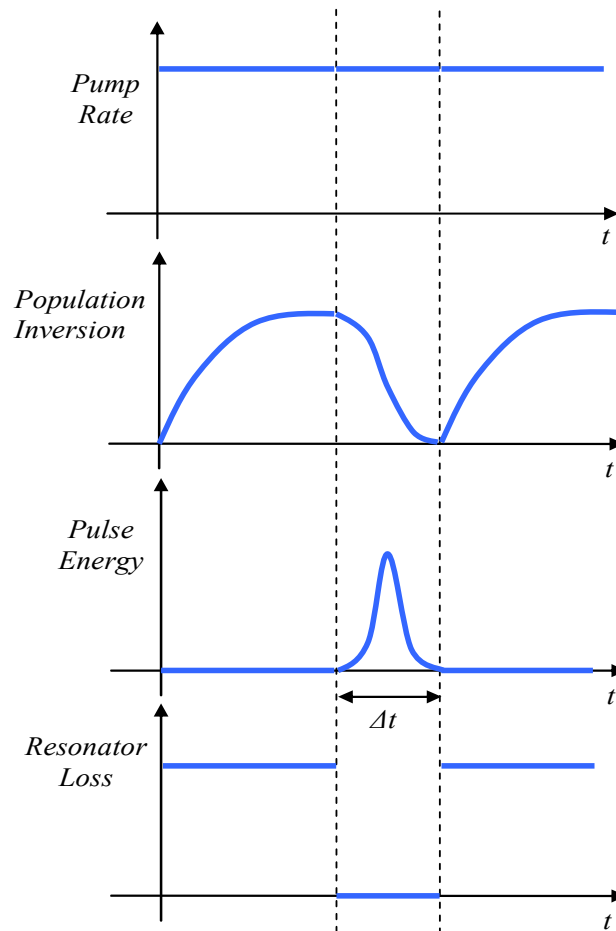


Figure 2-8: Graphical representation of laser behaviour during Q-switching.

Once the Q-switch is turned off and the induced loss is removed, the energy that was stored in the gain medium, during the on-time of the Q-switch, is rapidly released in the form of a laser pulse. The pulse rapidly depletes the population inversion within the gain medium. Once the pulse had been released the Q-switch turns on, the gain medium is excited by the pump light and the process repeats.

Q-switching with the aid of an acousto-optic modulator has been a favourable approach for operating Thulium doped fibre lasers in pulsed mode. The purpose of the

AOM as an intra-cavity element is to alter the ‘quality’ of the resonator, i.e. from a low loss to a high loss resonator. As discussed, this is referred to as Q-switching. It does this via the acousto-optic effect, which is the process whereby the refractive index within a material is varied, due to the presence of an acoustic wave. The acoustic wave is generated by the vibration of transducers surrounding the medium of the AOM. The variation in refractive index gives rise to a Bragg like structure within the medium of the AOM. The incoming light can be made to diffract completely out of the resonator by the variation of this Bragg structure within the medium (Figure 2-9).

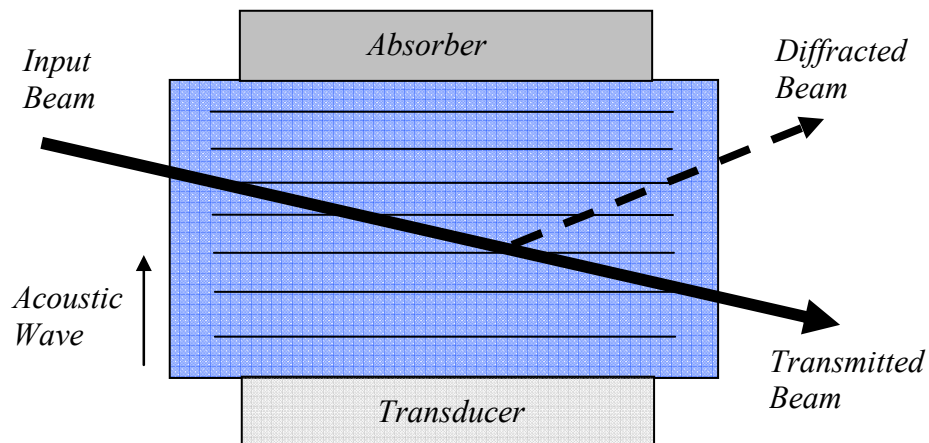


Figure 2-9: Representation of an AOM during operation or Q-switching.

Thus when the AOM is ‘turned on’ (radio-frequency (RF) power is applied to the AOM and an acoustic wave is generated in the medium), the light will diffract out of the resonator and the quality of the resonator is changed to a high loss one. This gives time where the pump may continue to excite the gain medium (Thulium ions), but no lasing occurs. When the AOM is ‘turned off’, (no RF power is applied) the light ceases to diffract out of the resonator and it becomes low loss (high quality or high Q factor) and the energy stored within the gain medium is released rapidly in the form of a pulse. There are a number of considerations when selecting the correct AOM. These are listed below:

- The medium or crystal of the AOM should have a high degree of transparency at the appropriate wavelength. In our case, the medium should be transparent for wavelengths around $2\mu\text{m}$.
- The medium should have high diffraction efficiency and a low insertion loss. In other words, with the AOM optimized with regard to angle, most of the

light leaving the resonator should be diffracted and not absorbed or reflected by the medium. Anti-reflection coatings on the medium itself may help facilitate this.

- With the high peak pulse powers encountered, the material and anti-reflection coating should have a high damage threshold with regard to power as well as a means to mitigate or minimize thermal effects.
- The switching time of the AOM would need to be chosen accordingly. The switching time of the AOM needs to be faster than the build up time of the pulse. If the switching time is too long, this may result in double pulses or instabilities.

2.3.1.2 Literature Review of Pulsed Thulium-Doped Fibre Lasers

The first actively Q-switched Thulium-doped fibre laser was demonstrated in 1993 [43]. The fibre was pumped at low power with a Ti:Sapphire laser at ~ 790 nm. The modulating element used for Q-switching was an acousto-optic modulator. The laser produced 4 watt, 130 ns pulses at a central wavelength of $1.92 \mu\text{m}$ and at repetition rates of 4 kHz. These results demonstrated the feasibility of a pulsed setup with an acousto-optic modulator as the Q-switching element. In 2003 a Thulium doped fibre laser pumped by a CW Nd:YAG laser ($\sim 1.319 \mu\text{m}$) was developed, generating a peak pulse power of 4.1 kW at pulse durations of 150 ns and repetition rates of 100 Hz [44]. S.D Jackson and M.Eichhorn developed a pulsed Thulium-doped fibre laser, with 30 W average output power, 41 ns pulse duration and $270 \mu\text{J}$ pulse energy with varying repetition rates in 2007 [52], utilizing an acousto-optic modulator to facilitate Q-switching. Pulsed Thulium doped fibre lasers have also been implemented using other techniques such as mode-locking [45], gain-switching [46] and passive Q-switching utilizing saturable absorbers [47].

Mode-locking is a method by which picosecond or femtosecond pulses are generated, with small pulse energies (~ 100 nJ). A fixed phase relationship is introduced between the cavity modes of the laser. This is achieved with some active or passive modulating element. The interference between these modes then gives rise to a train of stable pulses. Gain-switching can produce high-energy pulses with energies of 14.7 mJ being achieved [46], at the cost of longer pulse lengths. It is achieved by a fast modulation of the laser gain via the pump power. Some energy is suddenly stored in the laser gain medium via a fast pump pulse. Some delay is present before this energy

is extracted due to the build up of fluorescent light in the laser cavity. After a number of round trips of the fluorescent light, the energy is extracted and released in the form of a laser pulse. However, gain-switched systems showed a large amount of relaxation spiking, leading to low system reliability.

Other modulating elements for Q-switching have been used. These include Electro-optic modulators (EOM) as well as mechanical choppers. A comparison of Q-switching results generated via an EOM, AOM and mechanical chopper has been previously undertaken [48] and a summary of these results can be seen in Table 2-2.

Table 2-2: Table of results for Q switched Tm doped fibre laser, with varying modulating elements [48].

No	Q-switching technique	Pulse Duration	Peak power	Pulse energy	Pulse to pulse stability
1.	Chopper	300 ns	18.5 W	5.5 μ J	95 %
2.	AOM	150 ns	4.1 kW	0.6 mJ	99 %
3.	EOM	320 ns	3.3 kW	2.3 mJ	-

Recently, a Q-switched Thulium doped fibre laser was demonstrated by utilizing a photonic-crystal fibre [49]. In order to obtain larger output powers the core diameter, in step-index fibres, may be increased to allow more of the active ion to be incorporated into the fibre itself. This increase in core diameter will eventually result in multimode lasing. However, by employing photonic-crystal fibres a quasi-single mode beam may be generated while still increasing the core diameter, due to the inherent guiding properties of these photonic-crystal fibres. This work demonstrates the highest peak power recorded for Q-switched Thulium doped fibre lasers to date, with results of ~ 8.9 kW peak power, 49 ns pulse duration at a repetition rate of 10 kHz, however the average output powers were under 10 W and the fibre utilized did not have a step-index profile.

With regard to actively Q-switched fibre lasers, high output powers are required for applications such as non-linear media pumping. However, in general, an increase in repetition rate yields longer pulse durations but lower peak pulse powers. Due to the drop in high peak powers with increased repetition rates, Q-switched fibre lasers were seen at the time as an unattractive option for non-linear pumping. Research was undertaken into fibre amplifiers as an alternative which generated very favourable

results. The most recent results generated by such a system is 28 kW pulse peak power, 600 μ J with pulse durations \sim 20 ns [50]. However these systems were complex in design and required high amounts of control due to the build up of amplified stimulated emission (ASE). Owing to the complexity of such systems, much research has been undertaken into Q-switched fibre lasers utilizing a single oscillator. A thorough investigation of Q-switching theory yielded the conclusion that to avoid the detrimental build up of ASE and to obtain high pulse energies at short pulse durations, one would merely need to pump the fibre laser many times above its threshold value [51], [52]. In this thesis, attention will be drawn to Q-switched, single oscillator laser setups.

2.4 Review of General Fibre Laser Designs in Literature

In this section various design architectures utilized within the literature will be reviewed. Naturally some of these can be quite complex in design (such as fibre laser systems employing amplifiers and more than one oscillator). Therefore attention will be given to only single oscillator systems, i.e. a single fibre laser.

In its simplest form a fibre laser consists of a pump source, the active gain medium which is the fibre itself and a resonator (Figure 2-10) [14].

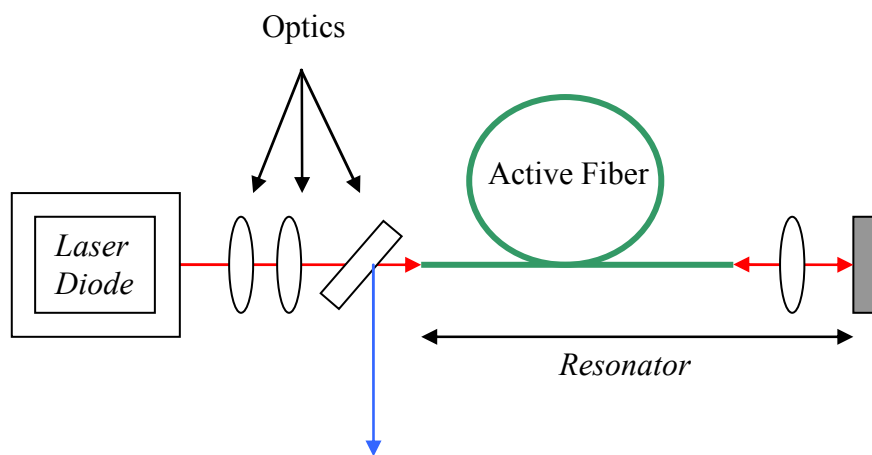


Figure 2-10: A simple fibre laser configuration

The pumping scheme in this case is optical, hence the pump source usually utilized is an AlGaAs diode laser [8]. Typical pumping powers for high-power applications are within the range of 5 – 300 W and pumping may be done with multiple diodes [39]. As was discussed in Section 2, Thulium has high absorption in the range \sim 790 - 800nm, which is the wavelength of many commercially available diodes.

Other pumping schemes have been used involving other fibre lasers (erbium), but these systems are more complicated in design [53]. The fibre may be dual pumped on both sides of the fibre to couple in more pump light [54]. Fibre-coupled diodes in the wavelength range of ~ 793 nm are readily available and are currently being scaled to higher powers. It is for this reason, and the strong absorption of Thulium at this wavelength, that these diodes are commonly employed as the pump source for Thulium-doped fibre lasers.

2.4.1 Resonator Designs

Feedback of the laser resonator is provided by a highly reflecting element, such as a mirror. Commercial, flat, broad band anti-reflection coated mirrors have typical reflectivity percentages of around ~ 99.9 % for $2 \mu\text{m}$ light and have a high thermal damage threshold. However, the use of a broadband mirror does not afford any spectral control into the thulium-doped fibre laser. Therefore spectral output of Tm^{3+} doped fibre lasers utilizing such a mirror is broad ($\sim 20 - 30$ nm) [40] and exhibits a large amount of temporal fluctuations [35]. Also, the use of free space optics increases the risk of misalignment due to mechanical disturbance.

In order to overcome these issues, alternative configurations may be considered (Figure 2-11). Certain applications require a very narrow wavelength output. Fibre Bragg gratings (FBG) written into the fibre core have been used successfully to achieve this [55,56]. A recent paper demonstrates the feasibility of an all-fibre laser utilizing FBGs [57]. With an output power of 137 W, this is the highest output power to date from a narrow-bandwidth, Thulium doped all-fibre laser.

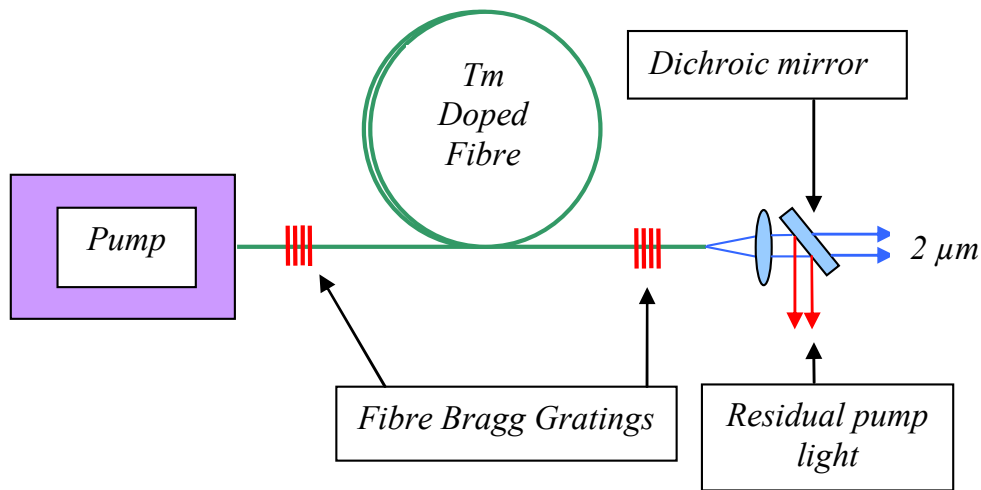


Figure 2-11: An all-fibre laser.

Such all-fibre laser configurations currently offer the best commercial solution [58]. High-coupling efficiencies ($\sim 95\%$) as well as the absence of misalignment issues offer a potentially compact and robust source of laser light. However, there is less flexibility with such designs in comparison with a fibre laser utilizing free-space optics.

Alternatively, Volume Bragg Gratings (VBG) have recently been utilized and offer an attractive alternative to gold mirrors and FBGs, offering the option of tunability and narrow wavelength output with little to no difference in overall efficiency [59,60]. However, the use of a VBG may require additional cooling for high power lasers [60].

A VBG is a bulk, transparent element that has a periodic variation of refractive index within its structure. This allows a large reflectivity to be obtained at a particular wavelength, provided the so-called Bragg condition is met. This condition is given as:

$$\frac{2\pi}{\Lambda} = 2 \frac{2\pi n}{\lambda} \cos \theta. \quad (2.6)$$

Where Λ is the period of the grating, n is the refractive index of the material, λ is the reflected wavelength and θ is the angle between the normal of the grating and the axis of the optical cavity. VBGs afford the option of a narrow and stable wavelength output, instead of the broad emission spectrum associated with Thulium doped fibre lasers.

2.5 *Conclusion*

Thulium-doped fibre lasers are robust and efficient sources of mid-infrared light. As was shown and discussed in Sections 2.3 and 2.4, much work has been undertaken in developing and improving these laser sources. This has led to the highest CW output of ~ 1 kW [8] from a single Thulium-doped fibre laser as well as the highest peak pulse powers of ~ 9 kW [49]. Further development and characterization of these devices continue in order to scale beyond these powers. As was discussed in Section 2, the three-level nature of the Thulium ion causes the laser performance and output values to be dependant on external factors such as fibre temperature. The following chapter investigates the dependence of the output power and wavelength on fibre temperature, for a CW Thulium-doped fibre laser.

3 Wavelength Characterization of a Thulium Doped Fibre Laser

This section details the author's evaluation of an existing Thulium doped silica based fibre laser. The fibre laser was re-built and its spectral output was characterized for different temperatures of the active fibre. As discussed in Chapter 2, a Thulium fibre laser has a quasi-three level lasing scheme, and as such the temperature plays an important role on the output of the laser. The aim was to investigate this behaviour and to fully characterize the fibre laser. Previous experiments conducted on this fibre laser [62], indicated a change in the central wavelength output for varying fibre temperatures. To achieve the aim of the experiments, the wavelength output was measured for different fibre temperatures.

3.1 Design Considerations & Experimental Setup

First, the experimental setup (Figure 3-1) will be discussed in brief as well as how the laser setup functions. Following this, a more detailed description of each component within the layout will be given.

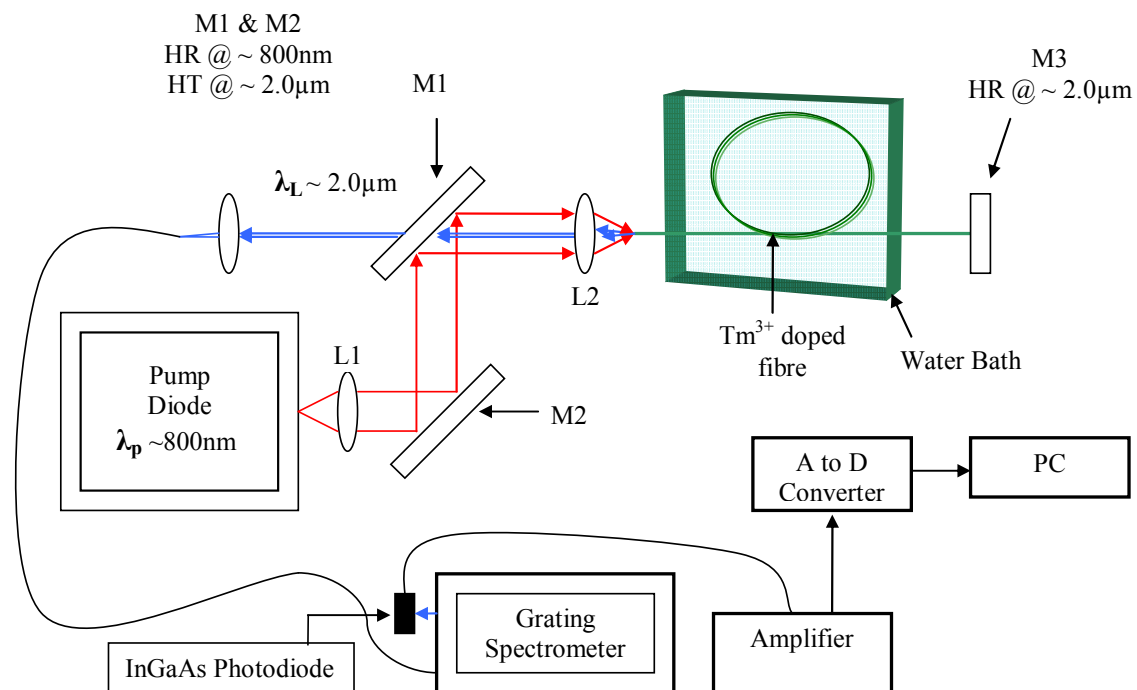


Figure 3-1: Schematic of the Tm: fibre laser setup.

The light out of the fibre coupled pump diode is first collimated via a spherical lens (L1) and is transmitted towards the first dichroic mirror (M2). M2 is orientated at an angle of 45° with respect to the propagation axis of the incoming collimated light. The light is then reflected towards another dichroic mirror (M1) which is also orientated at 45° to reflect the pump light towards the second spherical lens (L2). L2 was used to couple the pump light into the active fibre. The fibre end was placed in cylindrical copper tubes to allow for mild heat dissipation and fibre end stability. This in turn was mounted in a holder and onto a 3-dimensional translation stage (allowing for fine adjustment in the X-Y-Z axes). The fibre itself was coiled and placed within a water bath. The other end of the fibre was placed within another cylindrical copper tube and on its own 3-dimensional translation stage. A highly reflecting mirror (M3) was placed against the perpendicularly cleaved fibre end. The resonator for this fibre laser consisted of the reflective mirror M3 and the opposite perpendicularly cleaved fibre end, which provided sufficient feedback for laser operation.

The laser output leaves the fibre laser (e.g. the first fibre end acting as laser resonator output coupler) and passes through the second dichroic mirror (M1). This light was coupled into a standard transmission fibre with another focussing transmission lens. This fibre end was placed at the entrance slit of the monochromator. The light propagates through the monochromator, out of the exit slit and onto a $2\ \mu\text{m}$ photodiode. The photodiode is connected to a signal amplifier via a coaxial cable, which amplifies the signal obtained by a factor of ~ 10 . The signal is turned from an analogue to digital format via an analogue to digital (A to D) converter. This signal is then finally recorded onto a desktop computer and analyzed. The following sub-sections describe the operation of each sub-component in the setup.

3.1.1 Pump Source

In order to pump the active fibre, a fibre-coupled laser diode from Jenoptik AG (Figure 3-2) was utilized as the pump source [61]. Due to the laser diode being fibre-coupled, the diode laser beam was circularly symmetric. This simplified the pump-optic design to spherical optics for input coupling into the active fibre.

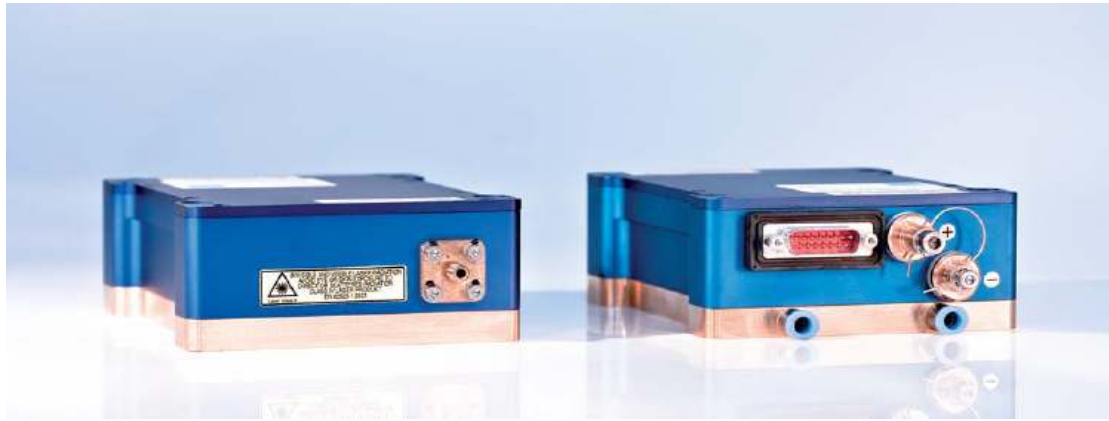


Figure 3-2: Fibre coupled laser diodes - Jenoptik (JOLD-75-CPXF-2P W).

The diode has a specified maximum output power of 75 W and a specified central wavelength of 808 nm. The wavelength variation is typically ± 3 nm at 25 °C. The diode fibre had a core diameter of 400 μm and a numerical aperture of 0.22. The laser was connected to a commercial diode laser controller. The diode laser was also water-cooled and had a flow rate of approximately 3 l/min. The laser diode also had a built in low power pilot laser (~ 650 nm), which was utilized for alignment purposes.

The diode laser was characterized with regard to its output power and the diode controller current (Figure 3-3). The threshold current for the diode laser was measured to be ~ 7 A with an operating voltage of 3V.

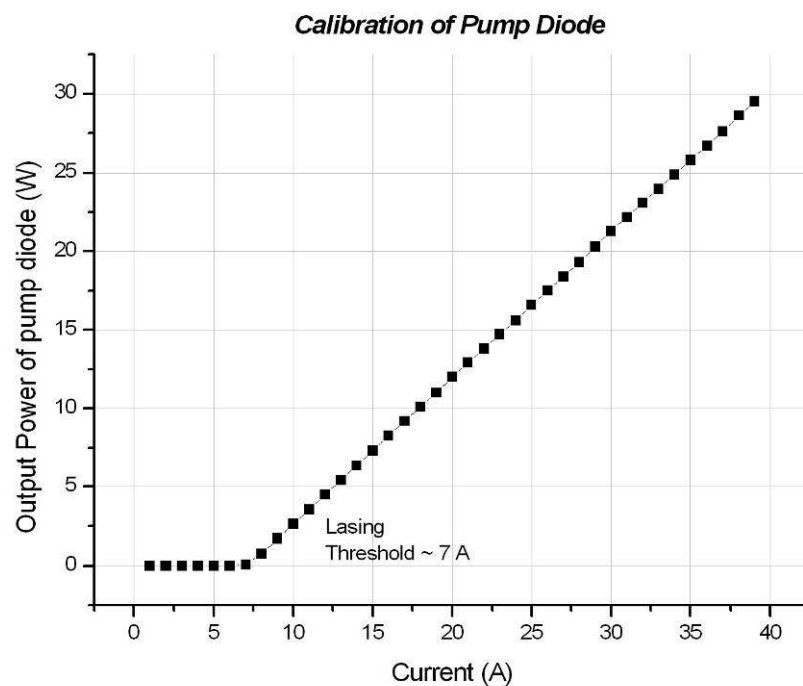


Figure 3-3: Laser diode output power (W) as a function of diode current (A).

Above laser threshold, a linear relationship between the output power of the pump diode and the input current was established. The electrical to optical efficiency of this laser diode was established to be $\sim 31\%$ (Figure 3-3). Further characterization of the wavelength of the diode was done previously [62]. The author reported a central wavelength of $\sim 801\text{ nm}$ for low temperatures ($18\text{ }^\circ\text{C}$) and $\sim 808\text{ nm}$ at higher temperatures ($25\text{ }^\circ\text{C}$), in agreement with the specification sheet for the diode laser.

3.1.2 Lenses & Mirrors

In order to effectively collimate and couple the pump light into the active fibre, the correct choice of lenses had to be made. The first lens (L1) and the second lens (L2) were both chosen to be spherical lenses, made of fused silica. L1 had a focal length of 25.4 mm and diameter $\phi = 25.4\text{ mm}$. L2 had a focal length of 12 mm and diameter $\phi = 12.7\text{ mm}$. Unfortunately, only L2 was anti-reflection (AR) coated for the pump wavelength. The lack of an AR coating on L1 introduced a loss of pump light within the laser setup, contributing a $\sim 8\%$ loss of pump light due to Fresnel reflections.

The first two mirrors employed (M1 & M2) were dichroic mirrors. Their function within the setup is to reflect the pump light towards the fibre as well as serve as a means of separating the pump light at $\sim 805\text{ nm}$ from the laser light at $2\text{ }\mu\text{m}$. Thus in order to achieve this end, they are highly transmissive ($\sim 98\%$) for wavelengths around $2\text{ }\mu\text{m}$ and highly reflective ($96\% - 98\%$) for wavelengths in the range of $795\text{ nm} - 805\text{ nm}$. The separation of the pump and laser light affords the option of investigating the laser light individually. These mirrors were previously characterized [62] and exhibited a loss of around $2 - 4\%$ at the pump wavelength.

Mirror three (M3) is a flat, protective gold coated, reflecting mirror with a diameter of 25.4 mm (1 inch). Gold mirrors have a reflectivity of $96\% - 99\%$ for wavelengths within the mid and far infrared. Its function was to provide feedback for the laser and directed the laser light back into the fibre. The mirror was placed directly against the fibre end.

3.1.3 The Thulium-Doped Fibre

The active fibre was provided by the company CorActive[®] [63]. The fibre is a step-index, double-clad fibre and is surrounded by a polymer coating (also called a buffer.) The specifications of the fibre are given in Table 3-1.

Table 3-1: Parameter values for the CorActive Thulium-doped fibre.

<i>Parameter</i>	<i>Core</i>	<i>Pump Cladding</i>	<i>Outer Cladding</i>
Diameter	18.1 μm	403 μm	548 μm
Numerical Aperture (NA)	0.11	0.23	-
Absorption coefficient	5.5 dB/m @ $\sim 790 \text{ nm}$.	-	-

A cross sectional representation of the fibre is given in Figure 3-4.

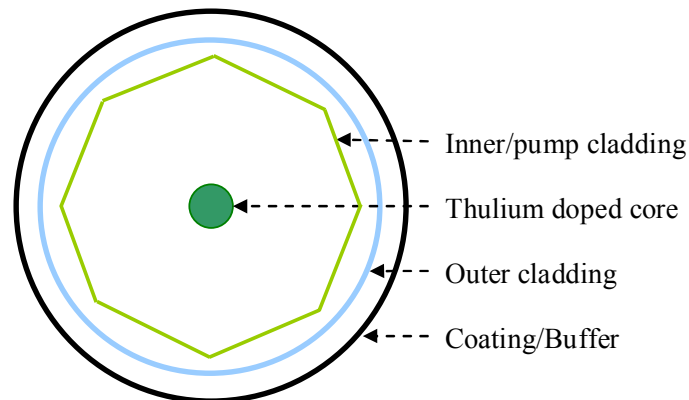


Figure 3-4: Cross sectional representation of the fibre (not to scale) [62].

The fibre core had a specified Thulium doping concentration of 5 wt %. As was discussed in Chapter 2.2, a high concentration is desirable for high pump conversion efficiency and to facilitate the cross-relaxation process between thulium ions. The high doping concentration also allows for shorter fibre lengths, which is favourable for pulsed operation of the fibre laser. The absorption in the fibre core at $\sim 790 \text{ nm}$ is specified to be 5.5 dB/m. The fibre core has a specified diameter of $\sim 18 \mu\text{m}$ and NA of 0.11. As was discussed in section 2.3, to obtain single mode operation, the so called “V-parameter” for a fibre needs to have a value less than or equal to 2.405. Applying Equation (2.4) and making use of the specified parameters for this fibre, the

V-parameter is calculated to be ~ 3.13 (for $\lambda = 2.0 \mu\text{m}$). Thus one would expect the laser output beam to be slightly multimode. However, this can be prevented by sufficient coiling of the active fibre (discussed further in Section 4.1.1.3).

The inner or pump cladding diameter is specified to be $400 \mu\text{m}$ allowing pump light to be coupled into the fibre. The cladding is shaped in a non-circular geometry (octagonal). This prevents the pump light from following a spiral path around the core and not being absorbed, resulting in a higher overall laser efficiency.

The total fibre length was 8 metres, with 2 metres un-doped/passive fibre spliced onto both ends of the 4 metre active fibre. This allowed cleaving the fibre ends without any loss of active fibre and also raised the damage threshold of the fibre ends. The fibre ends were perpendicularly cleaved on both ends using a standard fibre cleaver and polished, in the sequence of $5 \mu\text{m}$, $3 \mu\text{m}$, $1 \mu\text{m}$ and $0.1 \mu\text{m}$, with fibre polishing pads.

The fibre ends were also held in place with copper rods to introduce mechanical stability, with the auxiliary function of mild thermal management. The fibre was coiled to have a radius of $\sim 9 \text{ cm}$, which was convenient for placing the active fibre into a water bath for cooling. This was also considered to be large enough to avoid guiding losses within the fibre. If the fibre is coiled too tightly it is at risk of breaking due to mechanical stress and also will incur losses of laser and pump light due to the refraction angles being too acute to confine the light via internal refraction (macro-bending losses).

As was discussed in Chapter 2.2, the lasing transition of interest here (${}^3F_4 \rightarrow {}^3H_6$) follows a quasi-three level scheme and as such, thermal effects play a significant role in influencing the output of the laser. In order to get a better indication of this influence, and more specifically on its spectral output, a means to control the temperature of the water bath was employed. This was done by incorporating large amounts of crushed ice into the water bath of the fibre. The presence of the crushed ice lowered the overall temperature of the water bath and this temperature was measured to be $0 \text{ }^\circ\text{C}$. This is the temperature at which the phase transition occurs for ice, i.e. from a solid to a liquid. The temperature of the bath was monitored and measured with a standard mercury thermometer as well as a thermocouple.

The ice was placed into the water already present within the bath. The ice was placed in such a way as to ensure a homogenous distribution within the bath container. Also the water bath was isolated thermally from the breadboard via an insulating layer underneath the container. Further the coiled fibre was suspended onto a thermally conductive metal plate. In this way, the contact between the fibre and the ice water was maximized, while the contact between the fibre and other surface interfaces was minimized.

3.1.4 The Grating Spectrometer & Calibration

To measure the spectrum of the laser output a monochromator was utilized. The monochromator is from the company Jarrel-Ash and is a 0.5 meter Ebert scanning spectrometer with model number 82-001. The schematic of the monochromator is shown below (Figure 3-5).

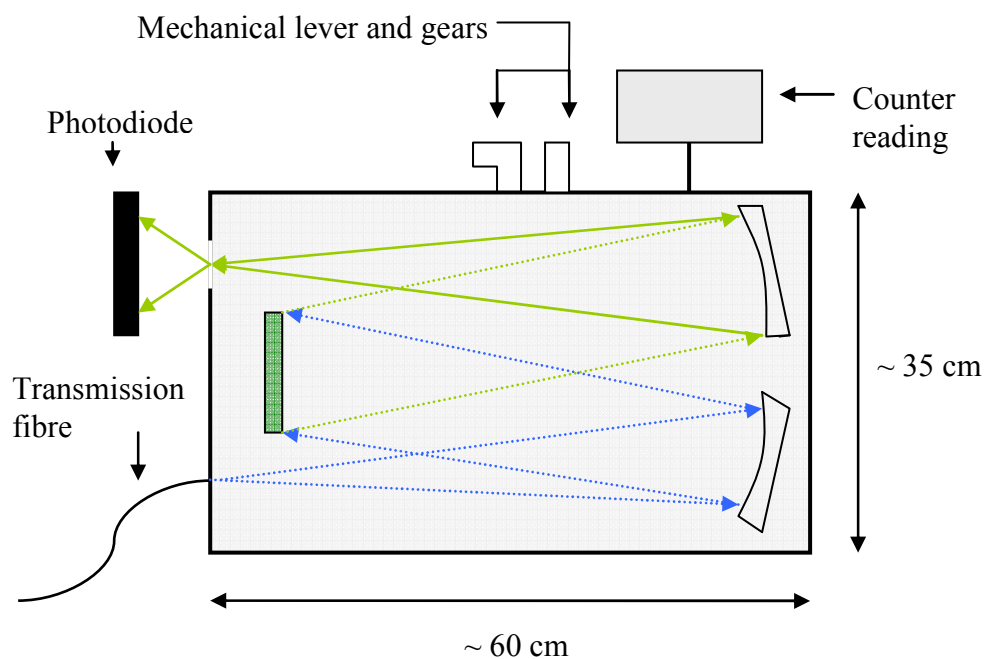


Figure 3-5: The monochromator, indicating the optical layout and auxiliary components.

The monochromator had an approximate length and width of 60 cm and 35 cm respectively. The entrance slit was removed and in its place a transmission fibre was mounted. Hence the core of the fibre would act as the entrance slit itself, removing the need for any alignment optics to couple the light into the monochromator. Additionally, since the fibre core was acting as the entrance slit for the

monochromator, the core diameter will ultimately affect the resolution of the monochromator.

The mirrors within the monochromator were concave and each had a radius of curvature of 150 mm. The mirrors served to first collimate the incoming light onto the grating, collecting the diffracted light and then focussing this light onto the exit slit and out the monochromator. The resolution of a diffraction grating spectrometer is directly proportional to the number of grooves *illuminated* by the incoming light. Optimal illumination of the monochromator mirrors ensured that the light would cover the entire grating. This is one way to ensure that the highest possible resolution is obtained from the monochromator. The exit slit was chosen to have a slit-width of 0.22 mm.

The photo-diode was an InGaAs photo-detector. The photo-diode has a wavelength range of approximately 1.8 μm to 2.1 μm , ideally suited for this specific fibre laser.

The monochromator is able to scan manually (middle gear) by rotation of the grating handle or automatically at different speeds by adjusting the gear settings accordingly. The following gear settings were available with their respective scanning speeds ($\text{\AA}/\text{min}$) (Table 3-2) [information taken from instrument].

Table 3-2: Spectrometer drive speeds ($\text{\AA}/\text{min}$).

Hi-Low Gear	In	2	3	Out
High	500	250	125	50
Middle	-	-	-	-
Low	20	10	5	2

The monochromator was calibrated using two different laser sources. The first was a standard He-Ne laser at 632.8 nm and the second a frequency doubled Nd:YVO₄ at 532 nm. In order to analyze the 1st order of the laser light at 2 μm , the grating was angled in such a way as to allow the 4th orders of the two light sources to be observed. In other words, if the 4th order of the He-Ne laser beam was observed, this would correspond to observing a wavelength of $632.8\text{nm} \times 4 = 2531.2\text{nm}$. Measured data for the calibration of the spectrometer is given below in Figure 3-6.

Calibration of Spectrometer with HeNe (~ 632.8nm) & freq. doubled Nd: YVO4 (~ 532nm)

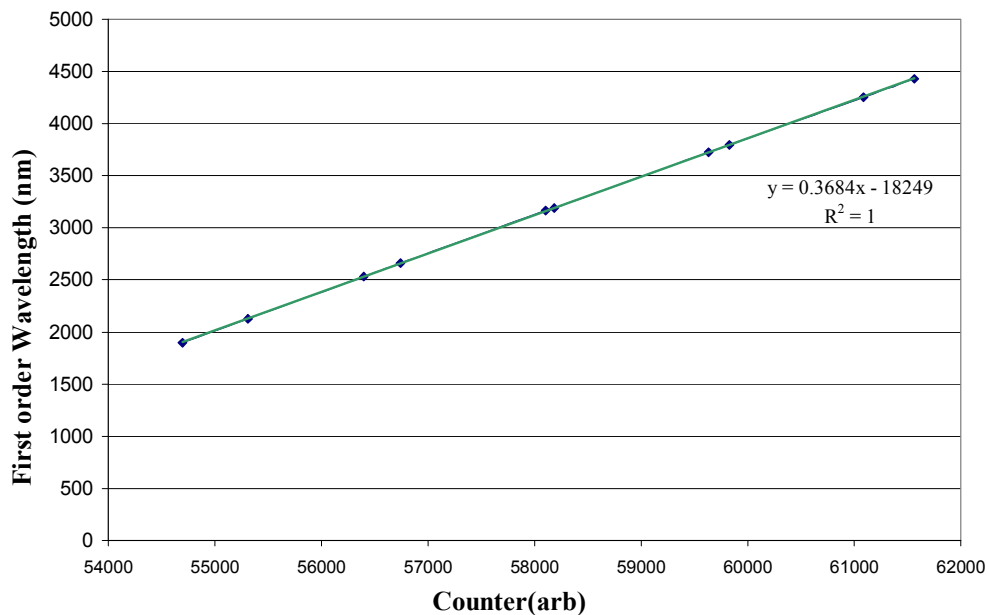


Figure 3-6: Calibration measurement of the Jarrel-Ash monochromator with two well known laser sources.

Using the measured data a linear fit was made of the form: $\lambda = mx + C$. The fitted line can be used to determine the unknown wavelengths of the Thulium fibre laser, in the expected wavelength range of 1.8 μm to 2.1 μm .

3.2 Experimental Results

3.2.1 Output Power Dependence on Temperature

The first measurement of the fibre laser was to determine the slope efficiency of the laser by plotting the output power as a function of the input pump power. This is done for a range of data points such that the slope or gradient of the graph can be determined. This is known as the slope efficiency and the graph for the CW laser configuration is given below (Figure 3-7).

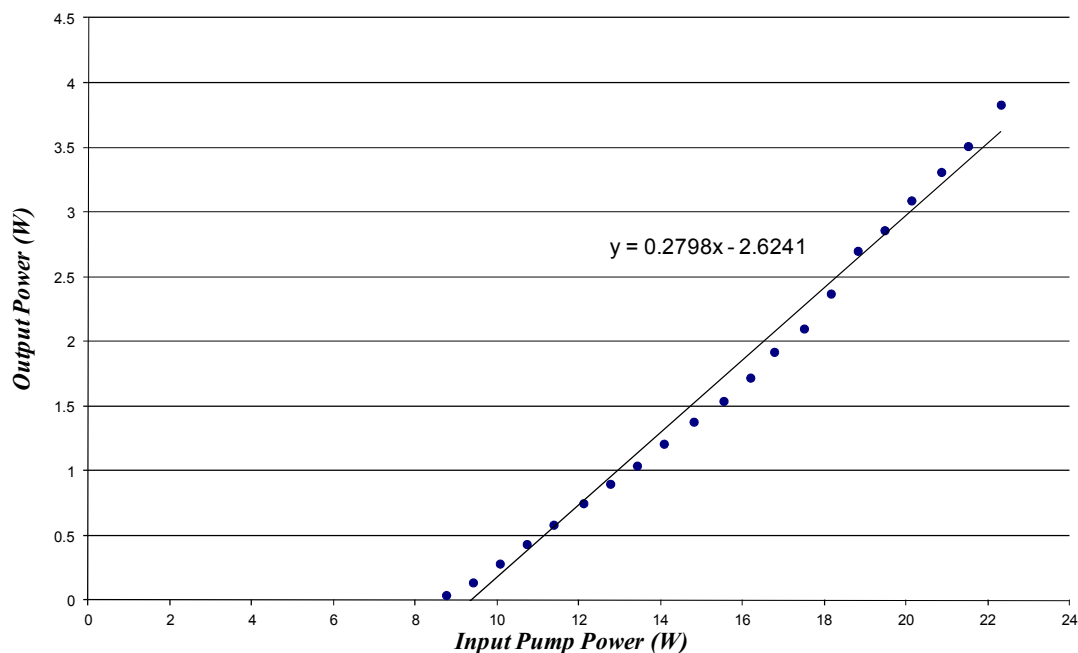


Figure 3-7: Slope efficiency plot for the Thulium doped fibre laser (room temperature).

A linear trend-line was fitted to the measured data points, above the threshold value. The gradient of this trend line is equivalent to the slope efficiency, which was measured to be 28 %. The threshold of lasing for the fibre laser was found to be at approximately 20 A of diode current or 12.0 W of initial pump power (using the calibration curve of Figure 3-7. Accounting for losses induced through the pump optics, the pump power incident to the active fibre end at threshold was calculated to be 8.7 W. The above data was measured when the water bath was stabilized at room temperature ($\sim 20^{\circ}\text{C}$).

When the water bath was cooled with crushed ice the temperature of the water bath was measured to be approximately 0°C . The threshold of the laser was lowered substantially for this water bath temperature and was found to be at approximately

6 W of input pump power, with an improved slope efficiency of 40 %. A discussion pertaining to the difference in these threshold values and other results is covered in the following section.

3.2.2 *Output Spectra and Wavelength Dependence on Temperature*

With the monochromator set up and calibrated, it was now possible to investigate the spectral output of the fibre laser. As was discussed in Chapter 2.2, Thulium is known to have a very broad emission bandwidth typically between 1.9 μm and 2.1 μm , therefore, an initial measurement over this wavelength range was undertaken to obtain an indication of where the central wavelength output of the fibre laser was situated. From the monochromator calibration curve (Figure 3-6), it is deduced that this amounts to scanning between the counter readings of 54693 to 55236.

The monochromator was scanned manually through the specified range and the signal at the exit slit was measured with an InGaAs photo-detector and oscilloscope. The measured value was averaged over 1024 measurements via the oscilloscope. The background noise was measured to be 45 μV . The resultant spectrum is given below in Figure 3-8. It should be noted that this result was taken when the water bath had stabilized at room temperature ($\sim 20^\circ\text{C}$) and with a constant pump power of 21.9 W (26 A) and constant laser output power of ~ 3 W.

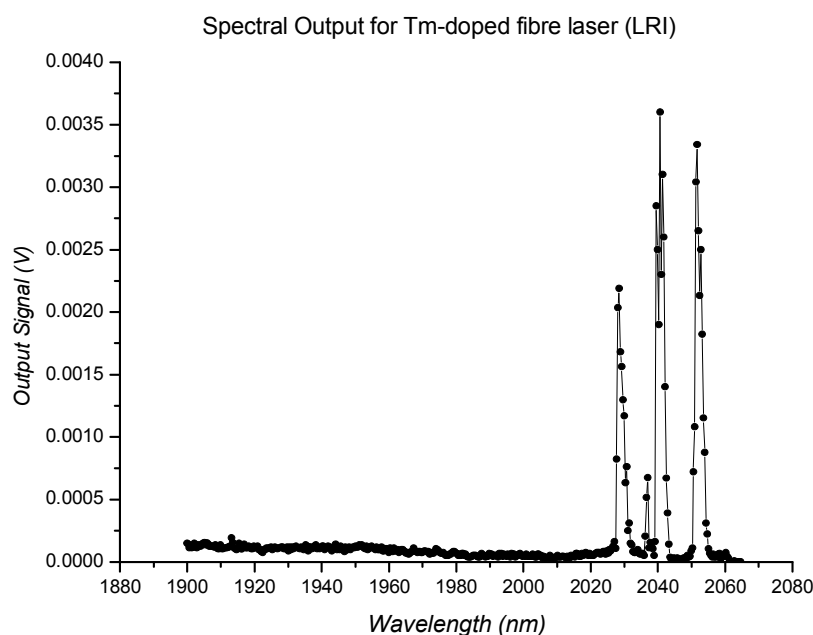


Figure 3-8: Initial spectrum for the Thulium doped fibre laser.

It was found that the central emission of the fibre laser was in the range of 2025 nm - 2065 nm with a broad bandwidth of 40 nm. This was consistent with what was expected.

In order to establish consistency with regard to this wavelength output, further measurements were undertaken (Figure 3-9 & Figure 3-10), while maintaining the bath at room temperature and constant pump power. In this case the automatic capability of the spectrometer was employed. The scan drive was set to the 2nd speed slot, while also shifting the gear of the spectrometer to its “low” position. Comparison with Table 3-2 indicates that this corresponds to a scan speed of 10 Å/min or 1 nm/min. The monochromator was allowed to scan over the range of 2025 – 2065 nm with these speed settings. The time taken over this range was measured to be roughly 10.32 minutes (632 seconds).

It was determined by means of comparison that 5000 data samples would be sufficient to obtain a good indication of the structure of the spectrum. Therefore the Analog to Digital converter was set to record a sample every 0.0632 seconds. There was a five second delay between the onset of the scanning and recording of data. This corresponds to a wavelength delay of 1.582 nm. This delay was incorporated and the appropriate correction was implemented into all of the following data sets.

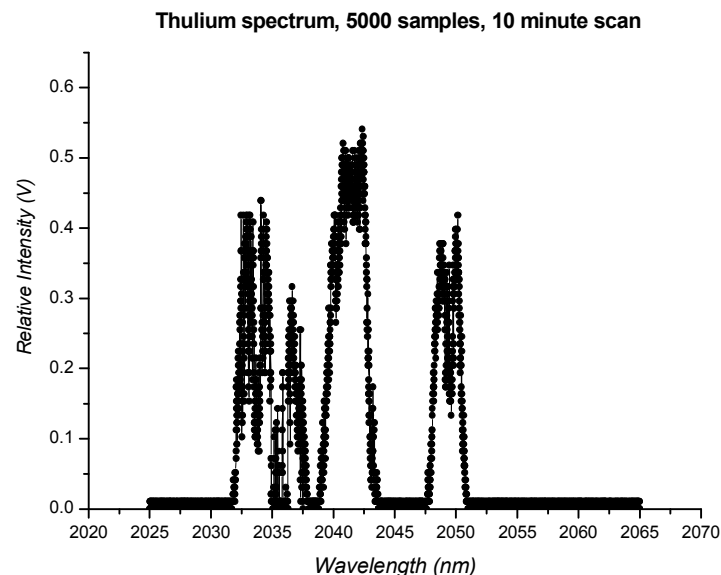


Figure 3-9: Measured Tm-fibre laser spectrum at constant temperature of 25°C and pump power of 21.9 W.

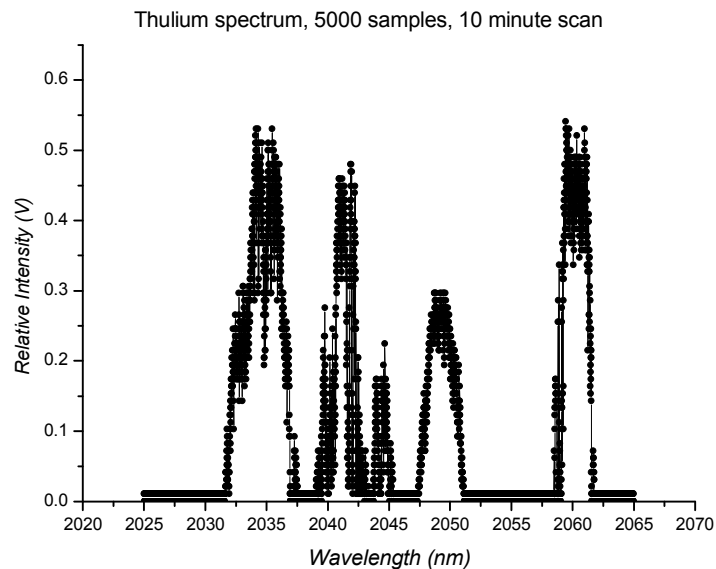


Figure 3-10: Measured Tm-fibre laser spectrum at constant temperature of 25°C and pump power of 21.9 W, second scan.

A 10 minute interval was chosen between each scan, thereby taking spectra from two different times. The spectrum given by Figure 3-10 shows a marked difference with respect to the location of the centre peaks. The temperature change was also monitored for each scan and a temperature shift of 0.5 °C was recorded. This temperature change is too small to effect the large variation apparent. As stated, the measured spectra were taken over a long time period (10 minutes) and incorporates the measured output spectrum which could have varied significantly over time. Temporal fluctuations of the central wavelengths would therefore be included in the measurement.

Another wavelength measurement was taken with the water bath temperature set to 0° C (Figure 3-11), while maintaining a constant pump power.

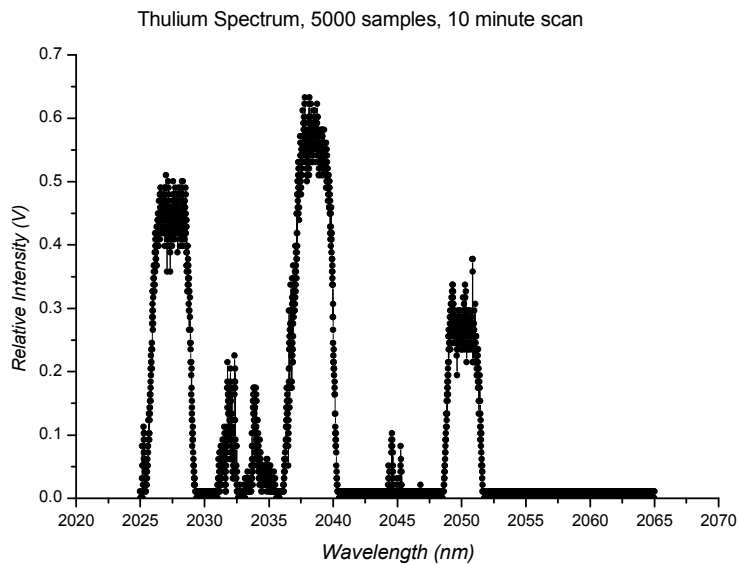


Figure 3-11: Output spectrum of the Thulium laser, with a cooled (0°C) water bath and constant pump power of 21.9 W.

A shift towards shorter output wavelengths was observed for lower water bath/fibre temperatures. The wavelength peaks were at 2027 nm, 2036 nm and 2050 nm. The centre peak at 2036 nm had a width of approximately 6 nm. To obtain a better indication of this shift a comparison was made between wavelength measurements taken for un-cooled and cooled water bath temperatures (Figure 3-12).

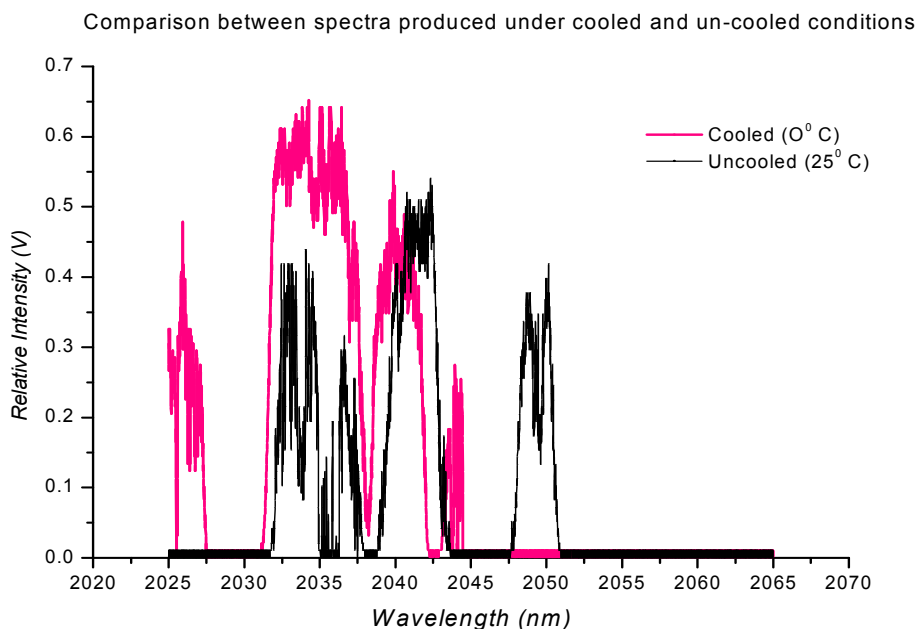


Figure 3-12: Cooled and un-cooled spectra of the LRI laser, at a constant pump power of 21.9 W.

3.3 Discussion

The results obtained in Section 3.2.2, are in good agreement with those found in the literature. As has already been discussed in Section 2.2, the three-level nature of the Thulium-ion, makes its behaviour susceptible to temperature. This is due to the fact that the lasing ground level 3H_6 is populated at room temperature. A temperature change will cause a re-distribution of the population in the ground level. Additionally, the laser losses attributed to re-absorption will differ for different fibre temperatures. As was shown by the McCumber relation (Equation 2.5), the emission and absorption cross sections of the lasing levels are also temperature dependent. Since all these factors are dependent on the fibre temperature, they will therefore play a role in determining the final wavelength output. It has also been suggested that the change in temperature may also influence the rate of non-radiative decay as well as energy transfer effects such as upconversion and cross-relaxation [64].

3.4 Recommendations

To conclude this chapter, listed below are a few points that may improve the existing laser setup as well as suggestions for further work.

- The use of the appropriate anti-reflection coated optics within the laser setup would decrease the overall losses of pump light substantially.
- A Volume Bragg grating may be implemented as a feedback element, for better wavelength control.
- Improved lab atmosphere control. A means of humidity control needs to be implemented in the lab, as atmospheric absorption is an important factor to consider, especially around the wavelengths of our output. This was one of the reasons for the temporal spiking of the observed laser output. For high powers this spiking may cause damage to optics within the setup. Also, a way to remove and keep dust out of the lab would be recommended, as this may have a detrimental affect on the optics and fibre.
- The transmission fibre used to transfer the 2 μm light to the spectrometer should be changed with a fibre better suited for infrared light. A fibre not suited for mid-infrared wavelengths will cause the original beam to be reduced in intensity and may distort the spectral profile. This will lead one to believe

that one is observing a strong/weak transition at a particular wavelength which may not be the case.

- A better cooling option may be employed (a circular, water-cooled mandrel for example).
- Implementing a Q-switch for pulsed operation.
- A cutback experiment could be undertaken to find the optimal fibre length for continuous-wave and pulsed operation. The spectral output, average powers, slope efficiencies, peak pulse power, etc. may all be determined for different fibre lengths.

4 Design & Development of a CW & Q-switched Thulium-Doped Fibre Laser

In this section the design and development of a Q-switched Thulium doped fibre laser is discussed. The previous fibre laser setup and results (Chapter 3), was studied and considered in the design of the following laser. Varying designs and configurations were considered. The components within the fibre laser, such as pump source, optics and active fibre are thoroughly discussed. The fibre laser output is characterized in CW mode for different design architectures. The laser output is also utilized to measure the wavelength and the temporal behaviour of this output is monitored. Following this, the fibre laser is made to operate in pulsed mode with the aid of an acousto-optic modulator as Q-switch. The initial design (Figure 4-1, Figure 4-2) was chosen to be similar to the design given in Figure 2-10 as this required the least amount of time to implement and was possible to develop with available optics. New fibre-coupled laser diodes were procured for pumping as well as new active fibre. It is this setup which we will elaborate on in the following sections.

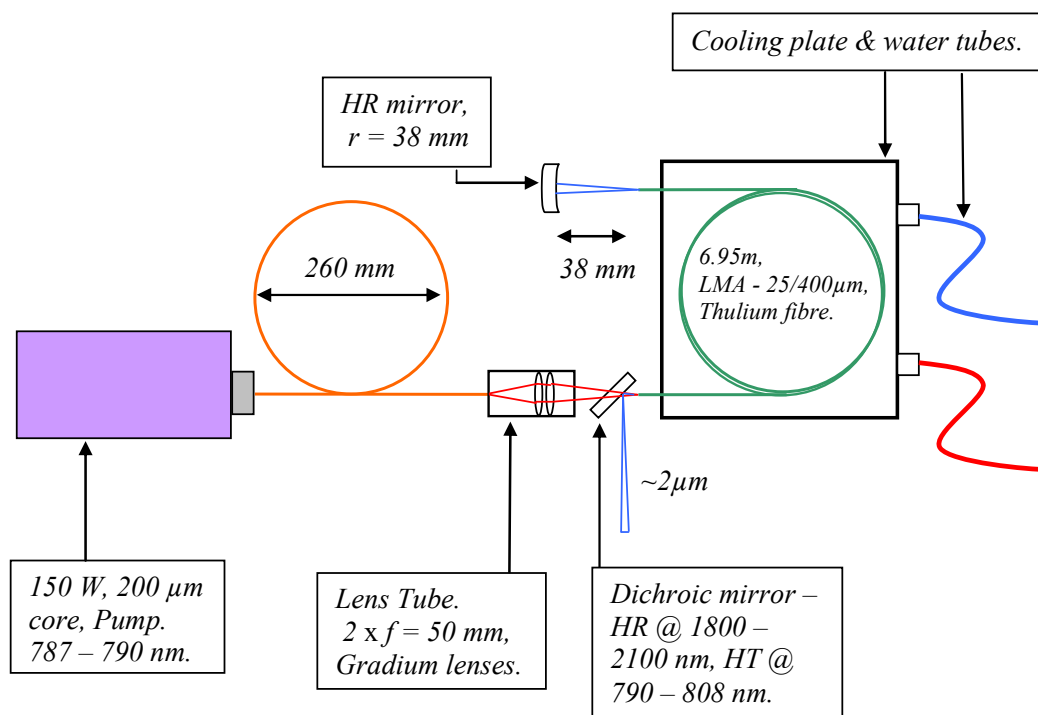


Figure 4-1: Schematic of the Thulium doped fibre laser setup.

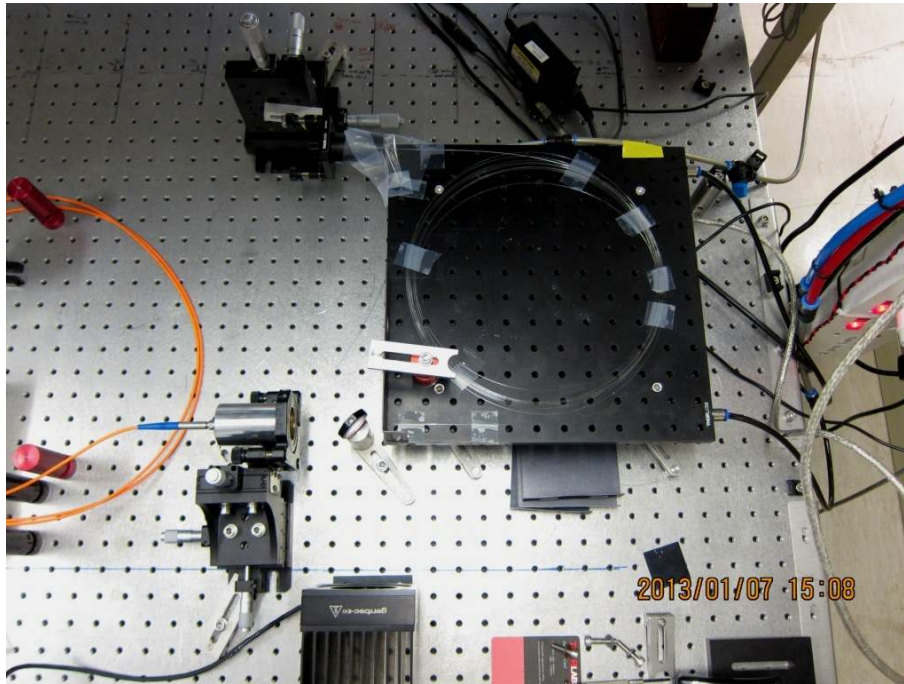


Figure 4-2: Top-view photo of the CW laser setup.

4.1 Design Considerations & Experimental Setup

4.1.1 The Active Fibre

The Thulium doped fibre was procured from Nufern. Nufern offers a range of products related to optical fibres (rare-earth doped and un-doped) and fibre lasers [65]. Two active fibres were selected and procured. These fibres are known as Large Mode Area (LMA) fibres and the specifications for each fibre are given below in Table 4-1.

Table 4-1: Parameter data for the doped Nufern fibres.

	LMA-TDF-25P/400	LMA-TDF-25P/250
Core N.A.	0.09	0.09
Cladding N.A.	0.46	0.46
Core Diameter	25 μm	25 μm
Pump Cladding Diameter	400 μm	250 μm
Buffer Diameter	550 μm	395 μm
Length	7 m	3 m
Cladding absorption	1.80 dB/m @ 793 nm	9.50 dB/m @ 793 nm

The initial experiments performed utilized the 25/400 μm fibre. As such the design considerations which follow, particularly with regard to the lenses in the setup, are

geared for the use of the 25/400 μm fibre. It is important to note that both fibres given in Table 4-1, were not polarization maintaining.

4.1.1.1 The Fibre Core

The specified fibre core diameter of 25 μm has a number of benefits for the laser. The large diameter raises the threshold for non-linear effects and thermal damage within the fibre. The fibre core is also small enough to yield single mode operation. Making use of Equation (2.4) to calculate the V-parameter yielded a value of 3.534. This is higher than the cut off value of 2.405 for single mode operation. However it is still possible to obtain single mode output by sufficient coiling of the fibre to prevent formation of the higher order modes, (discussed in Section 4.1.1.3)

Due to the low NA of the core and structure of the fibre, an excellent beam quality of laser light can be expected. The expected beam quality can be calculated making use of Equation (2.3). Theoretical calculations yield an M^2 value of 1.77. This is close to diffraction-limited beam quality ($M^2 = 1$).

To verify the specified core and pump cladding diameters, an imaging experiment was performed (Figure 4-3). Pump light was coupled into one end of the fibre. On the other end a lens with a focal length of 25.4 mm (Thorlabs – LA1951-B) was used to collimate the light leaving the fibre. This collimated light then falls incident onto a curved silver mirror with a radius of curvature of 400 mm (and hence a focal length of 200 mm). This effectively amounts to a 1-8 imaging layout, i.e. the image generated onto the camera would be eight times larger than the fibre core/cladding itself. A Spiricon CCD camera was placed 200 mm away from the mirror and the beam spot generated was observed (Figure 4-4).

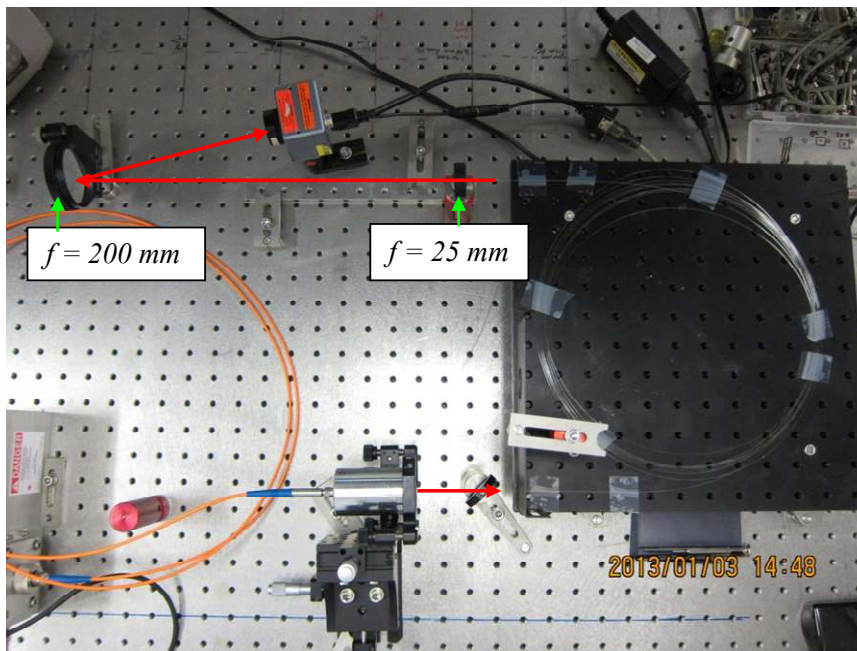


Figure 4-3: 1-8 Imaging layout used to confirm the core and pump cladding diameters.

Beam analysis software (Spiricon LBA) was used to image the fibre face and implement circular apertures around the core and pump cladding respectively. The aperture coinciding with the pump cladding was found to have a diameter of ± 3.20 mm. Bearing in mind the 1-8 imaging employed, this number was divided by a factor of eight obtain a value close to $400 \mu\text{m}$ for the pump cladding. This is in agreement with the specifications provided by the supplier.

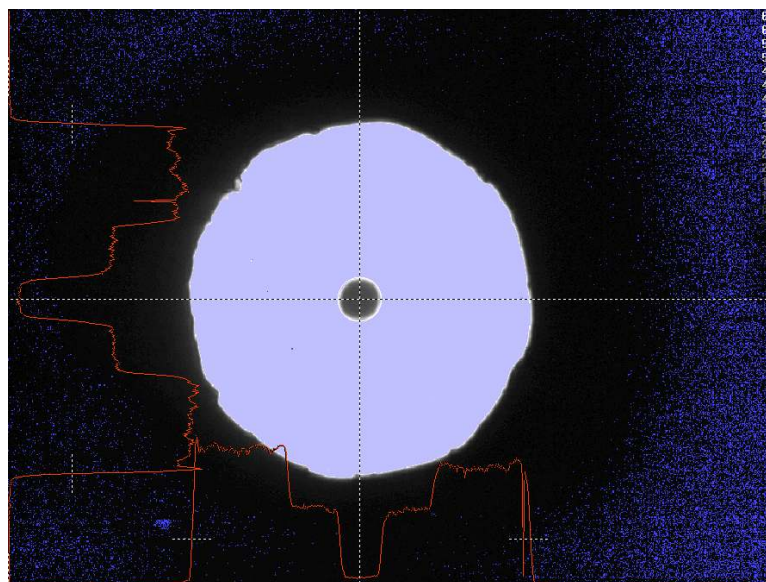


Figure 4-4: Imaged fibre face indicating the core and octagonal pump cladding – greyscale x 4.

Similarly for the core the aperture coinciding with the core was found to have a diameter of 0.410 mm. This effectively amounts to a core diameter of $51 \mu\text{m}$. This is

almost double the value specified by the supplier (25 μm). This discrepancy is explained by the introduction of an additional layer to the fibre core, consisting of germanium, a so-called ‘pedestal step’. The addition of this extra layer ensures that the NA of the fibre core remains small in the presence of aluminium-doping, which would raise the refractive index of the core [60, pg 94]. To ensure that the pump cladding was indeed correct, a micrometer was used to measure the outer diameter of the stripped fibre. The pump cladding was again measured to be $\pm 400 \mu\text{m}$.

4.1.1.2 *The Pump/Inner Cladding*

The large 400 μm cladding diameter affords the following advantages. Firstly, pump light is able to be focussed to a relatively large focal spot on the fibre end. This lowers the overall power density incident on the fibre end and in turn raises the damage threshold on the fibre end. The high numerical aperture of the pump cladding (NA = 0.46) allows for a large amount of pump light to be collected and guided within the fibre. These factors enable the use of high-power, poor-beam quality fibre coupled laser diodes to be utilized as pump sources. The guided pump light intersects with the doped core, enabling absorption of the pump light and subsequent excitation of the Thulium ions.

The pump absorption of the inner cladding was specified as 1.80 dB/m at 793 nm. Using this value, the length of active fibre needed for sufficient absorption to take place, was calculated. Let us require that 5% of the pump light reaches the other end of the fibre. In order to calculate this, the Beer-Lambert law is applied. This can be expressed via Equation (4.1) as [66]:

$$\alpha_{dB} = -\frac{10}{L} \log\left(\frac{P_T}{P_0}\right). \quad (4.1)$$

Where α_{dB} is the absorption coefficient (1.80 dB/m), L denotes the length of the fibre, P_T is the fraction transmitted pump power and P_0 is the incident pump power on the fibre ($P_0 = 1$). Therefore calculating the length of fibre L needed yields a value of 7.23 m.

4.1.1.3 Bending Radius of the Fibre

Pump and laser light within a fibre may be lost due to the mechanical bending of the fibre. Generally there are two losses associated with the bending of a fibre. The first are micro-bending losses and are incurred due to the presence of deformities within the fibre itself. The second is macro-bending losses which are more due to the overall bending of the fibre itself. If the fibre is coiled too tightly, the angle between the normal of the fibre interface and the light itself may become too acute. In this case total internal reflection will no longer take place and light will leak out of the core and pump cladding into the outer layers of the fibre. The radius of the coiled fibre where this macro-bend loss will begin to take place is known as the critical bending radius.

It was shown that by coiling the fibre to a sufficient radius, one is able to enjoy the benefits of a LMA fibre without having to worry about higher modes propagating through the fibre [67]. This is due to the fact the higher order modes can be ‘stripped off’ by the coiling of the fibre, provided the numerical aperture of the core is low enough to guide the light sufficiently within the core. Theoretical calculations have been previously undertaken to determine the bending loss of the respective modes for varying bending radii [68]. For the lowest order mode LP_{01} , the loss experienced was basically negligible for bending radii over 8 cm, for a fibre with a 25 μm core and 400 μm cladding. The loss incurred on the following higher mode (LP_{11}), also began to decrease. To ensure output that is fully single-mode, one would need to limit the loss on the LP_{01} mode whilst ensuring that the bending radius is small enough to still incur a loss on the higher order modes. An initial bending radius of 12 cm was chosen for the active fibre.

4.1.1.4 Fibre Preparation

When focusing light into a fibre, it is important that the fibre end has no deformities or irregularities in its structure. The presence of these will cause the light incident on the fibre end to scatter and not propagate into the fibre. It may also cause a deviation in the angle at which light is entering the fibre and therefore some of the light may not undergo total internal reflection, but will leak out into the surrounding fibre layers. For practical purposes, the fibre end acting as the output coupler should be cleaved perpendicularly to the fibre axis. This also ensures optimal input coupling on this end. At the perpendicularly cleaved fibre end, 4 % of the laser light is reflected back into

the fibre due to Fresnel reflections. This feature is used to provide the required feedback for the laser. This end also acts as the output coupler of the fibre laser.

The other end of the fibre (towards the feedback element) should, for this particular laser setup, be cleaved at an angle of ~ 8 degrees, to avoid Fresnel reflections back into the fibre core. The negation of these Fresnel reflections is important, in order to ensure no parasitic lasing takes place between the two fibre ends and that optimal Q-switching of the fibre laser takes place. The fibre cleaver available (Sony-Ericsson EFC-11 fibre cleaver, Figure 4-5) was meant for fibres with smaller diameters ($\sim 8/125 \mu\text{m}$), hence a perfect perpendicular cleave was not always ensured on the larger fibres. Therefore it was necessary to polish the fibre with specialized polishing pads. The polishing removes any micro deformities (and other particles which may have fallen on the fibre end). The polishing pads cater for a range of grit sizes and are available from many commercial suppliers.

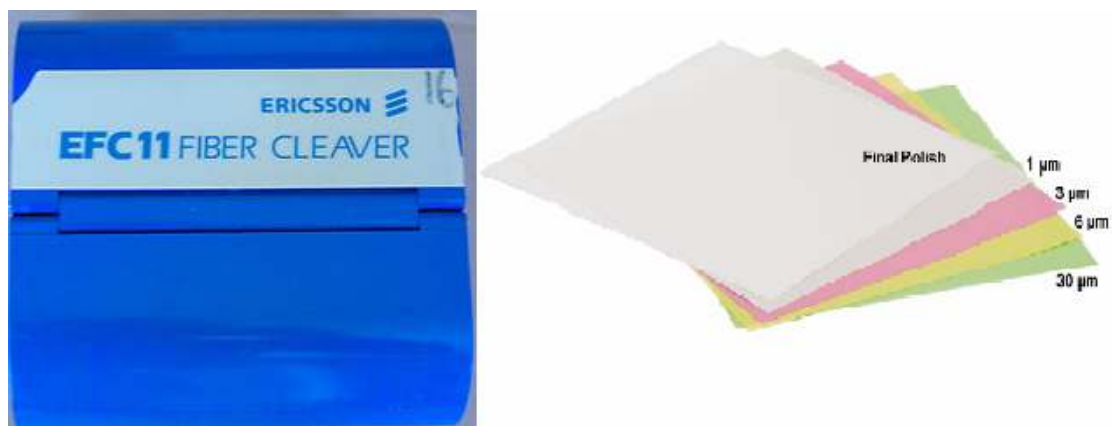


Figure 4-5: Sony Ericsson EFC-11 cleaver and optical fibre polishing pads.

Cleaving, followed by polishing of the active fibre can be seen in the figures below (Figure 4-6).



Figure 4-6: The active fibre after cleaving (left) and after polishing (right).

From side-view photos of the fibre in Figure 4-6, the fibre structure can be seen. Namely a central layer or fibre core, as well as the larger, octagon shaped pump/inner cladding. Before polishing there are clear defects on the fibre face due to the cleaving process. After cleaving, these defects are largely removed from the fibre face, with minor particle residual remaining. The remaining residue on the polished fibre face is easily removed by gently wiping with lens tissue doused in ethanol.

4.1.2 The Pump Source(s)

New fibre coupled laser diodes from Apollo Instruments (Figure 4-7), were available for this experiment.

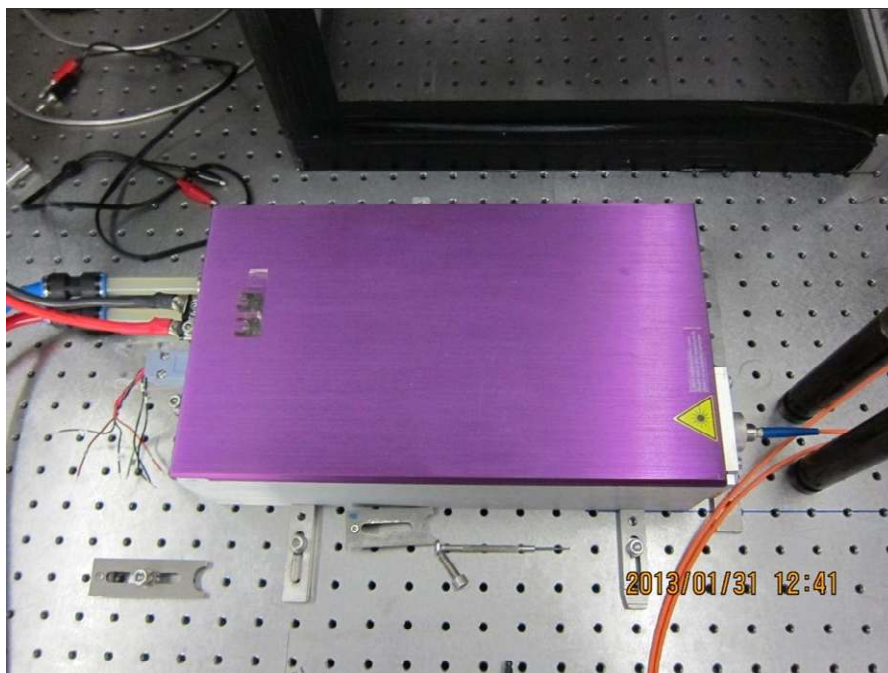


Figure 4-7: 150 W, 200 μm core diameter, fibre coupled laser diode - Apollo Instruments.

The specifications for these diodes are as follows:

- 65 W, 100 μm \O fibre, NA = 0.22, $\lambda = 792$ nm, $M^2 = 43.6$ - Apollo.
- 150 W, 200 μm \O fibre, NA = 0.22, $\lambda = 792$ nm, $M^2 = 87.3$ - Apollo.

A single 150 W Apollo diode was chosen to act as the pump source for the fibre laser, owing to the fact that this allowed the fibre to be pumped to higher powers. In addition, the specified central wavelength of the diode (792 nm) was nearer to the absorption peak (793 nm) of the active fibre.

The laser diode was connected to a Delta power supply to provide voltage and to set the operating current of the laser diode. According to the supplier's specifications, the diode was set to have a maximum voltage and current of 12 V and 60 A, respectively.

The minimum bending radius of the laser diode fibre was suggested to be 100 mm. In order to ensure no fibre damage or leakage of pump light, the diode fibre was coiled into a radius of approximately 130 mm.

The laser diode was water cooled via a chiller. The supplier specified an operating water temperature of 12-20 °C as optimal for the laser diode. The flow rate was suggested to be above 1.5 gallons per minute. This is equivalent to 5.68 litres per minute. The flow rate was monitored and measured to be 6.5 litres per minute, well over the recommended value. It was necessary to accurately determine the temperature of the water in order to ensure that the laser diode was being cooled sufficiently and not rising above its operating temperature (10-30 °C). The temperature of the water was measured with a mercury thermometer (taken as accurate) and via the chiller display. The water temperature was kept constant at an approximate value of 18.5 °C. Another means employed to monitor the diode temperature while under operation, was to measure the thermal resistance via an external thermistor and multi-meter. Using these values and the calibration data provided by the supplier, the temperature of the diode could easily be determined at any given time. The diode was in direct contact with the breadboard. This is not optimal as this effectively amounts to cooling the table in addition to the diode. In future it will be better to isolate the diode from the table via some insulating material for optimal cooling.

4.1.2.1 Pump Source Calibration

Since the diode is new, it was necessary to run a thorough characterization of its performance and output, ensuring that measured results matched those specified by the supplier. First, the output power was measured for increasing values of diode current. Two different power meters (600 W Gentec Maestro and 200 W Coherent) were used for the measurement. The results are given below (Figure 4-8).

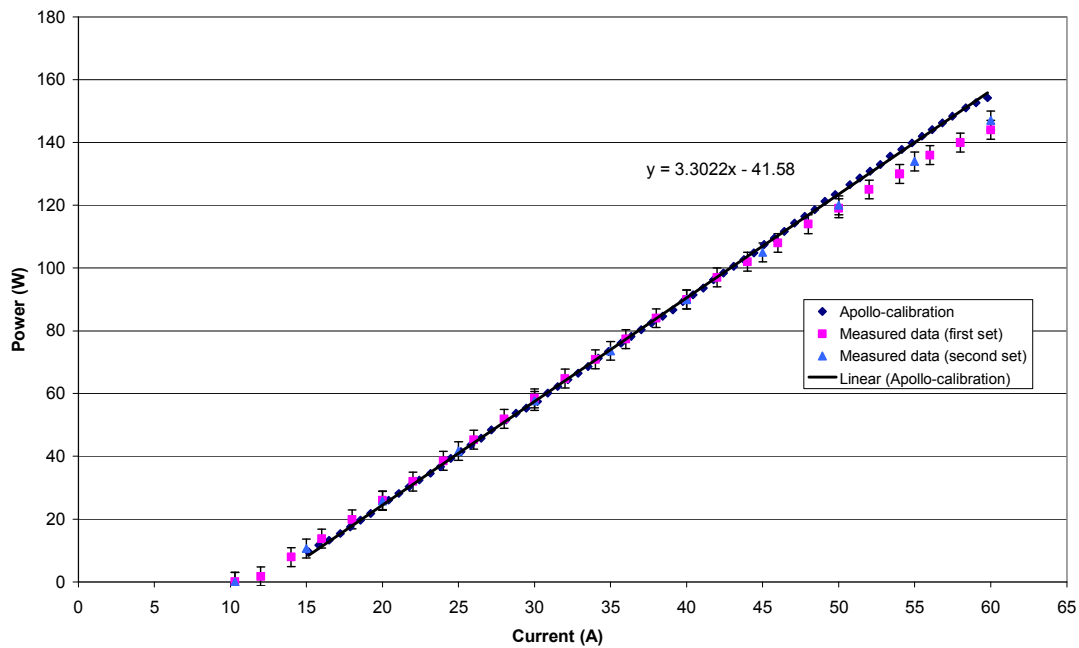


Figure 4-8: Power (W) vs. Current (A) calibration - 150 W, Apollo diode.

At the maximum current value of 60 A, the output power of the diode was measured to be 147 W with a measured fluctuation error of approximately ± 2 W. This corresponds to a 5 % difference between what was measured and the calibration provided by the supplier, which is within the measurement accuracy of the power meters. Threshold of the laser diode was found to be at an input current of 10.3 A.

The performance of the laser diode over a longer time scale was also investigated. The diode was set to full operating power (60 A) and the output power was logged for one hour. No significant deviation in output power was found during the test.

It was possible to establish the slope efficiency of the laser diode in the same way used for the Jenoptik diodes in the previous Chapter (Figure 3-3). The measured slope efficiency of the Apollo diode was calculated to be 28.5 %.

Another important part of characterization for the laser diode was establishing the wavelength output at maximum power, as well as the change in wavelength for varying diode operating temperatures. The wavelength was measured via an Ocean-Optics spectrometer (USB 4000), and yielded the following spectrum at full power and at 28°C (Figure 4-9).

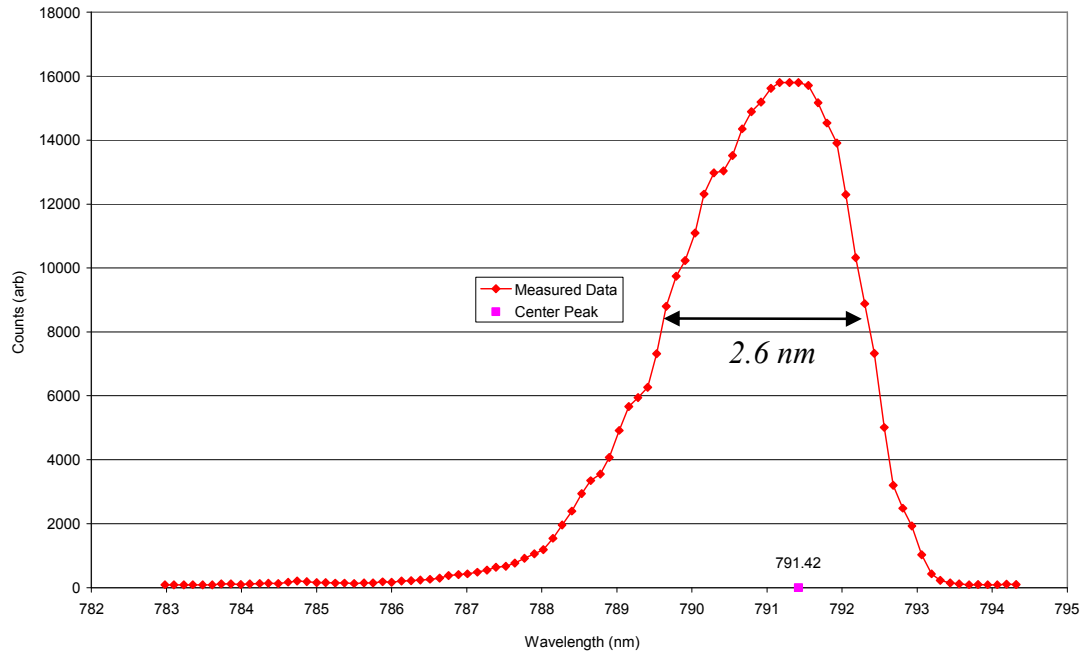


Figure 4-9: Spectrum of the 150 W Apollo diode at full power (60A), ~ 28 °C.

A centre peak at approximately 791.4 nm was measured, while operating the laser diode at full power. This is in close agreement with the wavelength specified by the supplier (791.7 nm at 60 A). The full-width half maximum was also calculated to be roughly 2.6 nm, within the specified value of approximately 3 nm.

The change in wavelength is actually dependent on the operating temperature of the laser diode. Therefore the wavelength was measured whilst simultaneously measuring the diode temperature (Figure 4-10).

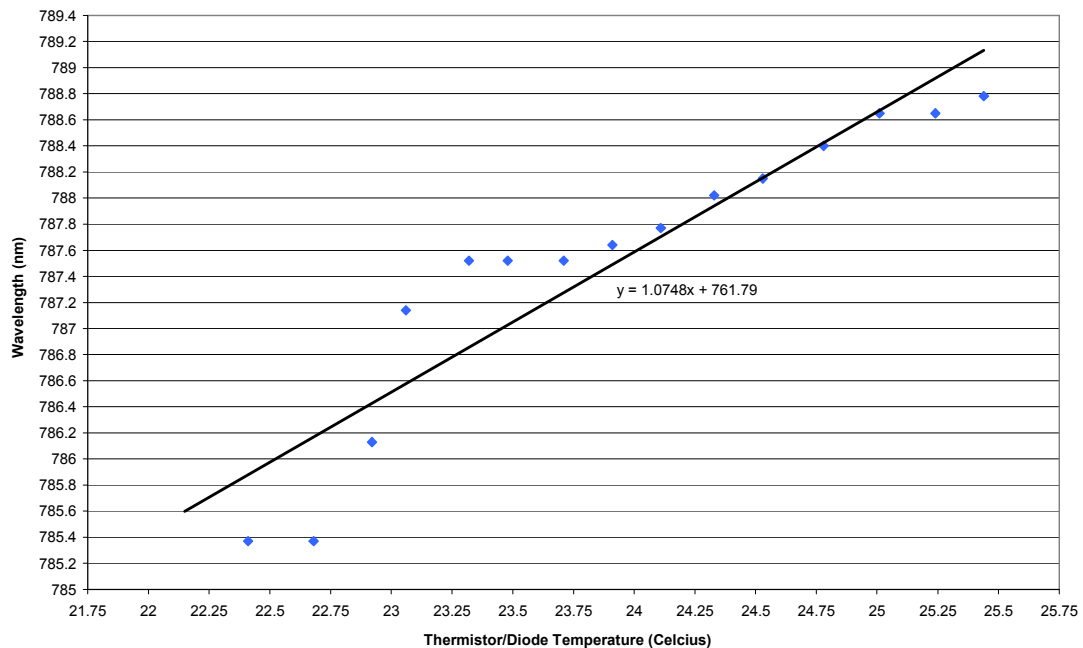


Figure 4-10: Wavelength dependence on diode temperature - 150 W Apollo diode.

Via simple calculations, the average change in wavelength over the measured interval could be determined. It was found that the wavelength change per degree Celsius was roughly 0.87 nm/C°. This value is quite high in comparison with other laser diodes, indicating the laser diode may need to be cooled more effectively. However, as can be seen from Figure 4-10, the output wavelength of the laser diode does not increase linearly with an increase in the diode temperature. This is due to the fact that there is a broad emission spectrum from multiple laser diode emitters in the laser diode module. A temperature change will affect each emitter by a different variation, resulting in the observed nonlinear increase in the wavelength. To summarize, the performance and output of the fibre coupled laser diode was measured to be close to the specified performance and output values.

4.1.3 Pump Optic Design

In order to proceed with the correct choice of lenses, it is necessary to know the variation of the pump beam size as a function of distance or propagation length. In order to do this the beam-propagation formula, given by Equation (2.1) in Section 2.1, is used to profile the propagation. This formula gives the beam radius w as function of distance z . In other words, for a known distance away from the fibre of the laser diode, it is possible to calculate what the beam spot size radius is at this position. This is important to know to prevent overfilling and beam clipping of the lenses in the optical layout.

4.1.3.1 Pump Light Collimation

This section will outline the choice of the lenses used for the pump light and the requirements on these lenses. With reference to the optical setup in Figure 4-1, it is indicated that there are two lenses after the laser diode fibre. The purpose of the initial lens is to collimate the light that comes out of the fibre coupled diode and the second lens focuses the pump light into the active fibre. A range of lenses with different focal lengths were considered. When choosing the lens for collimation, the following two criteria were considered:

- To avoid significant losses of pump light and spherical aberrations, it is required that the light incident on the lens does not overfill the lens. A good estimate would be that the diameter (D) of the lens is approximately three

times larger than the radius (w) of the incident beam to collect most of the light (99%). That is: $3w \leq D$ [69].

- $NA_{lens} \geq NA_{fiber}$. This criterion ensures that the collimating lens will collect and collimate all the pump light leaving the diode fibre. The NA of the pump cladding of active fibre is given by 0.22. The NA of the lens utilized (see below) was calculated to be 0.3. Therefore this condition is satisfied.

There are other considerations that need to be taken into account. One of these is the AR-coating on the lens. If light passes through a lens, a portion of the light will be reflected, due to Fresnel reflections. This is a loss in the laser setup and the reflected light might damage the laser diode by propagating back into the fibre of the laser diode.

Two Gradium[®] lenses with a focal length of 50 mm and diameter of 30 mm were available for use. These lenses are specially manufactured to have an index of refraction that varies radially throughout the lens (GRIN lenses - Graded Refractive INdex). This minimizes spherical aberrations induced by the lens considerably (Figure 4-11). They are therefore excellent for input coupling of the pump light into the active fibre.

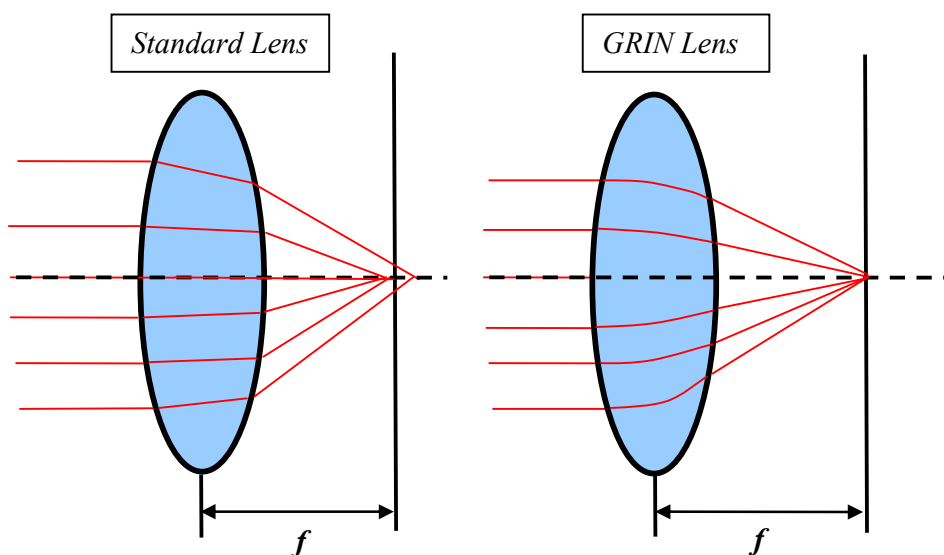


Figure 4-11: Comparison of light guidance between a standard lens and a GRIN lens.

In addition, this lens fulfils the conditions for collimation mentioned earlier. These lenses were also anti-reflection coated for the pump wavelength. Employing one-to-one imaging, the beam radius incident on the lenses would be 11 mm. This slightly overfills the lens as: $11 \text{ mm} \times 3 = 33 \text{ mm} \geq 30 \text{ mm}$. However since the lenses induce little aberration, the slight increase in loss should not present any significant problem.

The power density (at max pump power) incident on each lens was calculated to be approximately 39 W/cm^2 , which is well within the expected damage threshold of the lens or the AR coating. The power loss through both lenses was measured to be 0.4 % at a central wavelength of 788 nm. This corresponds to a loss of 0.2 % through each Gadium lens. These losses are relatively low, indicating an AR coating of good quality. This is adequate for the experiments and is a significant improvement on the laser setup covered in Chapter 3.

4.1.3.2 Pump Light Input Coupling

The other 50 mm focal length Gadium lens was used for focusing the input pump light into the active fibre. There are conditions that need to be satisfied in order to ensure optimal input coupling and these are the following:

- $NA_{lens} \leq NA_{cladding}$. This must be fulfilled in order to ensure that the light coupled into the active fibre will undergo total internal refraction and will not leak out into the surrounding layers of the fibre. This condition sets a limit on the smallest allowed spot size on the active fibre end, for a given pump source.
- The beam diameter of the focal spot should not exceed the diameter of the inner cladding.

The lenses were placed in a cylindrical tube (Figure 4-12). This held them firmly in place and also ensured that their optical axes were aligned with that of the pump fibre.

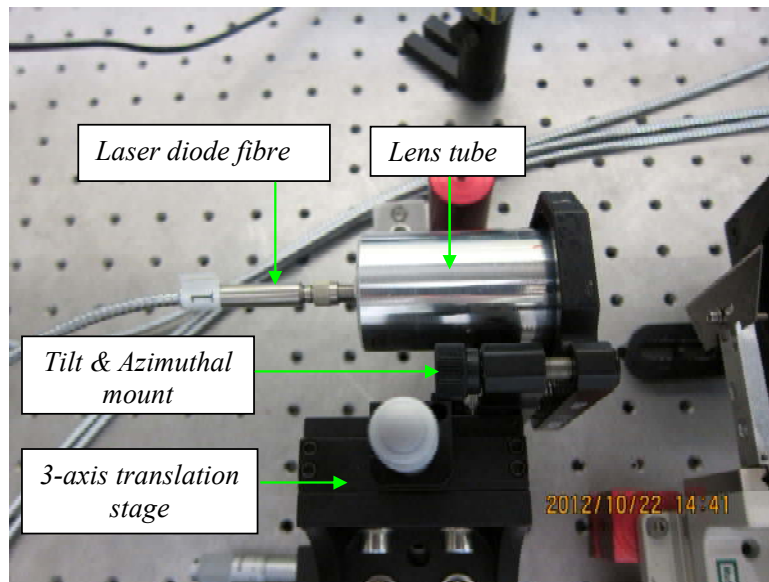


Figure 4-12: Mounted Gadium lenses.

Indicated in the schematic below is the interior of the lens tube in which the Gadium lenses were mounted (Figure 4-13).

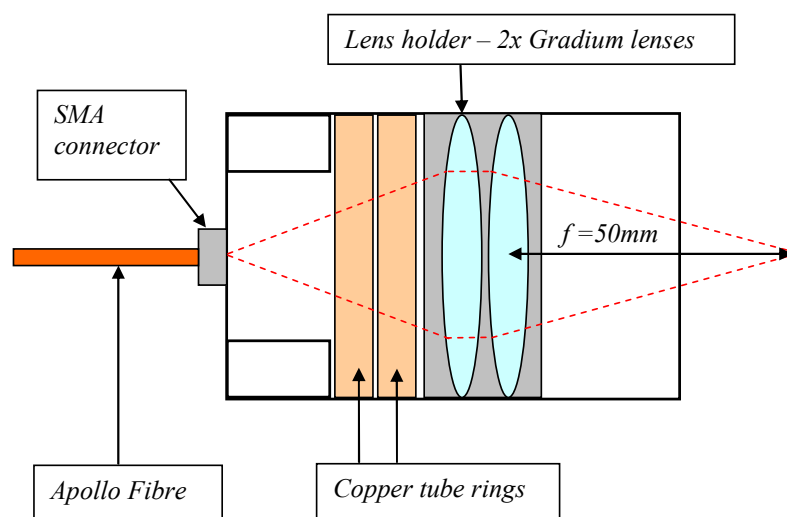


Figure 4-13: Interior structure of the Gadium lens tube.

The Gadium lenses were mounted in a single holder, effectively forming a compound lens. Inside the tube, copper rings with set widths were placed. By inserting or removing these rings, it is possible to shift the lenses further or closer to the pump fibre face. This is advantageous for it affords the option of changing the imaging ratio and therefore the diameter of the beam generated at the active fibre face.

Initially a one-to-one imaging scheme was employed. In other words, the front face of the laser diode fibre was imaged at the focus of the Gadium lens pair. Therefore the diameter of the beam at the waist was expected to be 200 μm , the same diameter as

the laser diode fibre core. This was confirmed with the aid a CCD camera (Spiricon-Scorpion LBW) and operating the laser diode with very little drive current using only fluorescence. The beam diameter with this imaging scheme was determined to be approximately 203 μm .

The propagation of the pump light through the Gradium lenses was also profiled, for varying beam diameters (i.e. various positions of the Gradium lenses within the lens tube). This is given below (Figure 4-14).

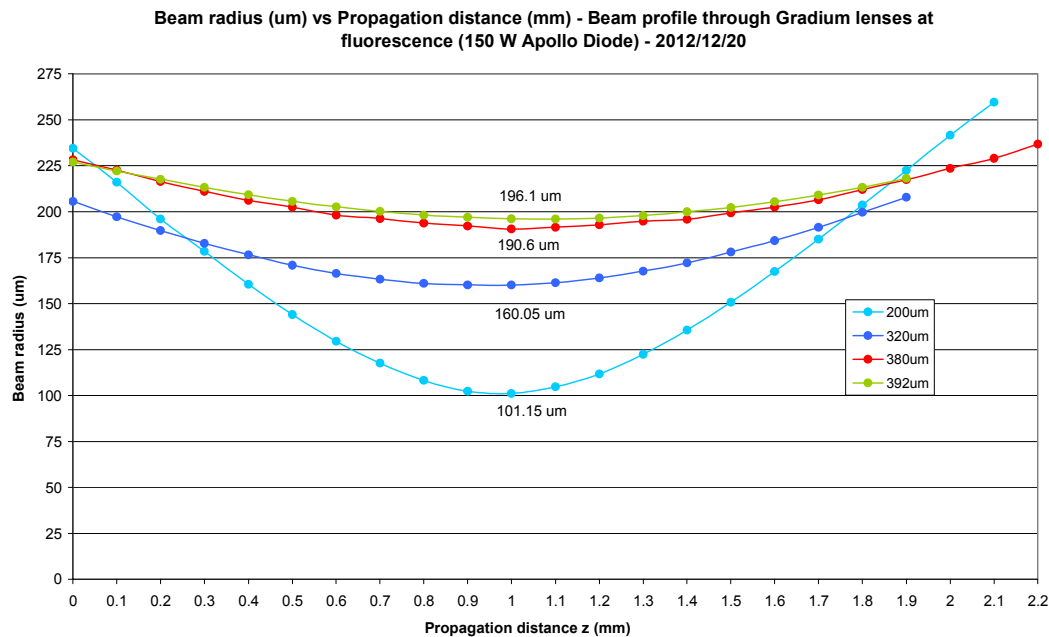


Figure 4-14: Propagation of pump light via the Gradium lenses.

This light was coupled into the active fibre. One of the crucial steps in obtaining a highly efficient laser is to obtain a high coupling efficiency. A 100 W Gentec power meter was placed at the other end of the active fibre and measured the transmitted pump power P_T for a set input pump power P_0 . Initially it was expected that by having a focal spot diameter (200 μm) much smaller than that of the pump cladding diameter (400 μm), a high coupling efficiency would be obtained. However, the results obtained did not agree with this assumption. In fact it was noted that by having a focal spot diameter closer to the diameter of the pump cladding, a much higher coupling efficiency was obtained (Table 4-2).

Table 4-2: Measured data for various beam diameters incident on the active fibre face.

Input Power (W)	Diode Current (A)	Measured Beam Diameter (μm)	Transmitted Power (W)
13.608	16	201	0.21
13.608	16	268.2	0.32
13.608	16	320	0.532
13.608	16	380	0.622
13.608	16	392	0.73

In order to obtain a percentage value for the coupling efficiency, pump light was coupled into a short piece of doped fibre (~ 1 cm) that had previously been cleaved. For this measurement it is sensible to use a short piece of fibre so that the percentage loss of pump light, due to absorption in the core, is negligible. This does provide a more accurate value of the coupling efficiency. Measuring the transmitted pump power and knowing the input pump power, the coupling efficiency came to 88 % for a beam diameter of 392 μm at the beam waist.

In summary, the imaging ratio of the Gradium lenses was chosen in such a way to have a beam diameter of 392 μm at the active fibre face, which was measured to yield the best coupling efficiency. In addition, the loss of pump light through these lenses was measured to be acceptable for laser operation.

4.1.4 Resonator Design for CW Operation

As was previously discussed a single end of the active fibre acts as the output coupler of the fibre laser. This is true provided the end is perpendicularly cleaved, resulting in 4 % Fresnel reflections back into the fibre. Therefore this fibre end is essentially a 96 % transmission output coupler. To constitute the other end of the laser resonator the appropriate high-reflector, serving as the feedback element, needs to be selected. For the initial CW setup (Figure 4-1) a $\frac{1}{2}$ " ϕ , highly-reflective (HR) curved mirror with a radius of curvature of 38 mm was chosen. The mirror was produced by Layertec. It has an AR coating for 808 nm (with a loss of 0.2 % at this wavelength). It is highly-reflective for wavelengths around 2100 nm, with a reflectivity greater than 99.9 % at this wavelength. The way in which this mirror functions has been indicated in (Figure 4-15).

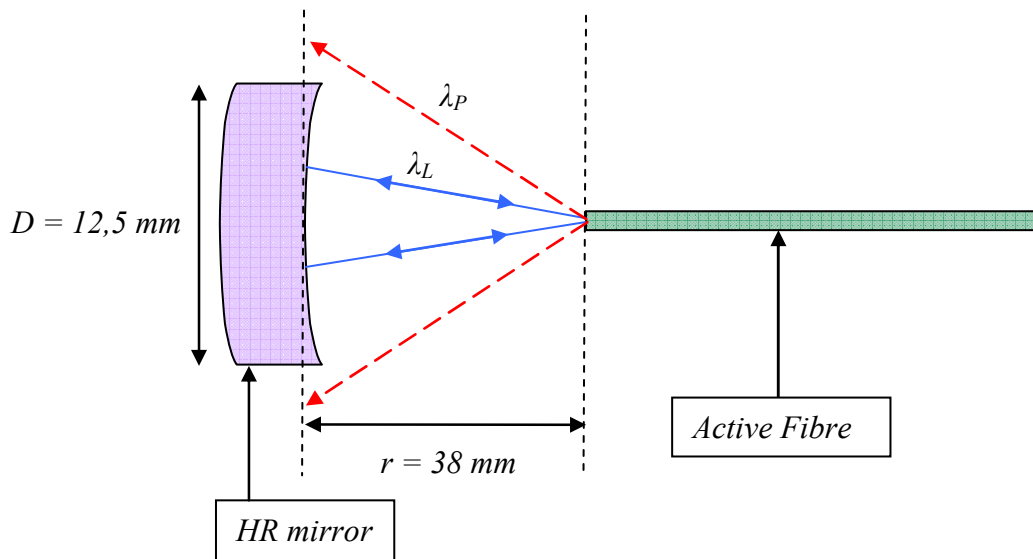


Figure 4-15: HR mirror functioning as feedback element within the resonator.

The $2\ \mu\text{m}$ light (blue) would propagate out the end of the perpendicularly cleaved fibre end. Since the NA of the core (0.09) and cladding (0.46) is known, it is possible to calculate what the beam radius would be 38 mm away from the fibre end, for both the laser light (λ_L) and pump light (λ_P). The beam radius of the laser light on the HR mirror was calculated to be 3.37 mm with the aid of the beam propagation Equation (2.1). This works well, as the spot does not over-fill the lens (i.e. $3 \times 3.37\ \text{mm} = 10.11\ \text{mm} \leq 12.5\ \text{mm}$), using the rule of thumb $3w \leq D$, discussed earlier in section 4.1.3.1. The beam radius of the remaining pump light is extremely large (17.5 mm), due to the larger numerical aperture of the pump cladding. However due to the length of the procured active fibre ($\sim 7.23\ \text{m}$), most of the pump light has already been absorbed so this does not pose a significant problem.

Once the light propagates out of the fibre, it falls onto the curved front of the HR mirror. The propagating light will make a perpendicular angle with the tangent to the mirror surface, at any specific point. Due to this, the light will be reflected back exactly along its incoming direction. The HR mirror was also held by a standard mirror mount (KM Thorlabs) which allowed us to adjust its azimuthal and tilt angles. In addition the mount was attached to a three-axis translation stage. However this proved to exhibit some instability in the laser performance with regard to its output power and beam profile. This is attributed to mechanical drift due to thermal expansion between the fibre end (due to the cooling plate) and mirror mount. A more stable solution was implemented, namely: a z-axis translation stage and a highly stable differential drive mirror mount (KS1D Thorlabs). This mirror mount was far

more stable and affords the option of tuning the azimuthal and tilt angles with much smaller increments.

It was also deemed necessary to create a dry air ‘box’ surrounding the mount (Figure 4-16). As the interior of the resonator cavity on this end was exposed to the atmosphere inside the lab, there could be atmospheric water absorption taking place. This is of particular concern for a laser operating at $2\ \mu\text{m}$, where atmospheric absorption is significant. This is detrimental to laser performance and will lead to intra-cavity spiking, which will in turn affect the characteristics of the laser and may lead to damage of the AR coating on the HR mirror.

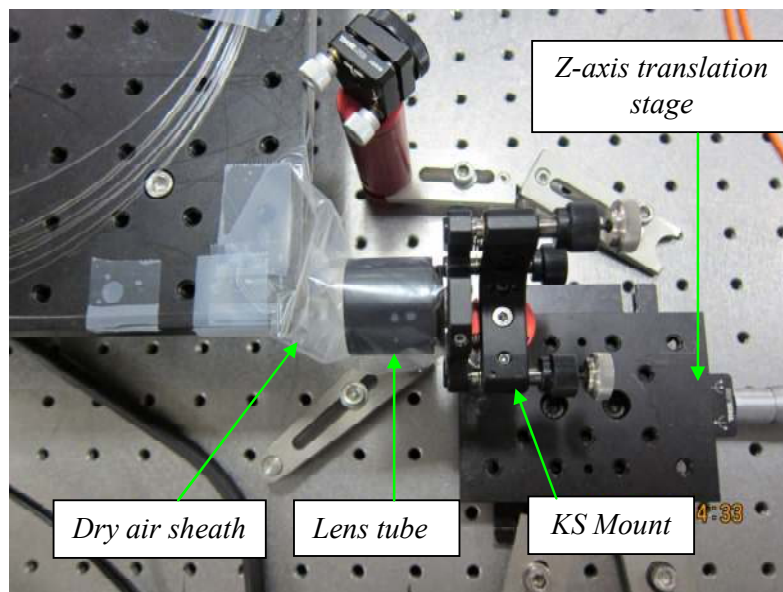


Figure 4-16: Mounted HR mirror with surrounding dry air enclosure.

The last point to be made concerning the resonator is that this laser configuration will only work for continuous-wave setups, as light entering a Q-switch (particularly an AOM), needs to be collimated to ensure optimal diffraction by the AOM. The modification of this configuration to implement Q-switching is discussed in Section 4.1.7.

4.1.5 Resonator Design for Locking the Laser Wavelength

A Volume Bragg Grating (VBG) was also used as a feedback element for a CW fibre laser setup and Q-switched setup (Figure 4-17). The VBG was used for a fibre laser setup with a fibre length of approximately 1 metre. As was discussed in section 2.4, VBGs afford the option of a narrow and stable wavelength output, instead of the broad emission spectrum associated with Thulium doped fibre lasers.

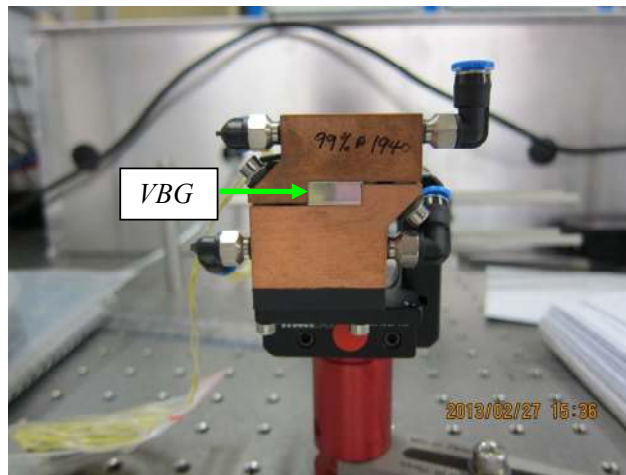


Figure 4-17: The mounted Volume Bragg Grating.

The available VBG was supplied by OptiGrate [70], a company specializing in quality volume Bragg gratings. The VBG was specified to be highly reflective ($\sim 99.9\%$) at ~ 1940 nm. The VBG was orientated to specific angles, relative to the optical faces of the VBG, to reflect at this wavelength. The specified angles required the VBG to be rotated horizontally by an angle of 1° and tilted by an elevation angle of 0.5° . This critical alignment was experimentally accomplished with the aid of alignment lasers. Shown in Figure 4-17, the VBG was mounted between copper slabs, in order to facilitate water-cooling. This is often necessary to prevent damage of the VBG itself when dealing with high power lasers.

4.1.6 Q-switch

As was discussed in Section 2.3.1, the purpose of the Acousto Optic Modulator (AOM) as an intra-cavity element is to alter the ‘quality’ of the resonator, i.e. from a low loss to a high loss resonator. This technique will lead to the generation of laser pulses.

A conduction cooled, crystal quartz AOM from Gooch and Housego (model number I-QS041-2C10V5-4-HC1) was available for this project [71]. The AOM has a specified wavelength range of 1900 nm to 2100 nm, with a specified AR coating on the optical surfaces of the quartz medium with reflectivity of 0.5 % per surface. The damage threshold for the coating and medium is specified to be larger than 500 MW/cm². The AOM is also specified to function with an RF frequency of 40.68 MHz and max RF power of 20 W. The RF signal was measured with the aid of a RF antenna and the signal displayed on an oscilloscope (Figure 4-18). The frequency of the RF signal was measured with the oscilloscope and confirmed to be 40.68 MHz, in agreement with the specified value.

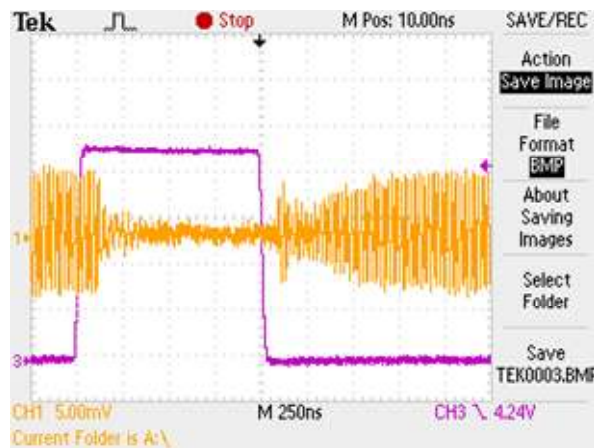


Figure 4-18: RF signal (orange) generated during specific time intervals.

The pink trace in Figure 4-18, represents the signal provided by the trigger signal generator. This signal provides intervals where RF power is applied (closed time – the laser cavity is turned to a high loss or the Q-switch is turned on) and where the RF power is not applied (open time – the laser cavity becomes low loss or the Q-switch is turned off). As can be seen from Figure 4-18, there is some delay in the decay of the RF signal during the open time. This is a feature of the RF driver itself. Likewise when the Q-switch is turned on, the RF signal takes a short time to build up.

In order to utilize the AOM effectively, an appropriate mount was constructed for it, which is shown in Figure 4-19.

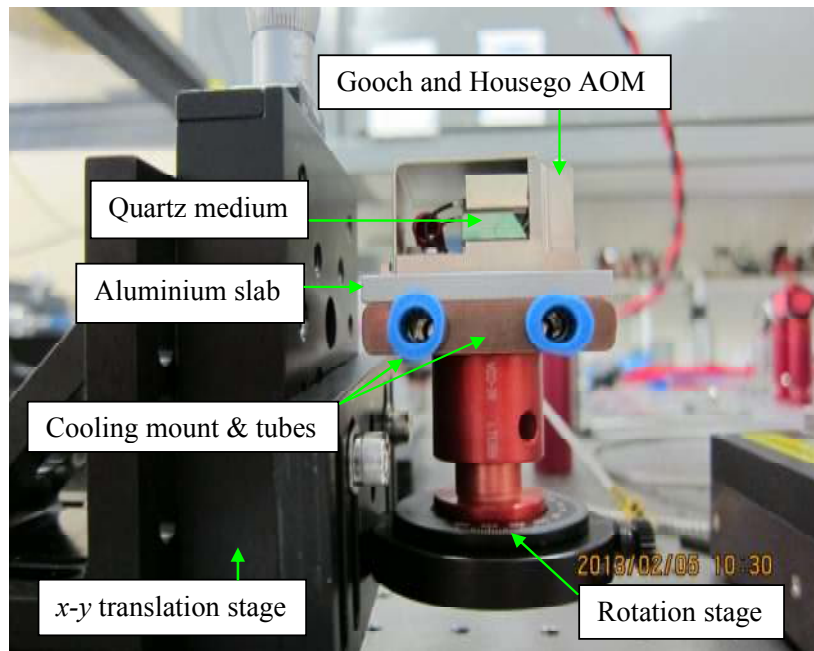


Figure 4-19: On-axis view of the mounted Acousto-Optic Modulator.

Heat is deposited into the AOM during operation due to the RF powers present (up to 20 W). Therefore it was necessary to devise a means to cool the AOM.

The AOM itself was connected to an aluminium slab, which served as an intermediate medium between the AOM and a copper cooling slab. The cooling slab had channels with which to facilitate water cooling, making it ideal for the cooling of the AOM.

The AOM and cooling assembly were placed onto a rotation stage with which the angular displacement of the AOM relative to the optical axis of the laser cavity could be varied. This was necessary to implement in order to obtain the maximum diffraction efficiency and thus facilitate optimal Q-switching.

Finally the entire assembly was mounted on a translation stage which allowed the AOM optical axis to be centred both horizontally and vertically with the optical axis of the laser cavity.

4.1.7 Optical Layout for Q-switched operation

The optical layout indicated in Figure 4-1 was modified appropriately to incorporate the Q-switch (Figure 4-20, Figure 4-21).

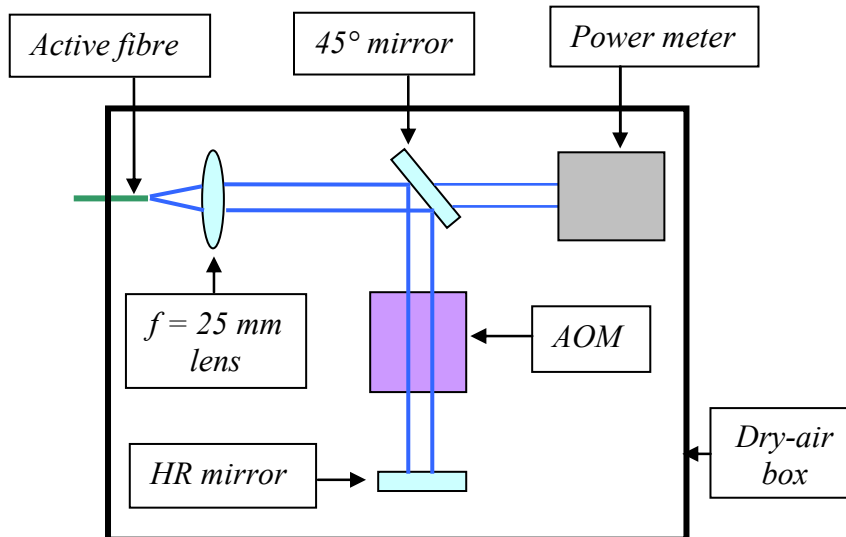


Figure 4-20: Schematic of the extension to the CW setup for Q-switched operation.

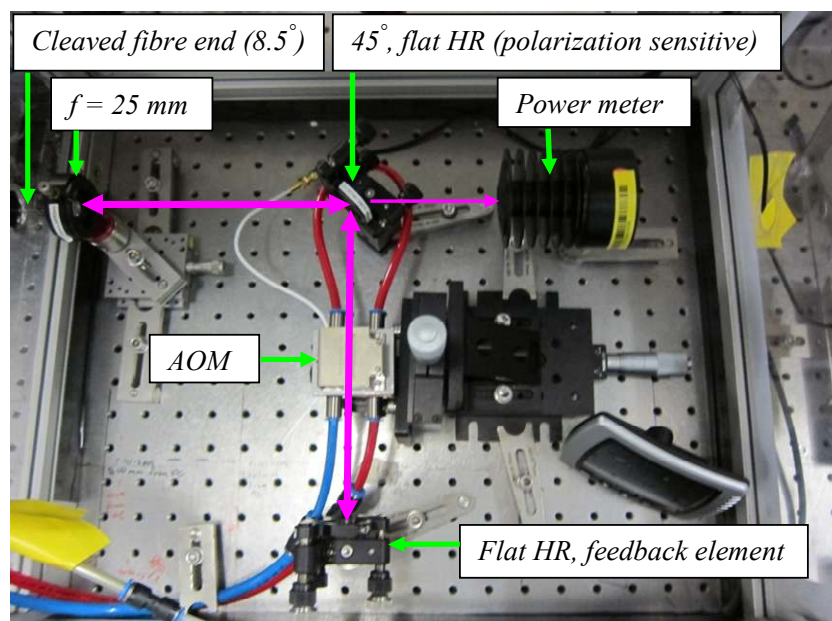


Figure 4-21: Optical layout for Q-switched operation.

The curved high-reflector (Figure 4-15) was replaced with a flat high-reflector, which has a broadband HR coating (1950 – 2340 nm). A lens with a focal length of 25 mm was used to collimate and re-focus the light leaving and entering the fibre. Collimated

light is required for optimal Q-switching. The angle of the AOM was adjusted in order to obtain high diffraction of the laser light.

The AOM is polarization sensitive while the light leaving the fibre is randomly polarized. Therefore a flat 45° high reflector was utilized to introduce a high loss for the horizontal polarization. The 45° mirror had a specified reflectivity of 99.9 % at 2054-2065 nm for the vertical polarization and a high transmittance for the horizontal polarization. This ensured that the fibre laser was polarized.

For the fibre laser with 1 metre fibre length (see experimental results in section 4.2.1), this mirror becomes inadequate. As shorter output wavelengths are expected for the fibre laser with a shorter fibre length, the reflectivity range of this mirror is not applicable. Therefore a thin-film polarizer was also used to introduce a loss on the horizontal polarization for this setup (Figure 4-22). The thin film polarizer was implemented and rotated at the Brewster angle of $\sim 56^\circ$ to allow transmission of only the vertical polarization.

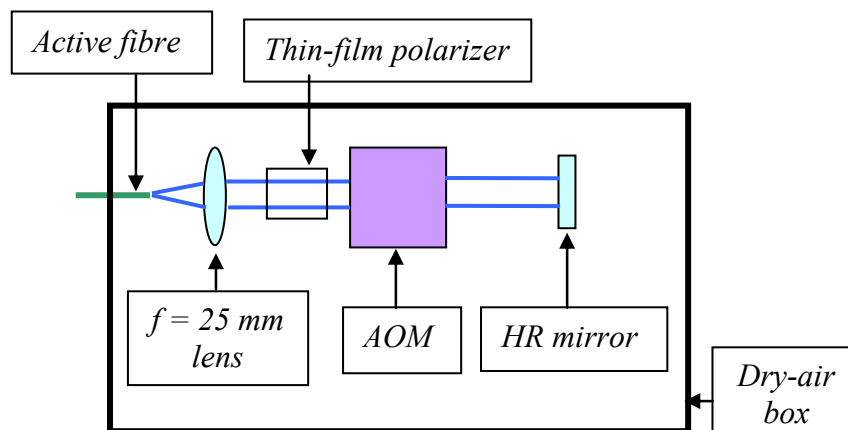


Figure 4-22: Optical layout for Q-switched operation with 1 metre active fibre length.

Another important modification introduced into the setup was the angle cleaving of the active fibre. The fibre was angle cleaved at 8.5° (confirmed optical measurement under a microscope). This suppresses Fresnel reflections of the laser light back into the fibre core. Essentially, the fibre end ceases to function as a resonator end. This is crucial for optimal Q-switching due to the fact that CW lasing might still occur simultaneously with the generation of laser pulses. Finally the intra-cavity setup, indicated above, was surrounded by a dry-air box, to prevent intra-cavity spiking and atmospheric absorption.

4.1.8 Cooling Design

Due to the heat load in the active fibre, it was required to cool the fibre. This was achieved via a water-cooled breadboard, indicated in the schematic in Figure 4-1. The breadboard consisted of water channels through which water was circulated from a chiller. The temperature of the water was set to 18 °C. The fibre itself was placed and attached on the breadboard via adhesive tape, ensuring sufficient contact between the fibre and the board. This cooling scheme is not as effective as the cooling scheme utilized by the fibre laser in Chapter 3. This is due to the fact that the fibre is only partially in contact with the cooling plate. Additionally, the temperature of the cooling plate was set to a minimum temperature of 18°C, to prevent build-up of condensation in the laser setup.

4.1.9 Diagnostic Layout

With the CW laser built, the next phase of the experimental layout involved incorporating diagnostic equipment to fully characterize the laser. It was necessary to determine the spectral output, beam quality factor (M^2), slope efficiency, polarization and observe other characteristics of the laser such as its beam profile and temporal behaviour. A diagnostic layout was devised as to observe many of these parameters simultaneously (Figure 4-23). This required the use of multiple partial reflectors to split the beam as well as the appropriate 45° high reflectors to guide the beam. A description of the diagnostic optical layout is given below.

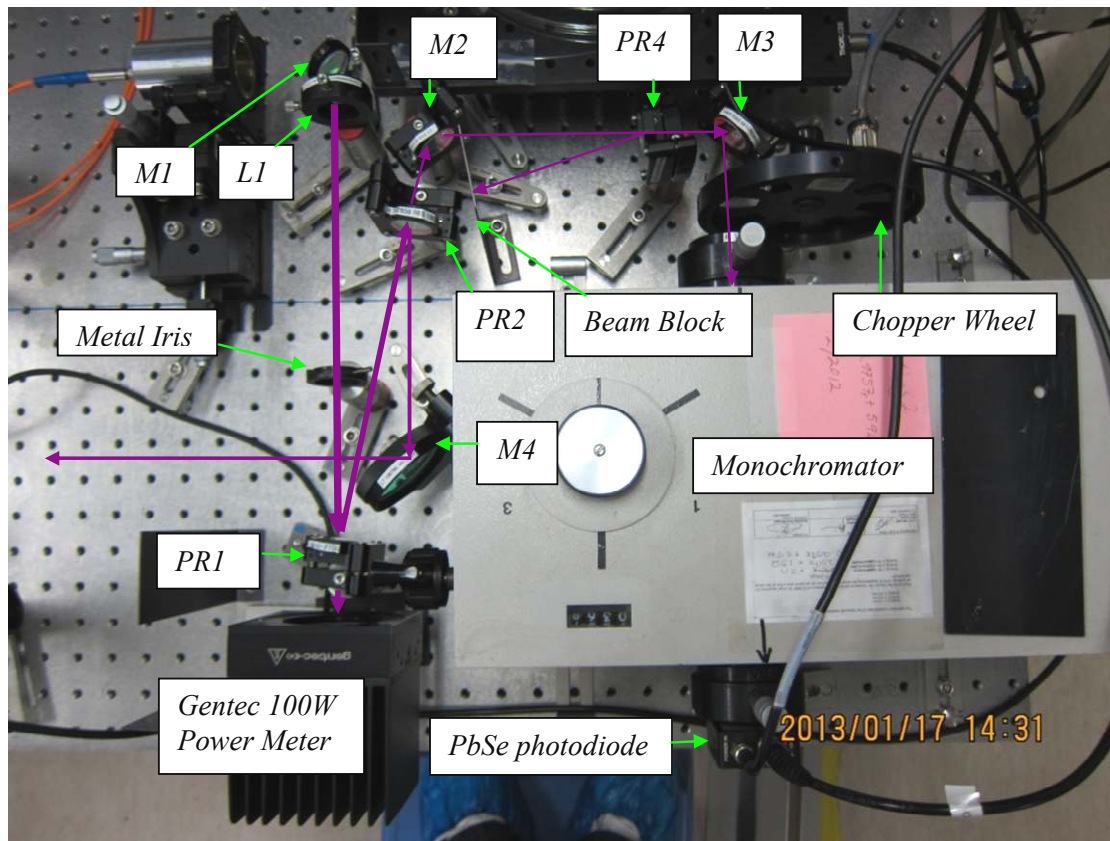


Figure 4-23: Diagnostic layout for the Thulium fibre laser.

- L1 – VLOC, $\frac{1}{2}$ " ϕ , $f = 25.4$ mm, plano-convex lens, $1.9 \mu\text{m} - 2.4 \mu\text{m}$.
- PR1 – VLOC, 1" ϕ , 0° partial reflector ($R = 30\%$), $1.8 \mu\text{m} - 2.1 \mu\text{m}$.
- PR2 – VLOC, 1" ϕ , 0° partial reflector ($R = 65\%$), $1.8 \mu\text{m} - 2.1 \mu\text{m}$.
- M1 – Layertec, 1" ϕ , 45° , high-reflector, $\sim 2 \mu\text{m}$.
- M2 – Layertec, 1" ϕ , flat 45° high reflector, $\sim 2 \mu\text{m}$.
- M3 – Layertec, 1" ϕ , flat 45° high reflector, $\sim 2 \mu\text{m}$.
- PR4 – VLOC, 1" ϕ , 0° partial reflector ($R = 90\%$), $1.8 \mu\text{m} - 2.1 \mu\text{m}$.
- M4 – Layertec, 2" ϕ , flat 45° high reflector, $1.7 \mu\text{m} - 2.3 \mu\text{m}$.

The perpendicularly cleaved fibre end acts as the output coupler as previously mentioned. The laser light is emitted by the fibre laser and falls incident on the 45° dichroic mirror (M1). This laser light is then reflected towards a collimating lens (L1), producing a collimated beam with an approximate diameter of 2.3 mm. The collimated light proceeds further down, through a metal iris (used during alignment) and falls upon a partial reflector (PR1). 70% of the light passes through and is measured by a power meter (Gentec 100 W, UP55N-100H-H9-D0). 30% is reflected to another partial reflector (PR2). 65% of this light is reflected towards the flat, 45°

high reflector M4, which guides the light to the end of the optical table. It was this portion of laser output that was used to observe the beam profile, temporal behaviour and for M^2 measurements for the fibre laser.

The remaining light passing through PR2 falls incident on M2 which directs the light towards PR4 and M3. This partial reflector (PR4) was used inter-changeably with the sole purpose of attenuating the laser light entering the monochromator. This prevented the PbSe photo-detector from being saturated and allowed the measurement of the spectrum at higher output powers. The light reflected by M3 first passed through a chopper wheel and scattering plate before entering the monochromator. The chopper wheel was required because the PbSe detector was AC-coupled. The scattering plate (ground glass) ensured that the grating of the monochromator was sufficiently illuminated.

4.1.9.1 Calibration of the Monochromator

A frequency doubled Nd:YVO₄ alignment laser (532 nm) was introduced into the setup, to assist with the alignment of the diagnostic setup. Another role the alignment laser served was for calibration of the monochromator. The monochromator is a Jarrel-Ash, diffraction grating spectrometer, mechanically different but otherwise similar to the monochromator employed in Section 3.1.4. This monochromator has a measured uncertainty of 2.5 nm. It was calibrated in the same procedure described in Section 3.1.4, with the resulting calibration plot given below (Figure 4-24).

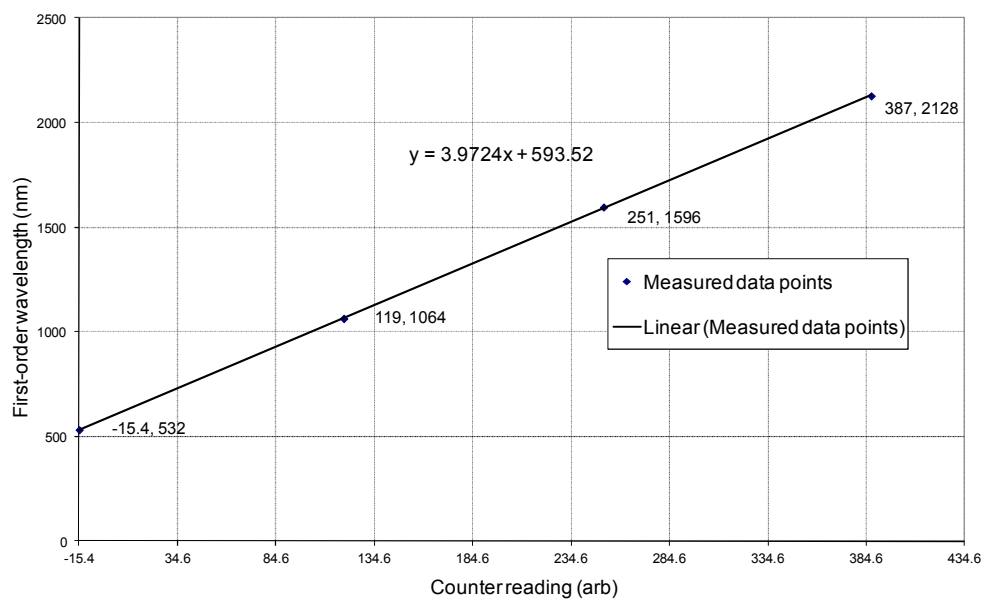


Figure 4-24: Calibration plot for the Jarrel-Ash monochromator, utilizing a frequency doubled Nd: YVO laser (532 nm).

The signal passes through the entrance slit of the monochromator, propagates through the monochromator, undergoes diffraction via the grating, and leaves via the exit slit. This signal is detected via a lead selenide (PbSe) photo-detector (PDA02H-EC). The detector has a specified response for wavelengths in the range 1.5 μm – 4.8 μm . The entrance and exit slit widths were made as small as possible by observing a signal on the oscilloscope, closing the slits so the signal disappears and slightly opening both until a signal is once again observed on the oscilloscope. Both slit widths were adjusted to be approximately 0.22 mm. A measurement using this monochromator in manual operation took approximately 20 minutes.

With these optical arrangements the parameters of the fibre laser, such as spectral output could be measured. The results are covered in Section 4.2.

4.2 Experimental Results

4.2.1 Laser Efficiencies

With the CW fibre laser built, with 6.5 m fibre length, and lasing (Figure 4-26), the output power was measured for increasing pump powers. The procedure is the same as the one employed in Section 3.2.1. In this case, the pump light passed through two Gradium lenses with a loss of 0.2 % at the pump wavelength. The loss of 0.5 % for the 45° dichroic mirror was also incorporated to obtain the measured slope efficiencies (Figure 4-25).

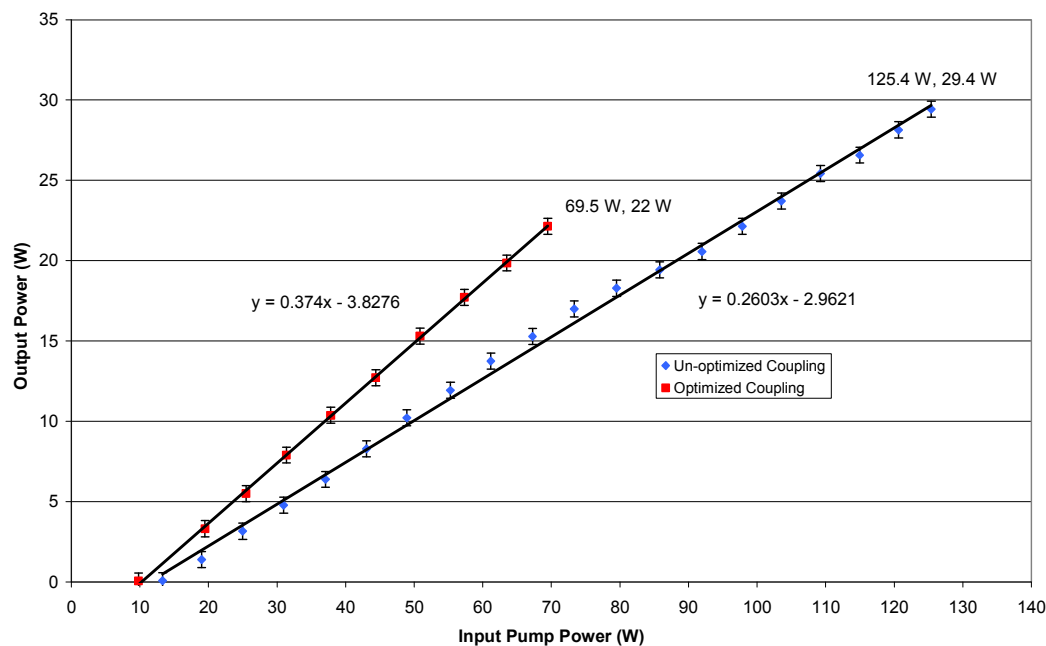


Figure 4-25: CW Slope efficiency with the curved HR mirror and ~6.5 metre fibre length.

Two slope efficiencies were measured. The initial slope efficiency recorded was 26 %. This is comparatively low compared to slope efficiencies obtained from the literature for Thulium doped fibre lasers. In this case, fluctuations in the output power of the laser (~ 0.5 W) were observed for a range of output powers. The reason for this was the instability of the HR mount and thermal drift between this mount and the fibre end. The input coupling was also not fully optimized with regard to the position of the beam waist. Therefore the beam diameter incident on the fibre face was larger than the waist size of 392 μm .

As mentioned in section 4.1.4, the KM mirror mount that housed the HR mirror was replaced with a differential drive KS mirror mount. More importantly, the input

coupling of the pump light was optimized, i.e. the beam waist of the pump light now incident on the fibre face. Following this, a second slope efficiency was measured. A significant increase in slope efficiency was found, reaching a value of 37 %. Also shown in Figure 4-25, the output power showed less deviation over time (~ 0.3 W), indicating the improvement of the KS mount stability for the end mirror.

The power density incident on the fibre end was far greater in the optimized case. As a result of this, the fibre was damaged at around 70 W of input pump power, with an output power of 22 W at this point. The un-optimized case allowed the fibre laser to scale to higher output powers, at the cost of a lower overall efficiency. The maximum output power for this case was ~ 29 W, with an incident pump power of ~ 125 W. The corresponding optical-to-optical efficiencies were determined to be ~ 32 % for the optimized setup and 23 % for the un-optimized setup. Threshold for lasing was found to be at pump powers of ~ 13 W for the un-optimized case and ~ 10 W for the optimized case.

During lasing the fibre was found to fluoresce and emit purple/ultraviolet light (Figure 4-26). This is commonly encountered in Thulium-doped fibre lasers, and is due to fluorescence from the 1G_4 energy level to the ground level 3H_6 , typically at a wavelength of ~ 400 nm. The indirect cause of this fluorescence is due to excited state absorption of the Thulium ion, from the 3H_5 level to the 1G_4 level.

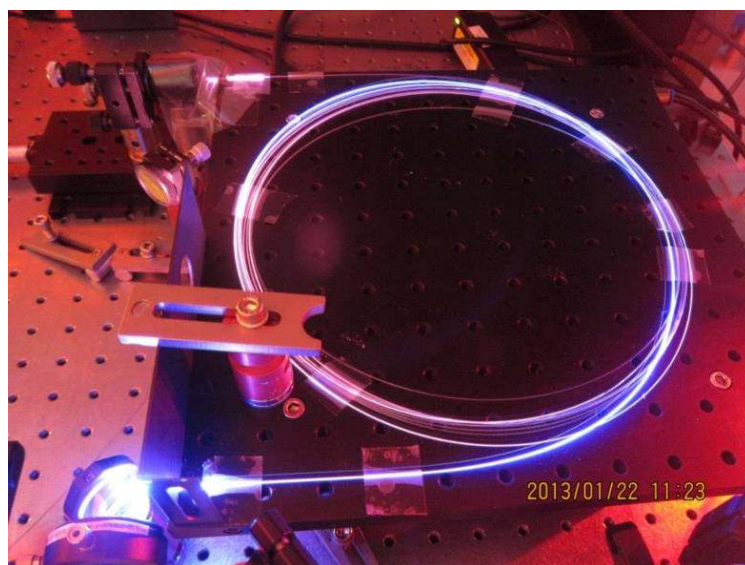


Figure 4-26: Photo of the Thulium fibre during lasing.

The slope efficiency of the setup modified for Q-switched operation (Figure 4-20) but operated in CW, was also measured (Figure 4-27). The setup was optimized with regard to the angles of the flat HR and AOM, as well as the alignment of the pump light.

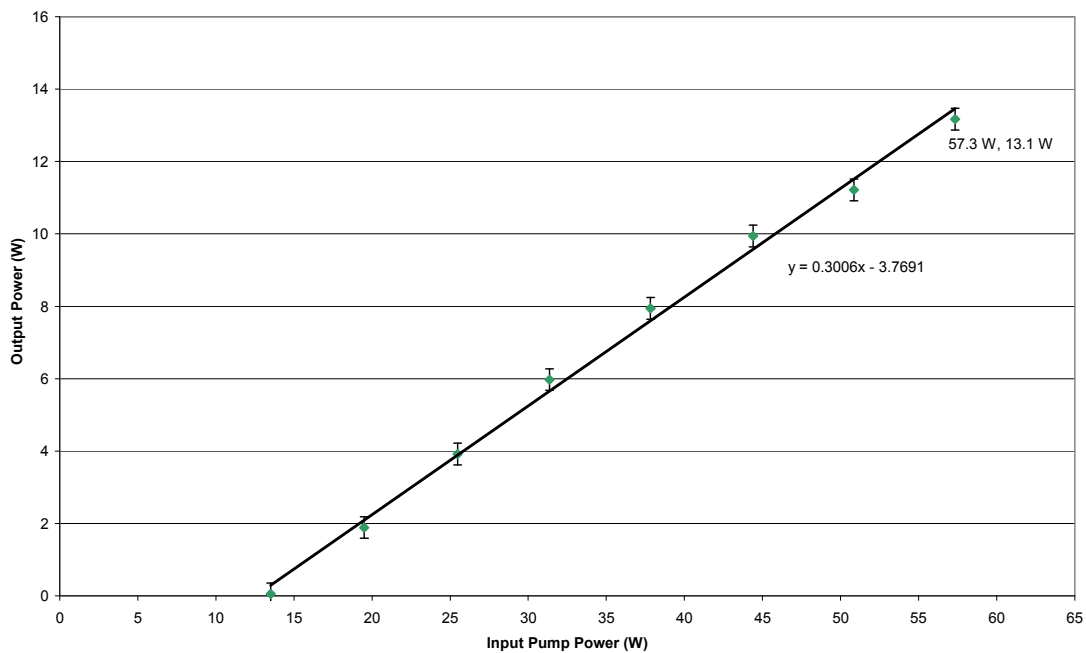


Figure 4-27: Slope efficiency of the Q-switched setup during CW operation, ~6.5 metres fibre length.

The slope efficiency was measured to be lower than the slope efficiency of the CW setup indicated in Figure 4-1. The intra-cavity elements introduced each incurred a loss within the laser setup. As a result a slope efficiency of ~ 30 % was measured and the corresponding optical-to-optical efficiency was determined to be ~ 23 %. The output power fluctuated by approximately ± 0.3 W. It was not possible to get the 6.5 m fibre laser to lase with the addition of the VBG. This is because the specified wavelength of the VBG (~ 1940 nm), is too far from the wavelength emission range of this laser.

4.2.1.1 Short Fibre Laser

The slope efficiency of the fibre laser with 1 metre of fibre was also measured (Figure 4-28). The fibre was angle cleaved at 8.5° to suppress lasing off this fibre end. Lasing was found to occur at approximately 30 W of pump power with two perpendicularly cleaved fibre ends and no HR element for feedback. With the introduction of the angle cleave, lasing was found to occur for much higher pump powers (~ 50 W), confirming some suppression of back reflections from the fibre end. The thin-film polarizer and AOM were also positioned inside the laser cavity for this setup as

discussed in Section 4.1.7. The pump beam size was optimized once again for this case, with a spot size of 392 μm incident on the fibre face. Using the same broadband, flat, HR mirror indicated in Figure 4-21, a slope efficiency of $\sim 20\%$ was measured with a corresponding optical to optical efficiency of $\sim 16\%$. Using the VBG as the feedback element of the laser, a slope efficiency of $\sim 16\%$ was measured, corresponding to a 4% drop in efficiency between this setup and the setup using the flat HR mirror.

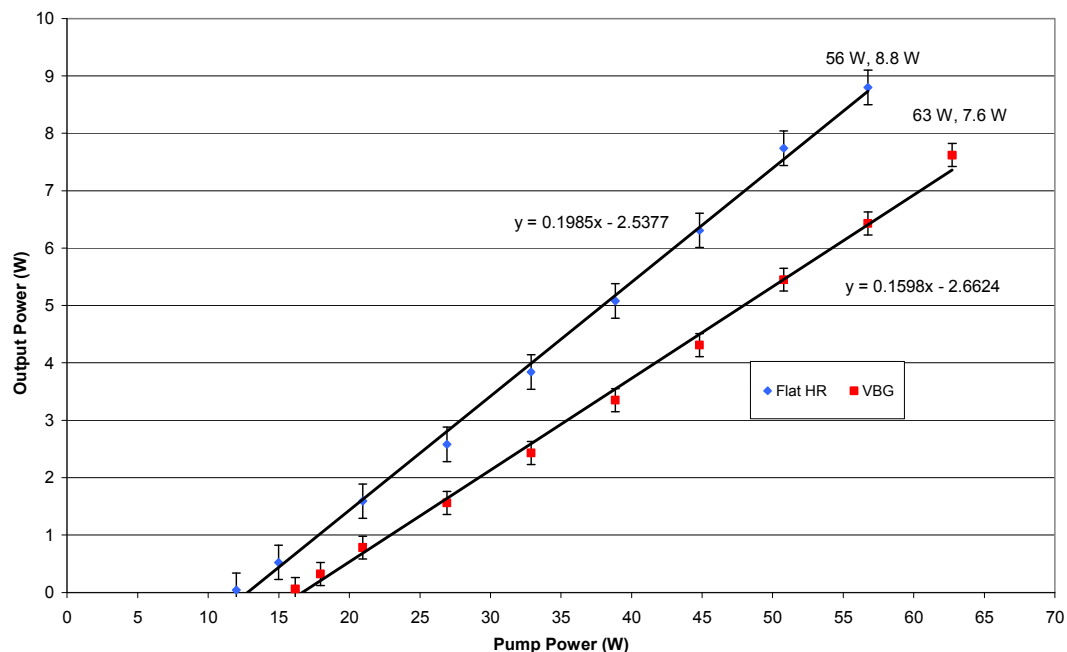


Figure 4-28: Slope efficiency for the 1 metre fibre laser, using a flat HR mirror and VBG.

Fluctuations in the output power were found to be approximately 0.5 W and 0.3 W, respectively, for each case.

4.2.2 Output Spectra

With the monochromator calibrated it was possible to determine the spectral output of the fibre laser for different fibre lengths as well as for different HR components. The spectral output of the following cases was considered:

- Case 1: Initial CW fibre laser, 6.5 m fibre length, low pump power (~ 15 W).
- Case 2: Initial CW fibre laser, 6.5 m fibre length, at 0.3 W, 3.2 W, 12 W, 27 W output power.
- Case 3: Short CW fibre laser, ~ 1 m fibre length, with broadband HR mirror.
- Case 4: Short CW fibre laser, ~ 1 m fibre length, with VBG.

In all cases that follow, the input pump beam was optimized, with a pump beam waist of 392 μm incident on the active fibre face.

4.2.2.1 Case 1

Scanning through the counter readings 328.89 to 379.24 (1.9 μm – 2.1 μm) of the monochromator, indicated signals in the range 361 – 373 (~ 2027 nm – 2075 nm) for the fibre laser with ~ 6.5 m fibre length. A signal was recorded on the oscilloscope via the PbSe detector. The peak to peak value (mV or V) was recorded. The background noise was also removed from all the spectra that follow.

An initial spectrum was measured at low output power (Figure 4-29).

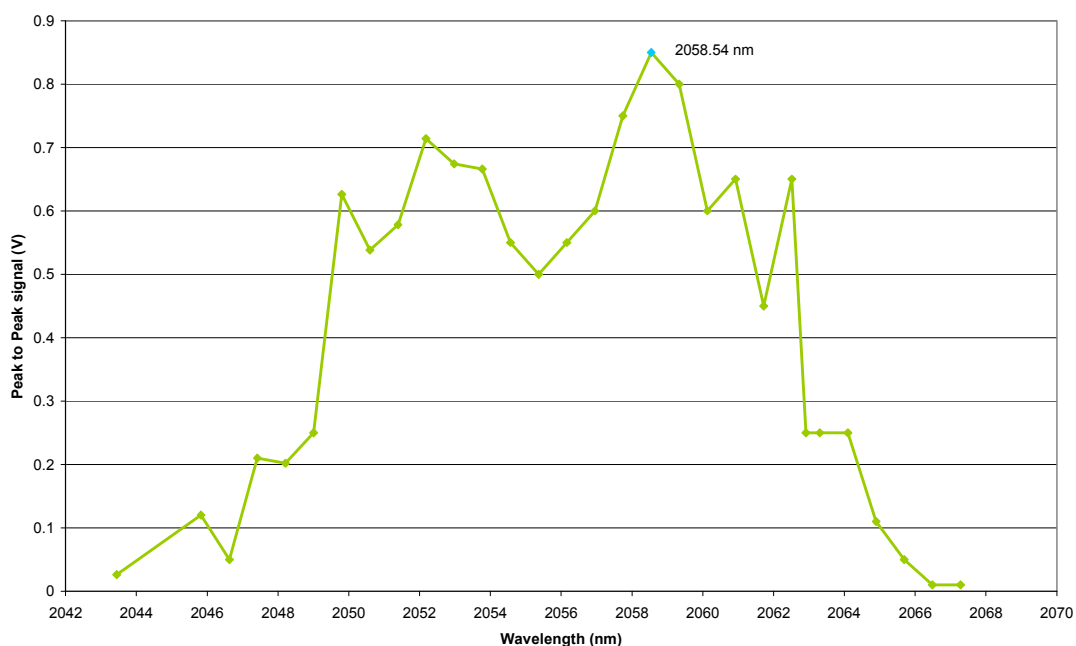


Figure 4-29: low power (0.336 W) spectrum for the Thulium fibre laser, fibre length of ~ 6.5 m.

Output signals were observed within the range of 2044 nm to 2066 nm, and a centre peak located at 2058.54 nm. This result is expected. As was measured in Section 3.2, for long fibre lengths and temperatures closer to room temperature, wavelengths around this region are measured.

4.2.2.2 Case 2

The next step was to obtain spectra for varying pump powers. Spectra for output powers of 0.3 W, 3.2 W, 12 W and 27 W were measured (Figure 4-30).

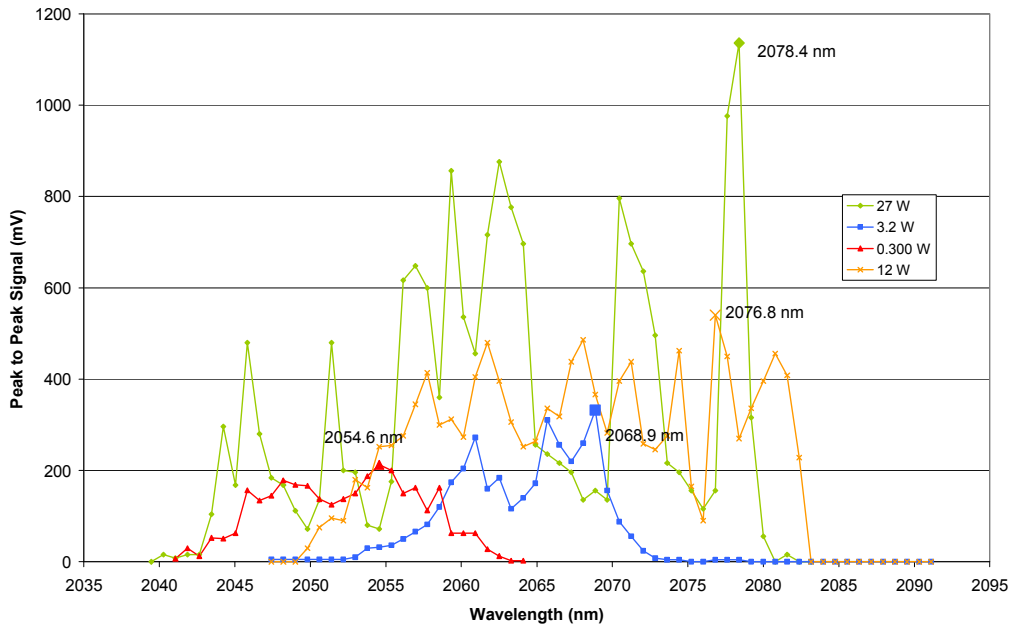


Figure 4-30: Spectral output for varying output powers, ~ 6.5 m fibre length.

An increase in the centre peak and bandwidth of the output spectra for increasing input pump powers was expected. This is due to the fact that the temperature of the fibre is increasing for higher pump powers. As has already been established in Section 3.2.2, higher fibre temperatures result in longer output wavelengths.

From the above spectra a definite shift towards longer output wavelengths was observed. The peaks of the output were also found to move towards longer wavelengths with an increase in the output powers. A large amount of temporal spiking (± 400 mV) of the output signal was observed for each wavelength observed at the exit slit. The output signal and therefore spectra was found to fluctuate rapidly over time. Determining the centre peak of the output was uncertain. It was expected that implementing wavelength control of the fibre laser would minimize these temporal fluctuations. It is possible, however, to observe a definite shift towards longer wavelengths and a broadening of the bandwidth for each spectrum for higher output powers. This is expected due to the fact that the temperature of the fibre is increasing for higher pump powers. As has already been established in Section 3.2.2, higher fibre temperatures result in longer output wavelengths.

The reasons for the fluctuating output signal could be attributed to:

- Water absorption in the atmosphere. The output laser light propagated through a substantial amount of free space (approximately 1.5 metres) before it was

incident upon the PbSe detector. Regions of air with a high H₂O concentration would lead to the intensity of the laser signal fluctuating.

- During the measurement time, it is possible that there was substantial mechanical drift, caused by thermal expansion, between the fibre ends and other mechanics within the optical setup. This leads to small misalignments of the input coupling of pump light, as well as misalignment of the high-reflective feedback element, causing a change in measured signal strength on the PbSe detector.
- The operating dynamics within the laser itself. Since a broad HR mirror was used to constitute the resonator and owing to the three-level dynamics of the Thulium ion, the laser output was found to lase on many different wavelengths. This resulted in a broad, fluctuating spectrum.

4.2.2.3 Case 3

The output spectrum for the fibre laser with 1 metre fibre length was also measured and compared to the 6.5 metre fibre laser at the same output power (Figure 4-31).

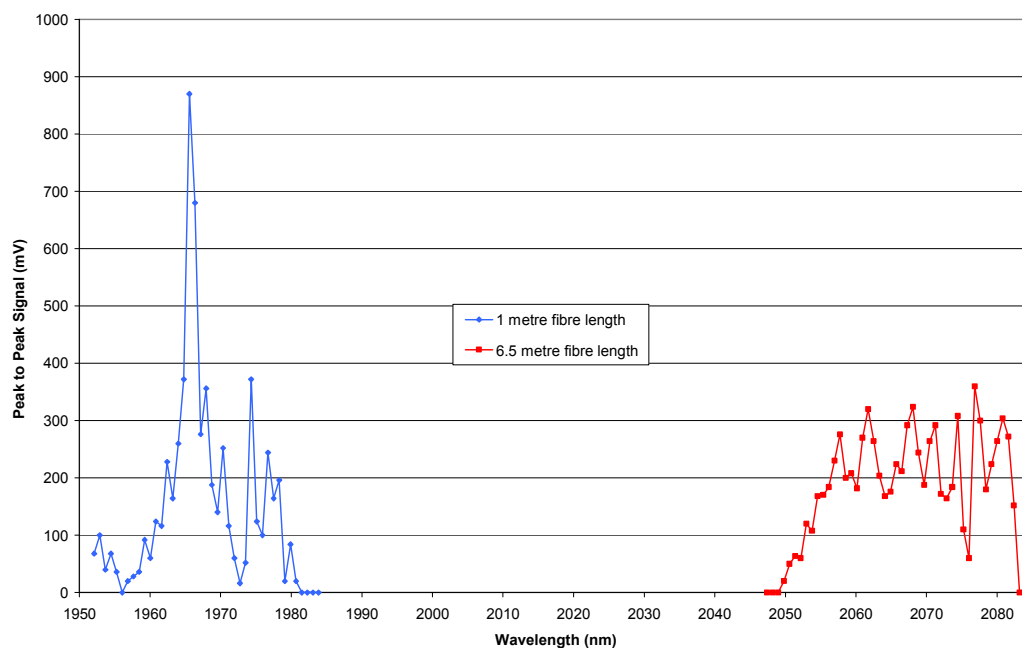


Figure 4-31: Output spectra for the two fibre lengths at constant output power of ~3W.

Shorter output wavelengths were measured for the 1 metre fibre laser, with a wavelength range of ~ 1955 – 1980 nm. The difference in signal strength between the 1 m and 6.5 m fibre laser output is due to different attenuating optics used in the

diagnostic layout (Figure 4-23). The shorter output wavelengths for the 1 m fibre length are expected, as there is less re-absorption/ground state absorption taking place within the fibre. Therefore shorter output wavelengths are encountered. The same fluctuations were present within the output signal for the short fibre laser.

4.2.2.4 Case 4

In order to attempt to limit the fluctuations observed in the measured output spectra and obtain a narrow wavelength output, the VBG was implemented into the setup and the output spectrum was measured (Figure 4-32).

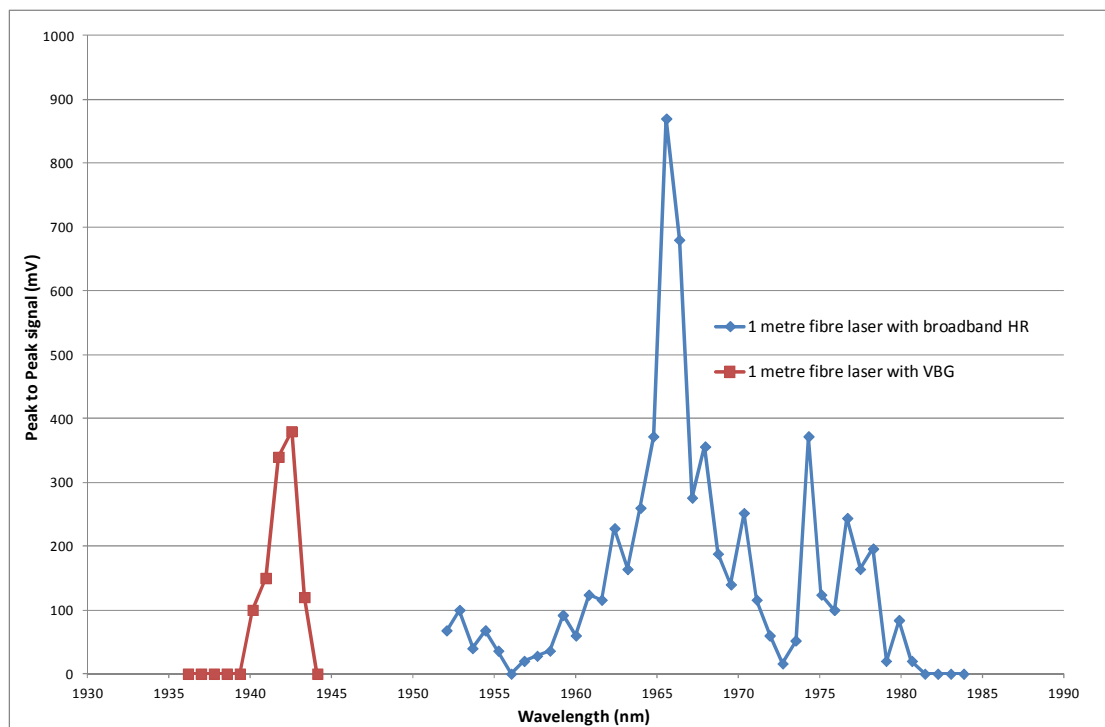


Figure 4-32: Output spectrum of the 1 metre fibre laser, with broadband HR and VBG, 1 W output.

The spectral output indicates that the fibre laser lased on a very narrow bandwidth, with a centre peak located at ~ 1942 nm. This is 2 nm higher than the specified operating wavelength of the VBG, which was 1940 nm. However, as was mentioned in Section 4.1.9.1, the monochromator has a measurement accuracy of 2.5 nm, therefore could not accurately resolve a difference between 1940 nm and 1942 nm. It is also possible that minor errors in the calibration of the monochromator could lead to a measured wavelength of 1942 nm instead of 1940 nm.

To conclude this section, the spectral output of the CW, Thulium-doped fibre laser was measured. The wavelength was measured for two fibre lengths. Shorter

wavelengths were encountered for shorter fibre lengths. Additionally the wavelength was measured for varying pump and output powers. An increase in longer wavelengths was encountered as well as a broadening in the output spectrum. A VBG was implemented into the 1 m fibre laser and the spectrum of this laser was measured. The measurement revealed that lasing was found for a narrow wavelength range, close to the specified operating wavelength of the VBG itself.

4.2.3 Temporal Behaviour/Fluctuations

The fluctuations in the temporal behaviour of the laser output were investigated. The laser light was reflected from a flat, 45° high reflective mirror (M_4) towards another flat partial reflector ($R = 98\%$), Figure 4-23. The reflected light was dumped onto a beam block. An InGaAs photo-detector (PDA10D-EC, $1.2 \mu\text{m} - 2.6 \mu\text{m}$) was orientated to face the beam block (Figure 4-33). The front of the detector was surrounded by a lens tube and iris which helped to reduce background signal and attenuate the signal incident upon the detector.

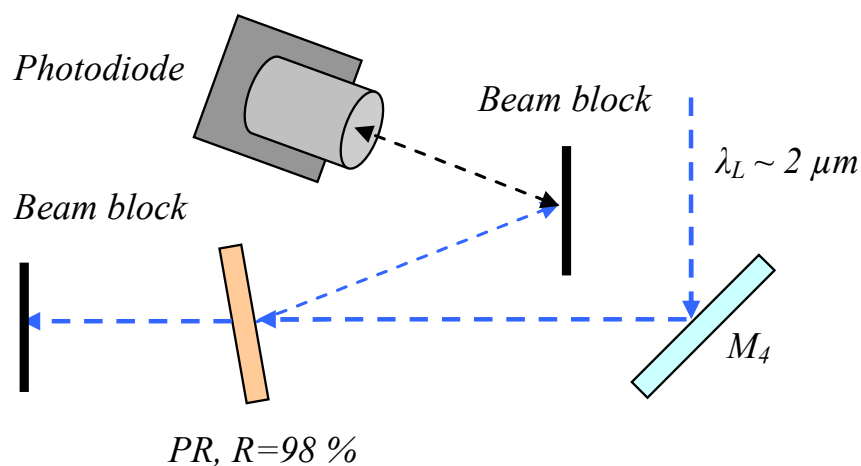


Figure 4-33: Schematic of the diagnostic layout used to observe temporal behaviour of the laser output.

The detector was connected to an oscilloscope and the temporal behaviour was observed (Figure 4-34).

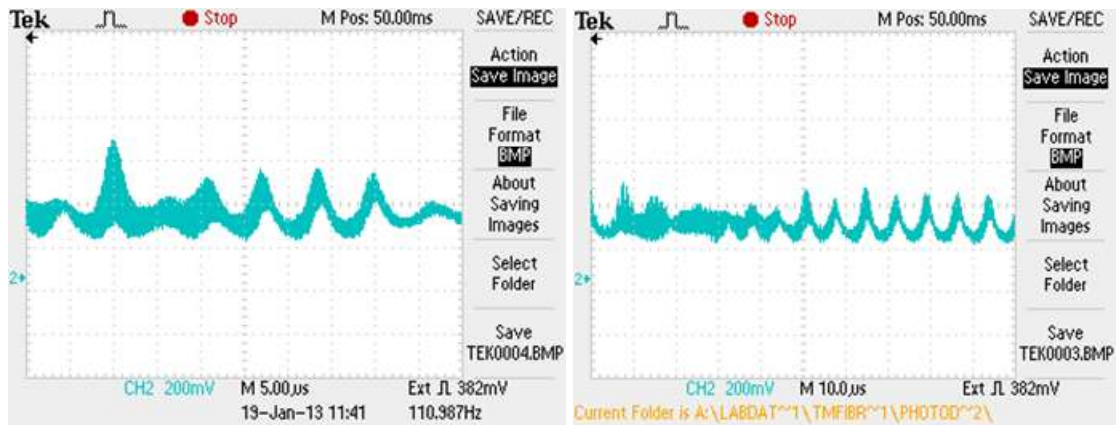


Figure 4-34: Temporal jitter of the 6.5 m fibre laser for two different time scales (1 W output).

The output signal was observed to fluctuate over time, with a certain periodicity. The period of these fluctuations was measured to be $\sim 5 \mu\text{s}$. The output contained periodic spiking or pulses. Initially it was thought that this temporal behaviour was due to relaxation oscillations. However, deliberate mechanical disturbances did not lead to a change in the observed behaviour or structure of the output signal. As was discussed in Section 2.2, this ‘self-pulsing’ has been a matter of continued interest. The self-pulsing behaviour was also observed for the laser with the VBG as the high-reflector (Figure 4-35).

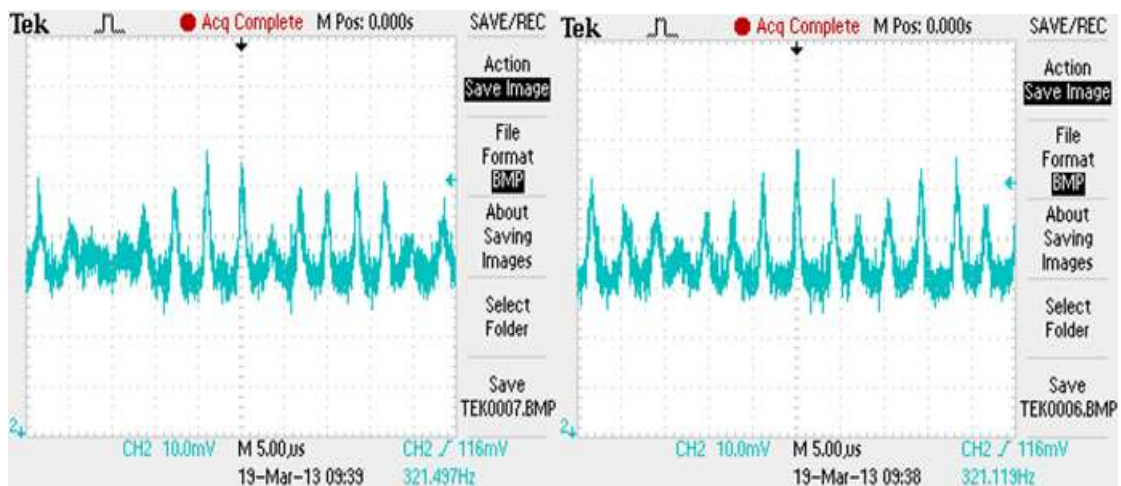


Figure 4-35: Output signal for the 1 metre fibre laser, with the VBG has feedback element (1 W output).

For each case, the spiking or pulses encountered constituted approximately 20 % of the total output signal. It was noted that the duration of these pulses was dependent on the fibre length. For the 6.5 m fibre laser, the self-pulses had durations of approximately $5 \mu\text{s}$, whereas for the 1 metre fibre laser the pulse durations decreased to approximately $1 \mu\text{s}$. It was also observed that the duration and frequency of these self-pulses were dependent on the amount of pump power (Figure 4-36).

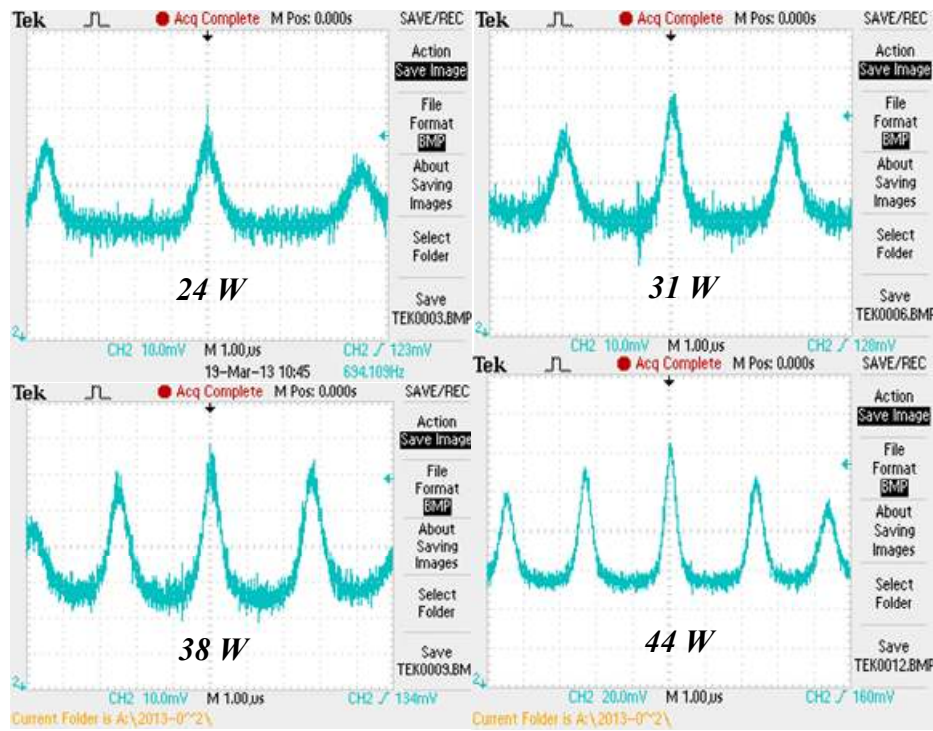


Figure 4-36: Self-pulses in the output signal for increasing pump powers, 1 metre fibre length, with VBG.

The pulse durations and frequencies were characterized for different pump powers (Figure 4-37).

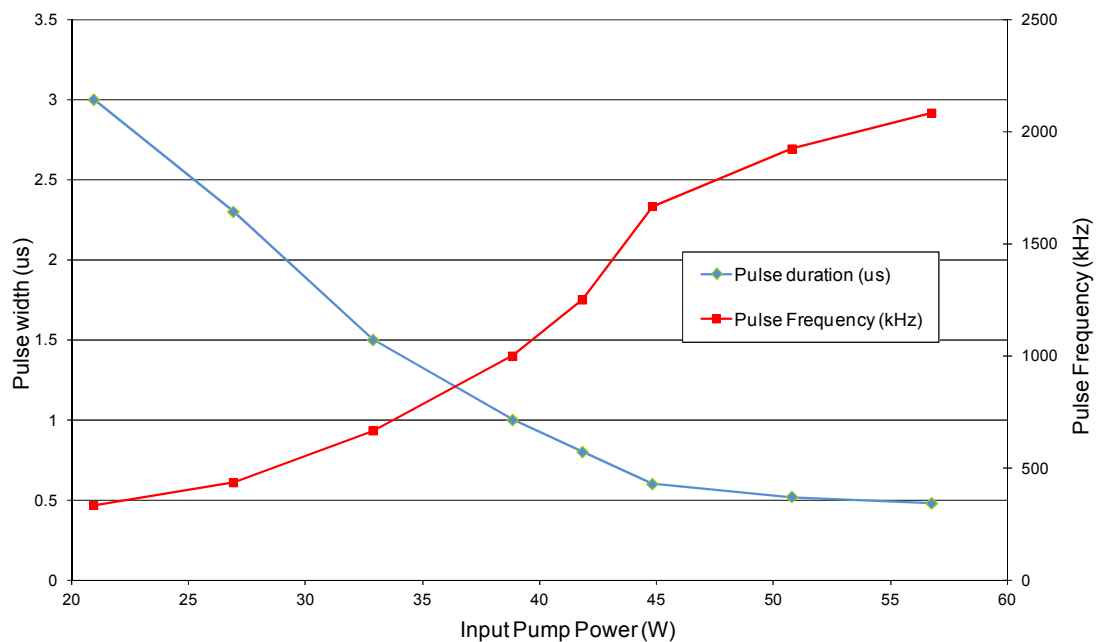


Figure 4-37: Self-pulse durations and frequency for varying pump powers.

It was observed that for increasing pump powers the duration of these self-pulses decreased almost linearly. However, for higher pump powers the pulse durations showed less of a decrease. The limit of the duration of these pulses is most likely

dependent on the total cavity length of the fibre laser. Similarly, for higher pump powers, the frequency of these pulses increased. These results are in good agreement with those reported in [34].

4.2.4 The Beam Profile of the Laser Beam

Certain applications require a laser beam with a stable and radially symmetric beam profile. It is therefore necessary to know the intensity distribution of the beam, how it evolves over time and what other laser parameters might affect this distribution. A Spiricon Pyrocam III was used to observe the beam profile of the fibre laser. Silicon based cameras are not compatible for wavelengths in the mid-infrared, therefore the Pyrocam proved to be ideal for these purposes. By making use of the Pyrocam it is possible to observe distinctive features in the beam profile, which in turn yield information related to the actual laser setup. It also affords the option of observing the stability of the laser beam profile over time and what components, in the laser setup, may have an influence upon this stability. The collimated light reflected by the 45° flat high reflector (M4, Figure 4-23), was directed towards the entrance aperture of the Pyrocam. The appropriate partial reflectors and filters were used to attenuate the laser beam sufficiently. The damage threshold of the Pyrocam is significantly lower than that of silicon based CCD cameras. The beam profile and its evolution over time, was observed for different output powers (Figure 4-38).

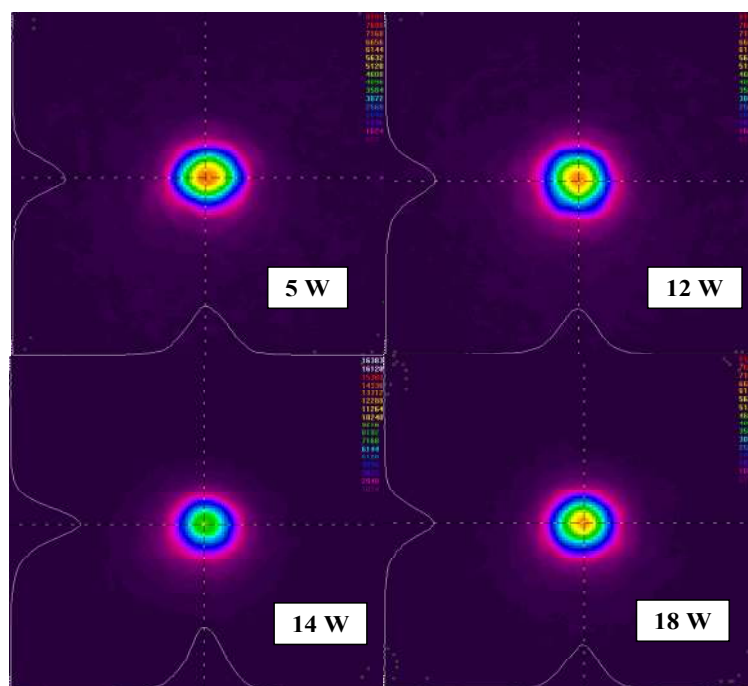


Figure 4-38: Beam profile of the laser beam for increasing output powers.

The observed intensity profile appeared to have a Gaussian structure. Also, the structure of the beam profile appeared to improve for higher output powers. The measurements suggest that a single-mode beam was obtained, and that the fibre laser was lasing on the lowest order mode LP_{01} .

Another observation made was the distortion of the beam profile with minor misalignments induced upon the high-reflective feedback element (Figure 4-39).

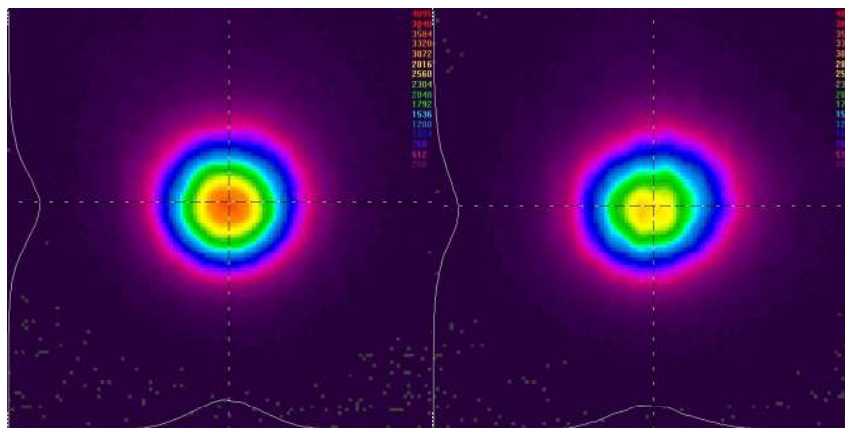


Figure 4-39: Distortion in the beam profile of the laser beam due to minor misalignment of the HR mirror – 3.7 W & 3.5 W output power.

The KS1D differential drive mounts offer a maximum angular adjustment of 1.5° . According to the supplier, a full rotation of the fine adjustment (via hex-screws) corresponds to an angular displacement of $660 \mu\text{rad}$ or 0.04 degrees. The high-reflector mount had previously been optimized, producing the symmetric beam profile in Figure 4-39. A half rotation (0.02 degrees angular displacement) was applied to the tilt-axis of the KS1D mirror mount. A drop in the output power (0.2 W) occurred as expected. What was also noted was a distortion in the intensity profile of the beam itself. The symmetry of the profile is lost with minor adjustments and the beam appeared to become slightly astigmatic.

The beam profile for the 1 metre fibre laser, utilizing the VBG was also observed (Figure 4-40). After initial alignment of the laser, the structure of the beam was heavily-distorted. To correct this, adjustments were made to the alignment of the VBG as well as for the pump diode optics. With adjustment, gradual improvement in the beam profile became apparent. It was concluded that the angle cleave of the fibre end-face distorted the symmetry of the beam profile. Improving this beam profile was challenging, as the VBG was not mounted onto a stable mirror mount (KS1D) but

rather a conventional KM mount (Thorlabs). Therefore fine-adjustments to the alignment of the VBG were not possible.

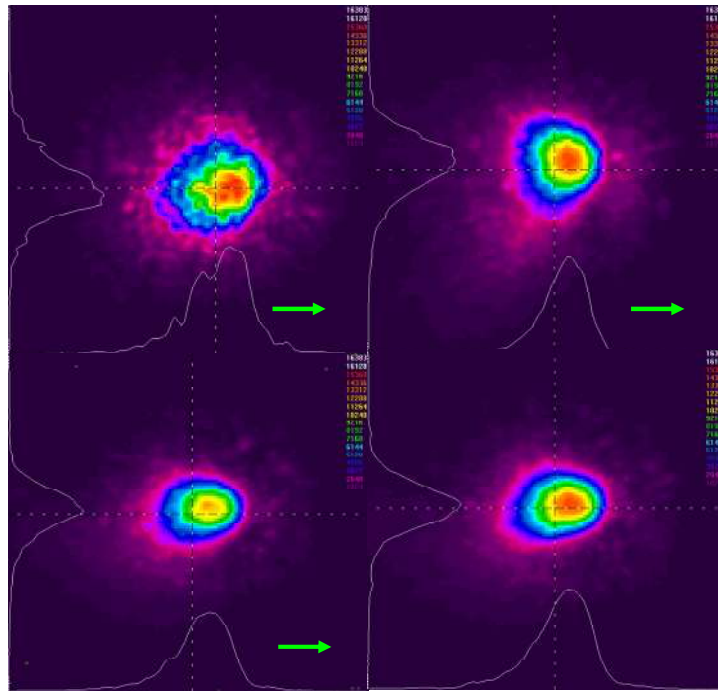


Figure 4-40: Gradual improvement of the beam profile for the 1 metre fibre laser with VBG. Angled cleaved fibre end. 1 W output power.

Beam wandering was also apparent in observing the beam-profile. This gives an indication of atmospheric absorption taking place. As the propagation distance of the laser beam to the Pyrocam was relatively large, this was plausible. This beam wandering was not observed for the beam profiles generated for the 6.5 metre fibre laser, with a broadband high-reflector (Figure 4-38), suggesting less atmospheric absorption at the longer output wavelengths.

In conclusion, the beam profile of the fibre laser was measured and observed for different fibre laser configurations. As the fibre had a small core diameter ($25\ \mu\text{m}$) and therefore small V-parameter value (~ 3.5), a single-mode beam was expected. This is slightly higher than the cut-off V-parameter value for single mode operation (~ 2.405). However, as was discussed in Section 4.1.1.3, Large-Mode Area (LMA) fibres can be coiled to suppress the formation of higher-order modes. The stability of the resonator optics was found to have an influence on the measured beam profile. Additionally, the angle cleave of the active fibre end-face was found to induce a distortion in the beam profile. This suggests the significance of the correct launch and alignment angles of the feedback element and pump optics.

4.2.5 M^2 measurement

As was discussed in section 2.1, the M^2 or beam-quality factor of a beam is a value which gives an indication of how closely the beam resembles an ideal Gaussian beam.

Initially it was attempted to determine the M^2 of the laser beam with the aid of the Pyrocam. A plano-convex lens with a focal length of 200 mm was used to focus the collimated beam. However, the spot size generated at the focus (and points near to this) were too small for the Pyrocam to accurately resolve. Also it was not practical to use a lens with a longer focal length, due to insufficient working space. Therefore, the 90/10 knife edge technique was employed to measure the laser beam diameter and determine the M^2 value. The measured beam radii at different propagation distances are shown in Figure 4-41, as well as the Gaussian beam propagation fit.

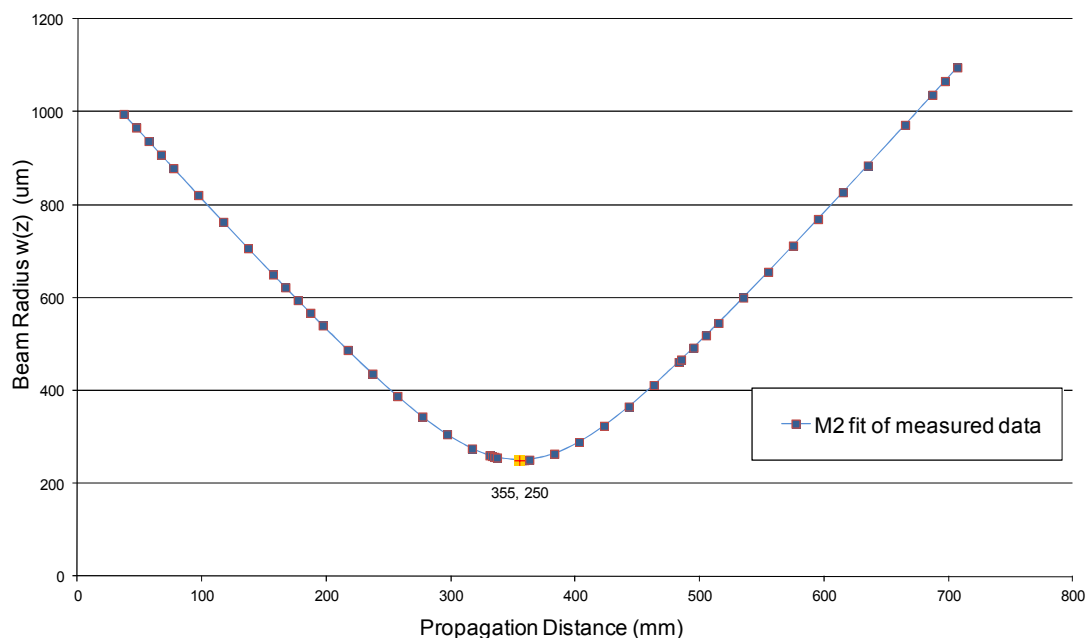


Figure 4-41: M^2 measurement for the Thulium fibre laser.

The measurement was performed for the 6.5 m fibre laser utilizing the broadband HR mirror described in section 4.2.1. The least-squares fit of the measured data resulted in an M^2 value of 1.15. This value is typical of fibre lasers and, as was discussed in Chapter 1, is one of their main attractions. The measurement agrees with the initial assessment of the beam quality by observing the intensity beam profile shown in Figure 4-38. A very low M^2 value was expected for the fibre laser, as the intensity profile of the beam resembled a symmetric Gaussian. The fit to the measured data is adequate considering the temporal fluctuations mentioned previously in Section 4.2.3.

The fluctuations increased the uncertainty of the beam radius measurements and made the experiment challenging.

4.2.6 Polarization

The polarization of the fibre laser output was determined with the aid of a polarizing cube. The cube was produced by CASIX and has a specified wavelength range of 1890 – 2064 nm. As was mentioned in Section 4.1.1, the active fibre used in these experiments was not polarization maintaining.

For the CW setup indicated in Figure 4-1, the laser output was found to be randomly polarized. That is, for any rotation angle of the polarizing cube, the power of the transmitted beam was always equal to 50 % of the total power.

The same measurement was done for the 1 metre fibre laser without any intra-cavity elements. The laser output for this case was also found to be randomly polarized, indicating that, for this laser configuration, the length of active fibre had no influence on the polarization of the output.

As was discussed in Section 4.1.7, it was necessary to establish or confirm that the laser output was vertically polarized for proper operation of the AOM. After the introduction of the 45° polarization sensitive mirror (Figure 4-20), the polarization of the CW output was measured with the polarizing cube.

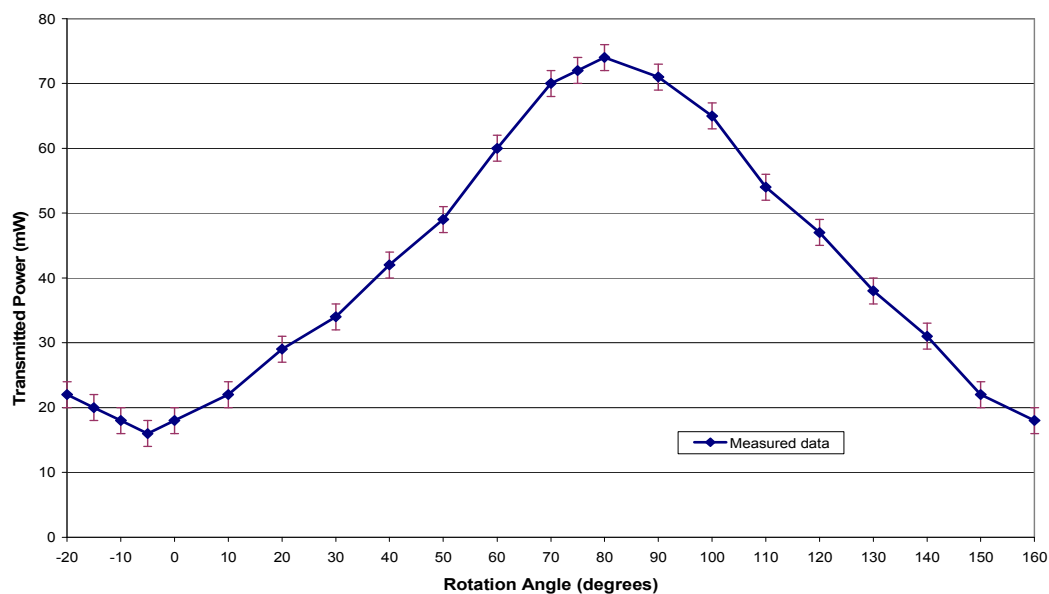


Figure 4-42: Transmitted output power through the polarizing cube, for different rotation angles. 80 mW total power.

The total laser output was measured to be ~ 3 W. The laser light was attenuated so that the total power incident on the polarization cube was 80 mW. The transmitted power through the cube was plotted for different rotation angles of the cube (Figure 4-42). The total power of 80 mW was never fully transmitted for any rotation angle. However a significant amount of power was still transmitted when the cube was rotated to allow the transmission of vertically polarized light. This suggests that the 45° mirror is introducing a loss on the horizontal polarization, forcing the laser to lase partially on the vertical polarization. Very little laser light, reflected by the cube, was observed.

With the addition of the thin film polarizer in place of the 45° mirror (refer to Section 4.1.7), the same result was obtained for the polarization of the output beam. Since the total power is never fully transmitted, this suggests that the fibre itself is partially influencing the polarization state of the output beam. It is likely that the bending/coiling of the active fibre is leading to stress-induced birefringence, causing slight de-polarization of the laser output. However, it is also possible that some of the laser light is being absorbed into the polarization cube, explaining the absence of the remaining power in Figure 4-42.

4.2.7 Q-switched Operation

As was discussed in Section 4.1.7, the optical setup was modified to operate the laser in Q-switch mode. The goal is to obtain stable laser pulses for different pulse repetition frequencies (PRF) and laser output powers. The AOM can be triggered at different repetition rates, resulting in a desired PRF of the fibre laser. Shown in Figure 4-43 is an oscilloscope screenshot of the output of the Q-switched fibre laser. The blue trace is the output signal of the laser, indicating its pulses (measured with a fast PEM detector). The green trace is the laser output measured with an InGaAs photo-detector. The purple trace represented the signals generated by the signal generator. Pulses generated become rapidly unstable and inconsistent over time.

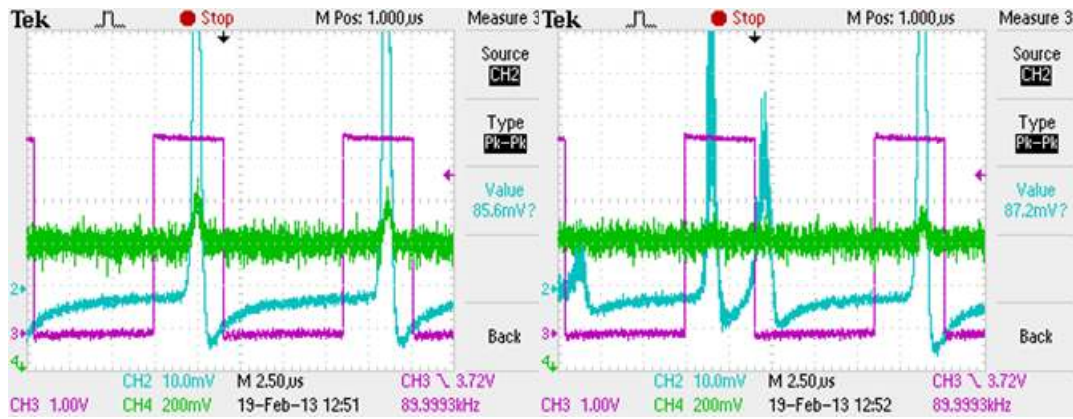


Figure 4-43: Stable pulse generation (a) followed by erratic pulsing (b), repetition rate of 90 kHz, 12 W output power, 6.5 metre fibre length.

By adjusting the pump power, repetition rate and other factors, it was possible to obtain stable pulses (Figure 4-44). However, there was uncertainty regarding these pulses due to the erratic pulsing encountered. More specifically, it was uncertain if this was purely Q-switched operation of the laser, or a mixture between CW and Q-switched operation.

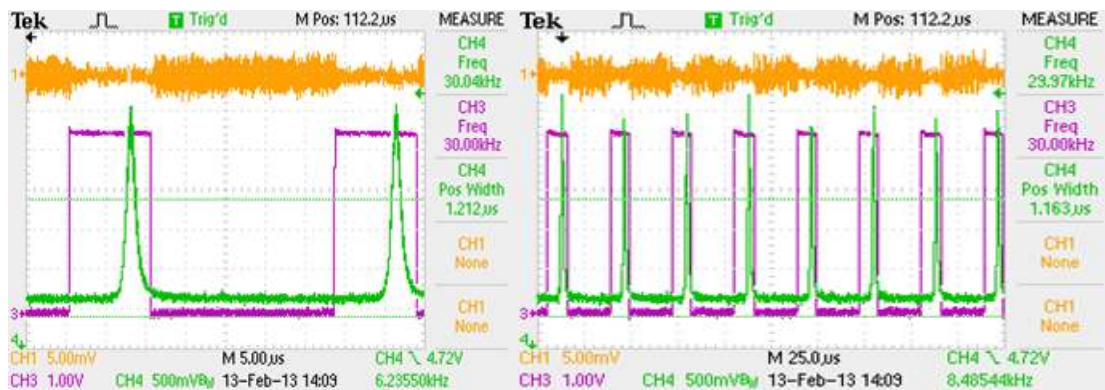


Figure 4-44: A stable pulse train at 30 kHz repetition rate, 2 W output power, 6.5 metre fibre length.

In order to correct this erratic behaviour and attempt to ensure the laser operates in one regime (CW or Q-switched), the fibre length was reduced to 1 metre. It was thought that this may reduce the amount of gain in the laser and therefore the loss introduced by the RF signal/AOM may be more effective. In addition the VBG was implemented into the setup to force the laser to operate on a very narrow wavelength output. The same behaviour occurred for this setup, with breakthrough (insufficient hold off or loss introduced into the setup, by the AOM) occurring for a range of pulse repetition rates and pump powers (Figure 4-45). For higher pump/output powers breakthrough lasing becomes more pronounced.

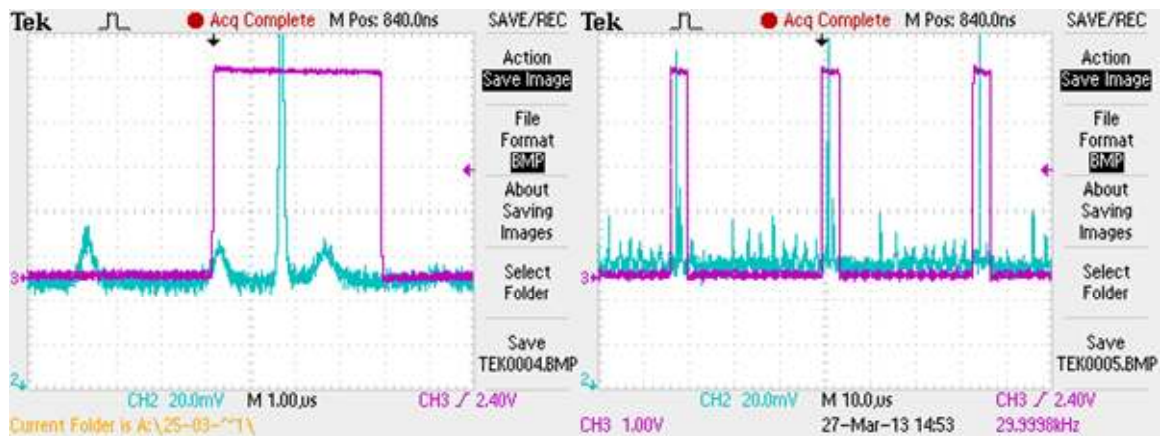


Figure 4-45: Breakthrough lasing during Q-switched operation seen at two different time scales and output powers. 30 kHz, 2W and 3W output power.

At very high repetition rates (> 90 kHz) a new behaviour was observed in the pulses generated. Pulses were ‘skipped’ and only occurred every second cycle (Figure 4-46). This behaviour was also apparent when the open time (or off time for the Q-switch) was made sufficiently small. The open time is too short for the pulse to be released every cycle and therefore the pulse occurs every second cycle.

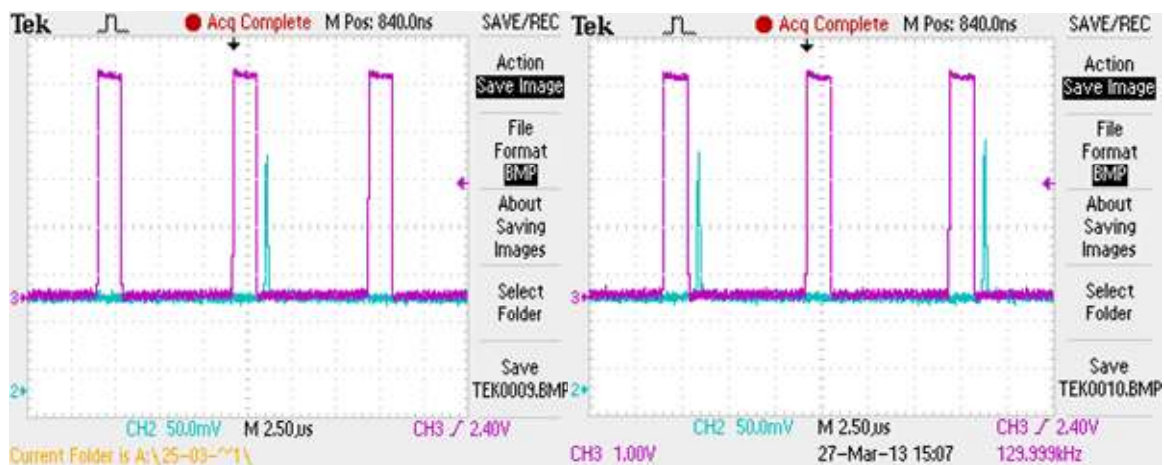


Figure 4-46: An irregular Pulse train, 150 kHz, 1 W output power.

A stable operating set of parameters was found, specifically with regard to the input pump power. Therefore it was possible to partially characterize the performance of this Q-switched laser, with regard to the energy of the pulses, their duration and peak powers. The pulse durations were measured with the aid of the oscilloscope. With the pulse durations and output power known (2 W), it was possible to characterize the pulse energy over a range of pulse repetition frequencies (Figure 4-47).

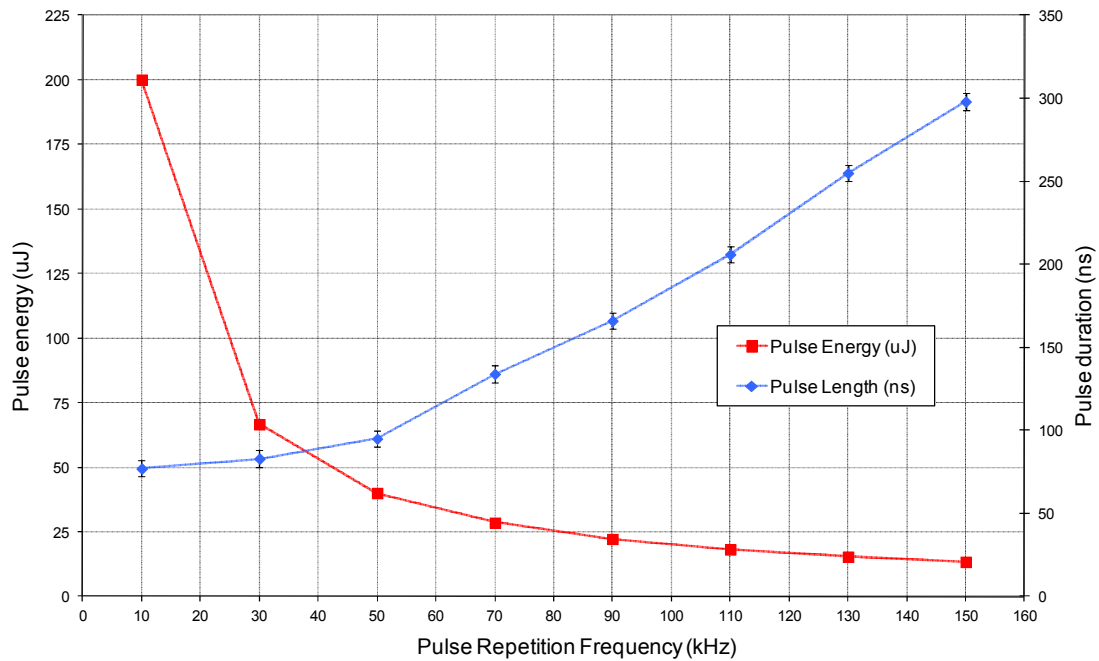


Figure 4-47: Pulse Energy (μJ) and Pulse Duration (ns) for varying repetition rates (kHz) at a constant output power of 2 W.

At a repetition rate of 10 kHz and laser output power of 2 W, pulses with an energy and duration of 200 μJ and ~ 77 ns respectively, were obtained. This yields a pulse peak power of ~ 2.6 kW. This behaviour is expected, namely the pulse energy decreased with an increase in the pulse repetition frequency and the pulse length increases. These trends agree with those found in the literature. This behaviour is due to the fact that there is less time for gain or energy to be stored in the gain medium before the onset of the next pulse. Therefore pulses with lower energy are generated for a higher repetition rates. For increasing repetition rates an increase in the pulse durations was measured. As was just mentioned with higher repetition rates there is less build of gain before the onset of the next pulse. Since the gain is less, the pulse takes longer to reach the saturation energy of the gain medium. This leads to a longer build up time of the pulse, implying longer pulse durations for increasing pulse repetition frequencies.

4.3 Summary & Discussion

In summary, a CW and Q-switched Thulium-doped fibre laser was designed and developed. The results obtained for the different laser configurations and mode of laser operation (CW or Q-switched), are summarized in the following table:

Table 4-3: Summary of results obtained for the Thulium doped fibre laser.

<i>Configuration</i>	<i>Feedback element</i>	<i>Fibre length (m)</i>	<i>Output Wavelength (nm)</i>	<i>CW Slope efficiency (%)</i>	<i>Fibre cleave</i>	<i>Polarization</i>	<i>Max. Output Power(W)</i>	<i>M² value</i>
CW	HR mirror	6.5	~ 2020 - 2070	37, 26	90°	Random	22, 30	1.15
CW	VBG	6.5	Non-lasing	Non-lasing	8.5°	Random	-	-
CW	HR mirror	1	~ 1960 - 1980	20	90°	Random	9	1.15
CW	VBG	1	1940	16	8.5°	Random	~ 8	-
CW (with 45° pol. mirror)	HR mirror	6.5	~ 2020 - 2070	30	8.5°	Vertical	13	-
CW (with thin-film pol.)	VBG	1	1940	16	8.5°	Vertical	~ 8	-
Q-switched	HR mirror	6.5	~ 2020 - 2070	30	8.5°	Vertical	13	-
Q-switched	VBG	1	1940	16	8.5°	Vertical	~ 8	-

A range of high-reflective elements were used to constitute the laser resonator. Two lengths of active fibre were used to develop the laser, ~ 6.5 metre and ~ 1 metre. For 6.5 metres of fibre length initial slope efficiencies of 37 % and 26 % were measured for CW operation, with total output powers of 22 W and 30 W respectively. The wavelength output was measured to be in the region of ~ 2020 nm – 2070 nm, dependent on the input pump power. For 1 metre of active fibre a slope efficiency of 20 % was obtained with a flat HR mirror to constitute the laser resonator. The wavelength output was measured to be in the region of ~ 1960 nm – 1980 nm. Replacing this with a VBG lowered the slope efficiency to 16 %, but offered a narrow wavelength output centred on ~ 1942 nm. The temporal behaviour of the CW output was also studied. Results indicate self-pulsing behaviour, consistent with results in the

literature. The parameters of these self-pulses were found to vary according to the pump power and were therefore characterized for different pump powers.

The beam profile of the fibre laser was also observed. The resulting profile resembles a symmetric Gaussian. The structure of the beam profile was found to be sensitive to alignment of the pump light as well as the HR element. The structure of the beam profile was also found to be dependent on the structure of the fibre ends. The angle cleave of the fibre end appeared to distort the symmetry of the profile. A 90/10 knife-edge measurement was performed to determine the beam quality factor (M^2) of the laser beam. Results yield an M^2 value of 1.15.

Q-switched operation was undertaken with an AOM acting as the Q-switch. Performance was studied for both the 6.5 metre and 1 metre length of active fibre. In both cases breakthrough lasing occurred, indicating insufficient hold off. For the 1 metre fibre utilizing the VBG as feedback element, stable pulses were obtained for a set output power of 2 W allowing partial characterization of Q-switched performance. At a repetition rate of 10 kHz, pulses with an energy and duration of 200 μ J and ~ 77 ns respectively, were obtained. This yields a maximum pulse peak power of ~ 2.6 kW.

The results obtained are in good agreement with those commonly reported in the literature. Future work and recommendations for further power scaling are discussed in the following section (4.4).

4.4 Recommendations & Future Work

The results achieved reveal much about the behaviour of the fibre laser developed. In addition, these results indicate important factors which influence performance and stability of the laser itself. It is believed that the fibre laser developed can be improved in the following ways:

- Ideally the laser should be encased in a dry-air box. The water absorption at the wavelengths measured will lead to spiking in the output signal. Additionally, water absorption will lead to beam wandering of the actual beam, as was encountered in section 4.2.4.

- There is passive/un-doped fibre available. The core and cladding diameters of this fibre match those of the active fibre. It is therefore possible to splice the un-doped fibre onto the active fibre. This affords the opportunity of cooling the active fibre ends directly, providing more efficient cooling and improved laser performance. This should also allow further power-scaling of the Thulium-doped fibre laser.
- Results encountered in Sections 4.2.1, 4.2.2 and 4.2.4 highlight a large amount of mechanical instabilities within the fibre laser setup. The fibre ends are currently mounted onto a cooling plate via standard adhesive tape. This is not the most stable solution and a more robust mounting option is essential. In addition, pump light is incident upon the high-reflective element leading to thermal drift and hence misalignment. Cooling the feedback element may be necessary to ensure long-term stable performance.
- As mentioned in Section 4.1.2, there are two 65 W fibre coupled laser diodes that were procured from Apollo Instruments. It is possible to make use of both of these diodes and dual pump the active fibre. This could lead to an increase in the laser efficiencies encountered so far (Section 4.2.1). For a single pumped end, there will be less pump power at the other end of the active fibre due to absorption in the core and attenuation in the fibre material. This is especially true for long lengths of active fibre. By pumping the fibre from both ends, this would provide more pump power through out the total length of fibre. In addition, since the damage threshold of the active fibre end was found to be around 70 W of pump power, the fibre ends are essentially safe from damage in this configuration.

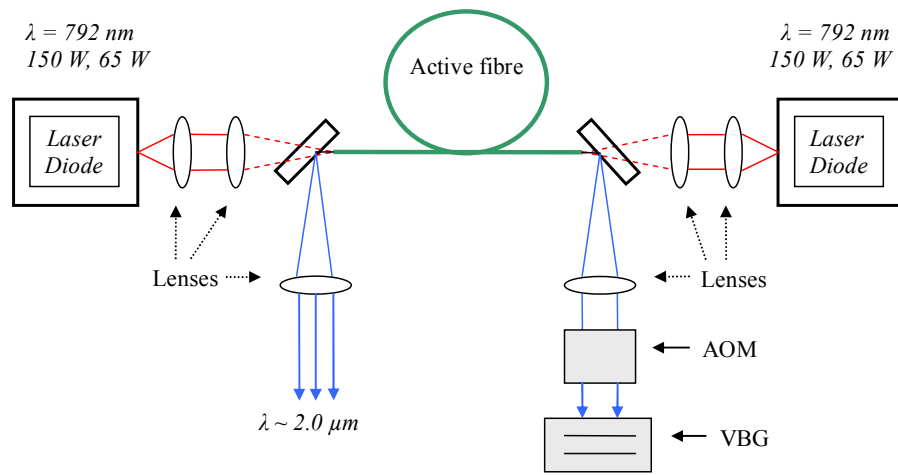


Figure 4-48: Proposed Dual end pumped configuration for the Thulium-doped fibre laser.

- The length of active fibre needs to be optimized with regard to the slope efficiency.
- As encountered in Section 4.2.7, the AOM is not providing sufficient hold off or loss in the laser cavity. The angle of the AOM was adjusted by hand. A mount which will allow finer adjustments of this angle will lead to a better diffraction efficiency and hence better hold off. It is also possible that the 20 W of RF power is insufficient for optimal Q-switching. Additionally the AOM is polarization sensitive, requiring some means of polarization control into the laser setup. This incurs additional losses into the setup. As the polarization was measured (Section 4.2.6) and the output was found to be only partially polarized, an AOM that is polarization insensitive would therefore be more suitable.
- Another active fibre with a core and cladding diameter of 25 μm and 250 μm was procured from Nufern. Another fibre laser could be developed with this active fibre.

5 Conclusion

Thulium doped fibre lasers are promising sources of mid-infrared ($\sim 2 \mu\text{m}$) light. There are a range of applications which require light that is centred on this wavelength. These include, but are not limited to: LIDAR and remote sensing [1], medical surgery [2], directed infrared counter measures (DIRCM) [3] and optical pumping of other laser systems [4,5,6]. Fibre lasers have certain properties which make them ideal for these applications. They are robust, potentially more efficient and can be scaled to very high powers ($> 1 \text{ kW}$). Motivated by these reasons, ongoing research has led to the highest CW output from a Thulium-doped fibre laser of 1 kW [8]. A pulsed peak power of $\sim 9 \text{ kW}$ was recently reached for Q-switched operation [49]. These results indicate that Thulium-doped fibre laser are promising laser sources, where $\sim 2 \mu\text{m}$ light is required. Therefore, in light of this and recent results obtained in the literature, the aim of this thesis was to establish expertise in Thulium-doped fibre lasers.

Chapter 1 and Chapter 2 covered background theory and information relevant to the functioning and design of fibre lasers. The favourable properties and advantages of fibre lasers were highlighted. The main factors limiting power-scaling of these devices were underlined. In Chapter 2, the energy-level structure of the Thulium ion was discussed as well as energy transfer processes relevant to lasers utilizing Thulium as the active ion. Common fiber laser configurations out of the literature, for both CW and Q-switched operation, were discussed. These included different feedback elements used to constitute the laser resonator. A brief literature review of CW and Q-switched results was given. The technique of Q-switching was briefly discussed. Results of Q-switched fibre lasers using different modulating elements, out of the literature, were highlighted.

In Chapter 3, an existing diode-pumped, CW Thulium-doped fibre laser was characterized (Figure 3-1). Specifically, the influence of fibre temperature on the spectral output and slope efficiency of the Thulium-doped fibre laser was investigated. The fibre laser was pumped at a wavelength of $\sim 808 \text{ nm}$ with a fibre-coupled laser diode. The active fibre was generously supplied by CorActive[®]. The fibre had specified core and pump cladding diameters of $18 \mu\text{m}$ and $400 \mu\text{m}$

respectively. The core absorption was specified to be 5.5 dB/m at ~ 790 nm. At room temperature a slope efficiency of 28 % was measured. With the fibre cooled to 0 °C, the slope efficiency rose to ~ 40 %. The spectral output was measured with the aid of a monochromator. The wavelength of the fibre laser was measured at room temperature with a wavelength range of ~ 2030 nm – 2060 nm. With the fibre cooled to 0 °C, the measured wavelength shifted towards shorter wavelengths, with a wavelength range of ~ 2025 nm – 2040 nm. The results obtained agree favourably with those found in the literature. Improvements in the design of the fibre laser were discussed and areas for future work are highlighted.

In Chapter 4, a CW and Q-switched diode-pumped, Thulium-doped fibre laser was designed and developed (Figure 4-1). The design process and considerations were discussed in detail. The fibre laser was diode-pumped at a wavelength ~ 792 nm. The doped fibre was procured from Nufern. The fibre used had specified core and pump cladding diameters of 25 μm and 400 μm respectively. The specified core absorption was 1.8 dB/m at ~ 793 nm. The CW fibre laser was characterized with respect to its slope efficiency, spectral output, beam profile, polarization and temporal behaviour. Different feedback elements were used to constitute the laser resonator, such as a broadband, high-reflective mirror and volume Bragg grating. Two lengths of active fibre, ~ 6.5 m and 1 m, were used to constitute the fibre laser.

For a fibre length of 6.5 m, a maximum output power of ~ 30 W was obtained with corresponding slope efficiency of 26 %. Optimization of the pump beam position increased the slope efficiency to 37 %, with thermal damage of the fibre ends occurring at ~ 70 W of pump power. The laser beam was observed with the aid of a Pyrocam, revealing near-diffraction limited beam quality or single-mode operation of the laser. Additionally the sensitivity of the feedback and pump alignment on the beam profile was investigated. M^2 measurements using the 90-10 knife edge method yielded a beam-quality factor value of 1.15. The spectral output of the fibre laser was measured to be in the range of ~ 2045 nm – 2065 nm. The wavelength output was characterized for increasing pump powers, revealing a broadening of the wavelength range and shift towards longer output wavelengths with an increase in pump power.

For a fibre length of 1 m, a maximum output power of ~ 9 W was measured, with a corresponding slope efficiency of 20 %. Using a broadband mirror, the wavelength

output of this fibre laser was measured to be in the range of ~ 1950 nm – 1980 nm. A VBG was introduced as the feedback element for this length of fibre. The VBG had a specified operating wavelength of ~ 1942 nm. Wavelength locking was confirmed at 1940 nm, with a slight decrease in the slope efficiency of the laser at 16% and maximum output power of ~ 8 W.

The temporal behaviour of the laser output revealed ‘self-pulses’ or fluctuations. The duration and frequency of these pulses was found to be dependent on the input pump power, as well as the length of active fibre. These results are in good agreement with those reported in the literature.

Q-switching of the fibre laser was performed with the aid of an Acousto-Optic Modulator (AOM) as Q-switch. The Q-switched fibre laser was found to lase during the on-time of the Q-switch, indicating insufficient hold-off or errors within the experimental setup. Erratic pulsing as well as pulse-skipping was observed in the laser output.

Stable pulse generation occurred for low output powers allowing for partial characterization of the Q-switched fibre laser. At a pulse repetition rate of 10 kHz, pulse energies of 200 μ J were measured with a pulse duration of 77 ns. This yields a pulse peak power of ~ 2.6 kW.

Possible improvements on this Q-switched fibre laser were discussed.

This thesis demonstrates the potential of Thulium-doped fibre lasers as efficient sources of mid-infrared (2 μ m) light. The efficiency and output power of these devices are expected to scale beyond the current results achieved. It is the author’s hope that this thesis may be of service to the scientific community and further development in this field. The aim of the work has been achieved by establishing expertise in diode-pumped Thulium-doped fibre lasers in CW and Q-switched mode.

6 List of Presentations

- 1) “*Characterization of a Thulium-doped fibre laser*”, South African Institute of Physics (SAIP), Pretoria, South Africa (2012). 1st Prize, MSc Oral Presentation.
- 2) “*Thulium-doped fibre lasers*”, IONS Conference, Drakensberg, South Africa (2012), Oral presentation.
- 3) “*A CW and Actively Q-switched Thulium-doped fibre laser*”, South African Institute of Physics (SAIP), Durban, South Africa (2013). MSc Oral Presentation.

7 References

-
- [1] N.P Barnes, et al “*Tm: fiber lasers for remote sensing*”, Optical materials 31, 1061 – 1064 (2009).
- [2] J. Geng, et al “*2 μm fiber laser sources and their applications*”, Proc. of SPIE, Vol. **8164** (2011).
- [3] M. Eichhorn, “*Pulsed 2 μm fiber lasers for direct and pumping applications in defence and security*”, Proc. of SPIE Vol. **7836** (2010).
- [4] D. Creeden, et al “*Thulium fiber laser-pumped Mid-IR OPO*”, Proc. of SPIE Vol. **6952** (2008).
- [5] D. Creeden, et al “*Mid-infrared ZnGeP2 parametric oscillator directly pumped by a pulsed 2μm Tm-doped fiber laser*”, Optics Letters. Vol. **33**, No. 4, February 15 (2008).
- [6] I. Elder, “*Thulium fibre laser pumped mid-IR source*”, Proc. of SPIE, Vol. **7325** (2009).
- [7] S.Christensen, G. Frith, B. Samson, “*Developments in Thulium-doped fibre lasers off higher powers*” SPIE Newsroom, DOI: 10.1117/2.1200807.1152, 11 July (2008).
- [8] T. Ehrenreich, R. Leveille, I. Majid, et al “*1-kW, all glass Tm:Fibre laser*” in Fibre Lasers VII: Technology, Systems, and Applications (2010), Session 16.
- [9] M. Taher, et al “*Novel approach towards cross-relaxation energy transfer calculation applied on highly thulium doped tellurite glasses*”, Optics Express Vol. 19, Issue 27, pp. 26269-26274 (2011).
- [10] S.D Jackson “*Cross relaxation and energy transfer upconversion processes relevant to the functioning of 2μm Tm³⁺-doped silica fibre lasers*” Optics Communications, **Vol.** 230, pp 197-203 (2004).
- [11] F. Di Teodoro “*High-Power Laser Handbook – Chapter 16: Pulsed Fiber Lasers*”, pp 463 (2011).
- [12] D.N Payne “*Rare-Earth Doped Fibre Lasers and Amplifiers*”, <http://eprints.soton.ac.uk/350285/1/307.pdf>
- [13] D.Z Yang, W. Liu, et al “*Linearly-polarized Tm-doped double-clad fiber laser*”, Laser Physics, **Vol.** 20, Issue 8, pp 1752-1755.
- [14] P.W. Milonni, J.H. Eberly “*Laser Physics*” Wiley (2010).
- [15] E. Snitzer, H. Po, F. Hakimi, et al “*Double clad, offset core Nd Fibre laser*” Proceedings of the Optical Fibre Communication Conference, Paper PD5, OSA (1989).

-
- [16] N. G. R. Broderick, H. L. Offerhaus, D. J. Richardson, et al “*Large Mode Area Fibres for High Power Applications*”, *Optical Fibre Technology* **5**, 185-196 (1999).
- [17] W. Shi, et al “*Kilowatt-level stimulated-Brillouin-scattering-threshold monolithic transform-limited 100 ns pulsed fiber laser at 1530 nm*”, *Optics Letters*, July (2010).
- [18] A. Osamu, M. Tadakuma, et al “*Four-Wave mixing in optical fibres and its applications*”, *Furukawa review*, No. 19 (2000).
- [19] A. Smith, et al “*Optical damage limits to pulse energy from fibers*”, *IEEE Journal – Quantum Electronics*, **Vol. 15**, No. 1, January/February (2009).
- [20] A.E Siegman, “*Lasers*” 01 Jan 1986, University Science Books.
- [21] ISO/TR 11146-3:2003 (E).
- [22] I.T. Sorokinam K.L. Vodopyanov (Eds.) “*Solid-State Mid-Infrared Laser Sources*”, *Topics in Applied Physics – Springer*, Vol. **89**, page 221.
- [23] F.H Kan, et al “*Optics and Spectroscopic Properties of Rare Earth Oxides in Inorganic Glasses. Ii. Absorption Spectra of Trivalent Rare Earth Ions*”, *NTIS*, AD-670 106, September (1967).
- [24] D.A Simpson “*Spectroscopy of thulium doped silica glass*” – PhD Thesis.
- [25] <http://www.limo.de/en/limo-produkte/diodenlaser/fasergekoppelte-pumpmodule/>
- [26] F. Auzel, “*Upconversion and Anti-Stokes Processes with f and d ions in Solids*”, *Chem.Rev.*, 104(1), 139-174, (2004).
- [27] P. Zhao, J. Liu, “*The slope efficiency of 2 μ m thulium doped fiber laser*”, *Proc. SPIE 7843*, High-Power Lasers and Applications V, 784306 (November 16, 2010);
- [28] J. Swiderski, “*Mid-infrared supercontinuum generation in a single-mode thulium-doped fiber amplifier*”, *Laser Phys. Lett.*, **10**, 035105 (2013).
- [29] M. Eichhorn, “*Quasi-three-level solid-state lasers in the near and mid infrared based on trivalent rare earth ions*”, *App. Physics B*, Vol. **93**, pp 269-316 (2008).
- [30] B.M Walsh, “*Spectroscopy and Excitation dynamics of the trivalent lanthanides Tm³⁺ and Ho³⁺ in LiYF₄*”, - PhD thesis.
- [31] S.D Jackson “*The spectroscopic and energy transfer characteristics of the rare earth ions used for silicate glass Fibre lasers operating in the shortwave infrared*”, *Laser & Photon. Rev.* **3**, No 5, 466-482 (2009).
- [32] G. Lakshminarayana, et al “*Spectroscopic investigations of Nd³⁺-, Er³⁺-, Er³⁺/Yb³⁺-, and Tm³⁺-ions doped SiO₂-Al₂O₃-CaF₂-GdF₃ glasses*”, *Physics B: Condensed Matter*, Vol. **404**, Issue 20, November (2009).

-
- [33] F.Z Qam, T.A King, “*Self-induced pulsations, Q-switching and mode-locking in Tm-silica fibre lasers*”, Journal of Modern Optics, 52:7, 1031-1403.
- [34] Y. Tang, J. Xiu, “*High-power Pulsed 2- μm Tm³⁺-Doped Fiber Laser*”, Semiconductor Laser Diode Technology and Applications.
- [35] A. El-Sherif, T.A King, “*Dynamics and self-pulsing effects in Tm³⁺ doped silica fibre lasers*”, Optics Communications, DOI:10.1016/S0030-4018(02)01587-0.
- [36] I.T. Sorokinam K.L. Vodopyanov (Eds.) “*Solid-State Mid-Infrared Laser Sources*”, Topics in Applied Physics – Springer, Vol. **89**, page 221.
- [37] A.J Kenyon “*Recent developments in rare-earth doped materials for optoelectronics*” Progress in Quantum Electronics, Vol **26**, Issues 4-5, pp 225-284 (2002).
- [38] D.C Hanna, I.M Jauncey, R.M Percival, et al “*Continuous-wave oscillation of a monomode thulium-doped fibre laser*”, Electronic Lett, 24: 1222-1223 (1988).
- [39] P.F Moulton, G.A Rines, et al “*Tm-Doped Fiber Lasers: Fundamentals and Power Scaling*”, IEEE Journal, Quantum Electronics, Vol. **15**, No 1, February (2003).
- [40] G. Frith, D.G Lancaster, S.D Jackson “*High power 2 μm Tm³⁺-doped fibre lasers*”, Proceedings of SPIE Vol. **5620** (2004).
- [41] Y. Jeong, P. Dupriez, et al “*Thulium-ytterbium co-doped Fibre laser with 75W of output power at 2 μm* ”, Proceedings of SPIE, Vol. **5620** (2004).
- [42] S.D Jackson, A. Sabella, D.G Lancaster “*Application and Development of High-Power and Highly Efficient Silica-based Fibre lasers operating at 2 μm* ” IEEE Journal, Quantum Electronics, Vol. **13**, No 3, May/June (2007).
- [43] P. Myslinski, X. Pan “*Q-switched thulium-doped fibre laser*”, Optical engineering Vol **32**. No 9 (1993).
- [44] A. El-Sherif, T.A King “*High-peak-power operation of a Q-switched Tm³⁺-doped silica Fibre laser operating near 2 μm* ” Optics Letters, Vol. **28**, No. 1 (2003).
- [45] M. Eckerle, C. Kieleck, et al “*High-average-power actively-mode-locked Tm³⁺ Fibre lasers*”, Fibre Lasers IX: Technology, Systems and Applications, Proc. Of SPIE, Vol. **8237** (2012).
- [46] Y. Zhang, Y. Wang “*14.7mJ total output from a gain-switched Tm³⁺-doped double-clad silica Fibre laser*”, ICO20: Lasers and Laser Technologies, Proc of SPIE, Vol. **6028** (2005).
- [47] H.F Ma, Y.G Wang, et al “*A passively Q-switched thulium-doped fibre laser with single-walled carbon nanotubes*”, Laser Phys. **23**, 035109 (2013).

-
- [48] A. El-Sherif, T.A King “*Evaluation of High Power Q-switched Tm³⁺-Doped Silica Fibre Lasers Operating Near 2μm*”, Fibre Lasers III: Technology, Systems and Applications, Proc. Of SPIE, Vol. **6102** (2006).
- [49] P. Kadwani, R. Sims, L. Leick, et al “*CW and Pulsed Performance of Tm-doped Photonic Crystal Fibre Lasers*”, Laser Technology For Defense and Security VIII, Proc. Of SPIE, Vol. **8381 – 83811F** (2012).
- [50] Q. Wang, J. Geng, et al “*Q-switched pulses amplified with short thulium-doped silicate Fibres*” Fibre Lasers IX: Technology, Systems and Applications, Proc. Of SPIE, Vol. **8237 – 82371W-1** (2012).
- [51] M. Eichhorn, S.D Jackson “*High-pulse-energy actively Q-switched Tm³⁺-doped silica 2μm Fibre laser pumped at 792nm*”, Optics Letters, Vol. **32**, No. 19 (2007).
- [52] M. Eichhorn “*Pulsed 2μm Fibre lasers for direct and pumping applications in defence and security*”, Technologies for Optical Countermeasures VII, Proc. Of SPIE, Vol. **7836**, 78360B-1 (2010).
- [53] M. Meleshkevich, N. Platonov, et al “*415 W single-mode CW thulium Fibre laser in all-Fibre format*”, Proceedings of the European Conference on Lasers and Electro Optics CP-2-3-THU (2007).
- [54] M. Eichhorn, S.D Jackson “*High-pulse-energy actively Q-switched Tm³⁺-doped silica 2μm Fibre laser pumped at 792nm*”, Optics Letters Vol **32**, no 19 October 1 (2007).
- [55] S.A Babin, S.I. Kablukov “*Tunable Fibre Bragg Gratings for Application in Tunable Fibre Lasers*”, ISSN 1054-660X, Laser Physics, Vol. 17, No. 11, pp. 1323–1326 (2007).
- [56] J.M.O Daniel, J.S.P Chan, et al “*Novel technique for mode selection in a large-mode area fiber laser*”, OSA 140.3510 (2010).
- [57] Y. Tang, C. Huang, et al “*High-power narrow bandwidth thulium fiber laser with an all-fiber cavity*”, Optics Express 17539, Vol. **20**, No. 16, 30 July 2012.
- [58] IPG Photonics – www.ipgphotonics.com (2013).
- [59] F. Wang, D. Shen, et al “*Spectrum narrowing of high power Tm:Fibre laser using a volume Bragg grating*” Optics Express OSA, Vol. **18**, No. 9 8937 (2010).
- [60] T.S. McComb, L. Shah, et al “*High Power, Tunable Thulium Fibre Laser with Volume Bragg Grating Spectral Control*” SPIE Vol. **7580**, 75801F-1 (2010).
- [61] Jenoptik AG – 2013, <http://www.jenoptik.com>
- [62] W.I Ndebeka “*Characterization of thulium doped Fibre for mid infrared laser applications*” MSc Thesis (2011).

- [63] CorActive © – Specialty Optical Fibre Manufacturer, www.coractive.com (2010-2012).
- [64] G. Rustad, K. Stenersen, “*Modeling of Laser-Pumped Tm and Ho Lasers Accounting for Upconversion and Ground-State Depletion*”, IEEE Journal of Quantum Electronics, Vol. **92**, No 9. September (1996).
- [65] www.nufern.com
- [66] G.P. Agrawal, “*Nonlinear Fiber Optics*”, Third edition (2001).
- [67] J. P. Koplow, D. A. V. Kliner, and L. Goldberg, “*Single-mode operation of a coiled multimode Fibre amplifier*”, *Opt. Lett.* **25**, 442-444 (2000).
- [68] T.S McComb, “*Power Scaling of Large Mode Area Thulium fiber lasers in various spectral and temporal regimes*” – PhD Thesis, page 76 (2009).
- [69] W. Koechner, “*Solid-state Lasers: A Graduate Text*”, Springer (2003).
- [70] www.optigrate.com
- [71] www.goochandhousego.com